Adhesion Studies of T-lymphocytes: insights into the adhesion dynamics of integrin- mediated inside-out signaling in response to TNF

Dissertation

zur Erlangung des Doktorgrades
der Mathematisch-Naturwissenschaftlichen Fakultät
der Christian-Albrechts-Universität zu Kiel

Vorgelegt von
Qian Li

Kiel
2015

Erster Gutachter: Prof. Dr. Thomas C. G. Bosch
Zweite Gutachterin: Prof. Dr. Christine Selhuber-Unkel

Tag der mündlichen Prüfung: 08.07.2015
Zum Druck genehmigt: 09.07.2015

gez. Prof. Dr. Wolfgang J. Duschl, Dekan

C**ontents**

I. Abstract

Integrin-mediated T-lymphocyte adhesion to endothelial cells is a crucial step in the mammalian inflammatory response and for the elimination of pathogens. Outside-in signaling is the well-known pathway in the integrin-mediated leukocyte adhesion in response to proinflammatory events, which is stimulated by an important proinflammatory cytokine, the tumor necrosis factor (TNF). Many studies have been reported that TNF upregulates the expression level of endothelial cell surface molecules. This in turn activates the extracellular domain of integrins and thus facilitates the adhesion of T-lymphocytes both regarding biomolecular interactions and cell adhesion strength.

Recently, an inside-out signaling pathway of integrins in lymphocyte activation by TNF has been brought up. However, how this activation modulates T-lymphocyte adhesion strength and dynamics is still not understood. In the study presented here, T-lymphocyte (Jurkat E6-1) cell adhesion to fibronectin (FN)-coated surface was investigated. Such surfaces provide a biomimetic environment since FN is naturally present on top of endothelium and additional effects from the surface molecules, which are present on endothelial cells *in vivo*, can be excluded.

In detail, phase contrast microscopy and photonic crystal slabs (PCS) were applied for the quantification of cell amount and cell size on fibronectin as a function of TNF stimulation. No difference in these parameters was found for the cells with TNF stimulation compared to those without. An advanced optical strategy, reflection interference contrast microscopy (RICM), was applied for the measurement of the real cell adhesion area and the length of microspikes projected from the cell body. With this technique, cell adhesion dynamics and the fluctuation of subcellular structures were visualized, and again no significant effect of TNF stimulation was detected. To quantify the cell adhesion strength, single-cell force spectroscopy (SCFS) was employed to measure cell detachment forces and single ruptures dynamics. TNF significantly increased cell detachment forces and detachment energies, as well as the number of molecular ruptures and the force associated with single rupture events. Meanwhile, the most pronounced effect was obtained at the shortest cell-surface contact time of about 0.2 sec compared to the

longest contact time of 10 sec. To understand the behavior of T-lymphocyte cells in the initial capture and rolling phase, microfluidics, which mimics the shear stress in *in vivo* situations, was used to track and analyze the percent of adhering cells and the speed of rolling cells as a function of TNF stimulation. The preliminary data show that TNF facilitates more cells to adhere on the surface and decreases the rolling speed. To obtain a detailed understanding of the integrin distribution and the proteins close to the adhesion site in T-lymphocyte cells, functionalized gold nanopatterned structures were used as substrates. No significant effect of TNF stimulation on the cell number or morphology was observed.

Our results show that the TNF-stimulated inside-out-signaling pathway directly enhances T-lymphocyte adhesion, particularly cell adhesion strength.

II. Zusammenfassung

Die integrinvermittelte Adhäsion von T-Lymphozyten an Endothelzellen ist sowohl ein wichtiger Bestandteil der Entzündungsreaktion von Säugetieren, als auch grundlegend für die Abwehr von Pathogenen. Der von außen nach innen gerichtete Signalweg ist bereits in der integrinvermittelten Adhäsion von Leukozyten als Reaktion auf entzündungsfördernde Ereignisse bekannt. Diese Ereignisse werden durch ein wichtiges proinflammatorische Zytokin, genannt Tumor-Nekrose-Faktor (TNF), stimuliert. Viele Studien haben gezeigt, dass TNF die Expression von Oberflächenmolekülen von Endothelzellen verstärkt, was wiederum den extrazellulären Teil von Integrinen aktiviert und damit die Adhäsion von T-Lymphozyten in Bezug auf biomolekulare Interaktionen und zelluläre Adhäsionskräfte begünstigt.

Erst vor Kurzem wurde die Idee eines von innen nach außen gerichteten Signalweges in der Literatur erwähnt. Jedoch ist noch nicht bekannt, wie diese Art der Aktivierung die Adhäsionskräfte und die Dynamik von T-Lymphozyten reguliert. In der hier präsentierten Studie wurde die Adhäsion zwichen T-Lymphozyten (Jurkat E6-1) und Oberflächen, die mit Fibronektin (FN) beschichtet wurden, untersucht. Solche Oberflächen können als eine biomimetische Umgebung dienen, da das Endothel in der Natur von einer FN Schicht bedeckt ist und daher der Einfluss anderer Oberflächenmoleküle, die *in vivo* auf Endothezellen präsent sind, vernachlässigt werden kann.

Phasenkontrastmikroskopie und planare photonische Kristalle (PCS) wurden in der vorliegenden Arbeit genutzt, um die Anzahl und die Größe von Zellen auf FN in Abhängigkeit von TFN Stimulation zu bestimmen. Es wurde kein Unterschied bezüglich dieser beiden Parameter zwischen TNF stimulierten und nicht stimulierten Zellen beobachtet. Interferenzreflexionsmikroskopie (RICM) wurde als hochentwickelte, optische Technik angewandt, um die reale zelluläre Adhäsionsfläche und die Länge der aus dem Zellkörper herausragenden Mikrostacheln zu messen. Diese Technik ermöglichte es, Zelladhäsionsdynamik sowie Fluktuationen von subzellulären Strukturen zu visualisieren. Wiederum wurde kein signifikanter Einfluss der TNF Stimulation gemessen. Mithilfe von Einzelzellkraftspektroskopie (SCFS) wurden Kräfte und Dynamiken von Zell- und Einzelabrissen untersucht. TNF erhöhte

sowohl die Abrisskräfte und -energien der Zellen, als auch die Anzahl und Kräfte molekularer Einzelabrisseereignisse signifikant. Dieser Effekt wurde am stärksten für die kürzeste Kontaktzeit zwischen Zelle und Oberfläche von 0,2 s, verglichen mit einer Kontaktdauer von 10 s, beobachtet. Zum besseren Verständnis des Verhaltens von T-Lymphozyten während der anfänglichen Arretierungs- und Rollphase wurde die *in vivo* im Blutgefäß vorliegende Scherspannung mithilfe eines Mikrofluidikansatzes imitiert, um die prozentuale Menge adhärierender Zellen und deren Rollgeschwindigkeit in Abhängigkeit von der TNF Stimulation zu messen und zu analysieren. Die bisherigen Daten zeigen, dass TNF zu einer höheren Anzahl an adhärierenden Zellen und zu einer erhöhten Rollgeschwindigkeit führt. Für ein besseres Verständnis der Verteilungen von Integrinen und Proteinen nahe des Adhäsionskontaktes von T-Lymphozyten wurden funktionalisierte Gold-nano-Strukturen als Substrate genutzt. Es wurde kein signifikanter Effekt auf Zellanzahl oder -morphologie durch TNF Stimulation beobachtet.

Unsere Resultate zeigen, dass TNF stimulierte, von innen nach außen gerichtete Signalwege die Adhäsion von T-Lymphozyten und insbesonders die zellulären Adhäsionskräfte direkt verstärken.

1. Introduction

1.1 Acute Phase Inflammation

The mammalian immune system administers and protects organisms against bacteria, viruses and other external pathogens. Inflammation is the complex dynamic reaction through the transport of immune proteins, and/or cells to the wound or the infected tissues. Acute phase inflammation is the homeostasis reaction to the local or systemic disruption, such as wounds, infections, or immunological disorders. During this inflammation, cytokines, as pro-inflammatory proteins, are released and able to upregulate the expression level of acute phase proteins, which can in turn augment the amount of cytokines (Gruys et al., 2005). Acute phase inflammation also facilitates leukocytes to rapidly transmigrate from the bloodstream into inflamed tissue and to the infected site.

1.1.1 Leukocytes

Leukocytes (also called white blood cells) are derived from hematopoietic stem cells in the bone marrow and widely exist in lymphatic system and blood (Maton et al., 2008). In the immune system of vertebrates, there are five types of leukocytes: monocytes, neutrophils, eosinophils,

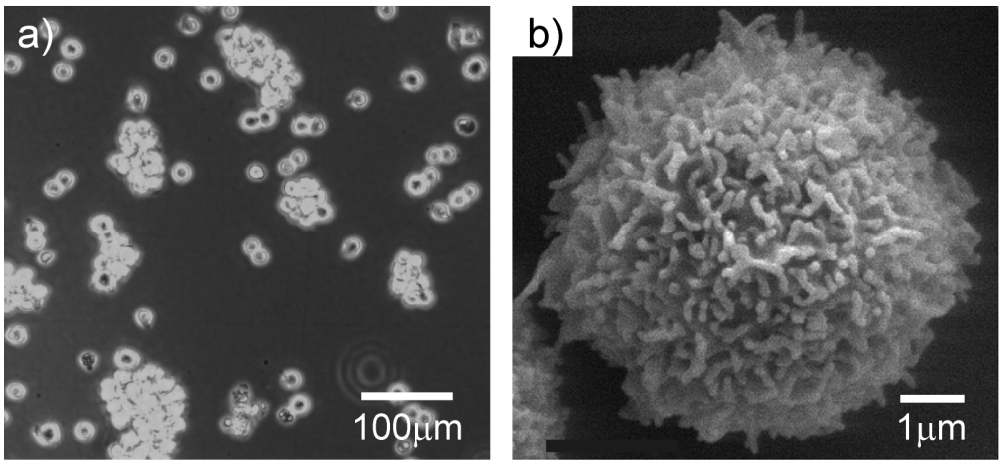

Fig. 1: (a) Jurkat E6-1 cells in tissue culture flask. They are cells in suspension. Cells are prone to form into clusters in healthy condition. **(b) A human blood lymphocyte cell under scanning electronic microscopy (SEM).** (modified from Majstoravich et al., 2004).

basophils and lymphocytes presenting in the blood and macrophages presenting in the tissue (LaFleur-Brooks, 2008). All lymphocytes are classified into three subtypes: T-cells, B-cells and natural killing cells. During the inflammation, when T cells enter the infected tissue, their activation relies on the contact with antigen-presenting cells (APCs) (Bradley, 2003). Afterwards, these T cells are able to kill virus-infected cells, activate macrophages and B cells. In my study, I used Jurkat E6-1 cells (Fig. 1a), which were originally isolated from Epstein Barr virus-negative, non-Hodgkin's lymphoblastic leukemia (Schneider et al., 1977). Followed by the immortalization as a cell line, they are widely used for studying signal transduction cascades (Osborn et al., 1989; Chan et al., 2000). On the surface of a typical human lymphocyte cell, microvilli are observed. These are cell membrane extensions composed of glycoprotein. The length of such microvilli is 0.3-0.4 μm while the diameter of the T lymphocyte cell is 5-6 μm (Fig. 1b, Majstoravich et al., 2004).

1.1.2 Cytokines & Tumor Necrosis Factor (TNF)

Cytokines are a category of proteins released during the acute phase inflammation. Numerous types of cells can produce cytokines, including macrophages, T cells, B cells, and many other kinds of cells (Ibelgaufts, 2013). Several typical types of cytokines can be found in these cells such as chemokines, interferons, interleukins, lymphokines and tumor necrosis factors (TNFs). Cytokines play important roles in the cellular immune response, in particular in cell population regulation and in transmitting intracellular effects from one type to another (Ibelgaufts, 2013).

Tumor necrosis factor (TNF), lymphotoxin-alpha and other 17 proteins consist of the tumor necrosis factors family. Known as TNF alpha (what we used in the study) or cachectin, TNF has the molecular weight of about 17 kD. It is produced mainly from macrophages as homotrimers and spans across the cell membrane. The transmembrane form of the TNF can be leaved into soluble TNF by the TNF alpha converting-enzyme (TACE). TNF is known by playing pivotal roles in physiological and pathological processes. Besides causing tumor necrosis, TNF can also induce its own expression and stimulate secretion of other cytokines and chronic inflammatory reactions (Chu et al., 2013). Prior to its functionalization, TNF initially binds with the cell surface TNF receptors TNF-R1 and/or TNF-R2, the former one of which uniquely expresses on

all nucleated cells, and the latter one only expresses on certain types of cells (Faustman & Davis, 2010). It is known that TNF-R1 plays the key role in activation of numerous signaling pathways, although it has no intrinsic enzymatic activity. TNF binding can activate the cytoplasmic domain of TNF-R1 and recruit the adaptor proteins like tumor necrosis factor receptor type 1-associated death domain protein (TRADD) and fas-associated protein with death domain (FADD) to mediate most of the cell-signaling pathways. These well-known pathways are activation of nuclear factor kappa-light-chain-enhancer of activated B cells (NF-κB), mitogen-activated protein kinases (MAPK) and death signaling (Chen & Goeddel, 2002) as shown in Fig. 2. Besides binding with receptors on cells, TNF is also found to bind with extracellular matrix to concentrate its activities to specific inflamed sites (Vaday et al., 2000).

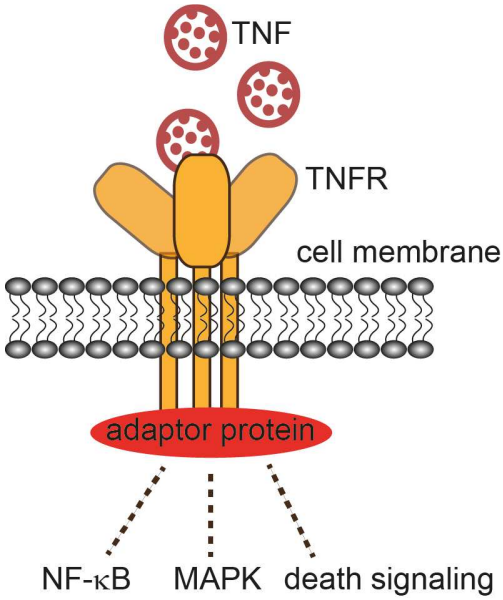

Fig. 2: TNF binds with TNFR and the downstream signaling pathways. The intracellular domain of TNFR recruits the adaptor proteins and mediates the signaling pathways such as activation of NF-κB, MAPK and death signaling.

1.1.3 Leukocyte Adhesion Cascade

Leukocytes generally circulate in the blood stream without adhesion to the vessels but can form temporal bonds with other leukocytes or the vessel. When there presents an inflammation, cytokines trigger transmigration of leukocytes into the inflamed tissue. Prior to this behavior, it

requires leukocyte adhesion to endothelial cells of the blood vessel with successive steps of rolling, arrest, adhesion, strengthened adhesion and migration out through the venular walls (Schmidt et al., 2013). All these partly overlapping steps together generate the "leukocyte adhesion cascade" (Nourshargh & Alon, 2014) with details shown in Fig. 3.

Tethering of leukocytes is usually observed with an obvious reduced velocity during rolling within less than a few seconds and a short adhesive contact to the endothelium (Ley et al., 2007). The primary adhesion of leukocytes to endothelial cells can occur both in fast mode or slow mode depending on whether there is synthesis of the corresponding proteins on endothelial cells (Pober & Sessa, 2007). In detail, leukocyte rolling is mediated by P-selectin, E-selectin on the endothelial cells and L-selectin on leukocytes. Additionally, the arrest process is facilitated by integrins on leukocyte (i.e., $\alpha_L\beta_2$ and $\alpha_4\beta_1$), and cells surface molecules such as intercellular adhesion molecule (ICAM) and vascular cell adhesion molecule (VCAM) on endothelial cells. Finally, other kinases and molecules mediate the following crawling and migration (Nourshargh & Alon, 2014).

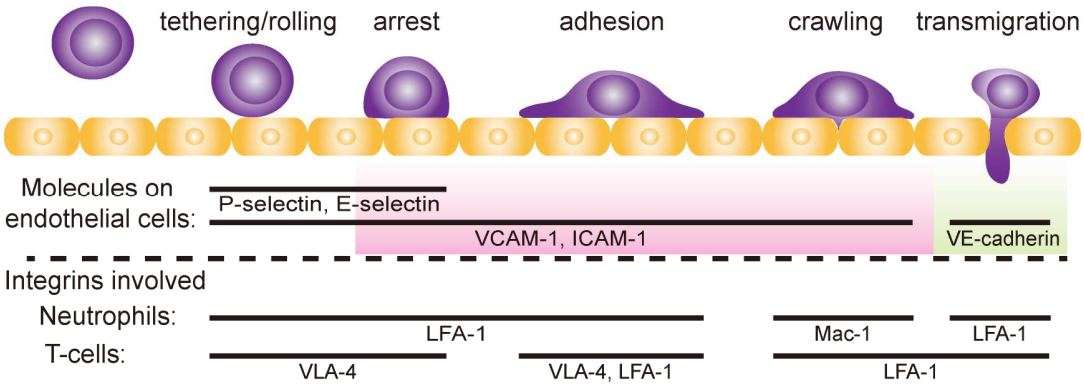

Fig. 3: Leukocyte adhesion cascade. VCAM: vascular cell adhesion molecule; ICAM: intercellular adhesion molecule; LFA-1: lymphocyte function-associated antigen 1, also named as $\alpha_L\beta_2$ integrin; Mac-1: macrophage antigen 1; VLA-4: very late antigen 4, also named as $\alpha_4\beta_1$ integrin. When there are danger signals released from the infected or wound tissue, effector cells are stimulated in specific phases. For instance, leukocytes and endothelial cells (pink) are activated during the arrest to the crawling, and sentinel cells (i.e., macrophages, dendritic cells, green) are activated in the transmigration (modified from Ley et al., 2007; Nourshargh & Alon, 2014).

1.2 Integrin

Integrins were first identified in 1986 as the transmembrane glycoprotein complex (Tamkun et

al., 1986). They link to the cytoskeleton, and can bind to fibronectin (FN). They mediate complex biological events across cell-cell and cell-matrix interactions that are relevant to cell adhesion, migration, invasion, cell signaling transduction, and differentiation.

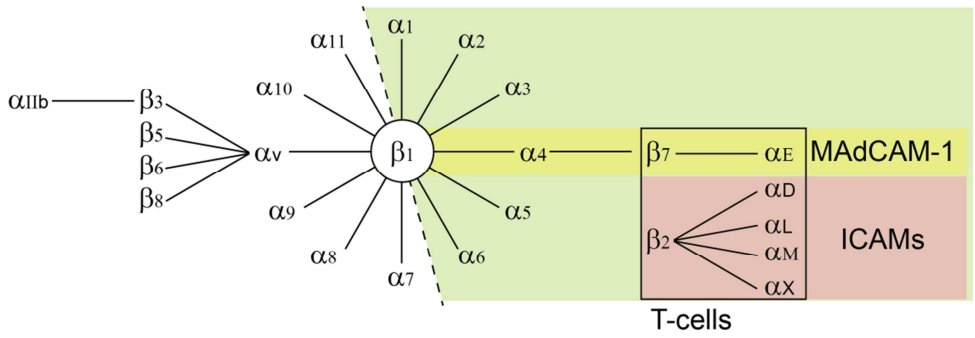

Fig. 4: Combinations of two subunits in integrins. Integrins expressed on T-cells are in green, those binding with mucosal vascular addressin cell-adhesion molecule 1 (MAdCAM-1) are in yellow and those binding with ICAMs are in pink. (Modified from Cox et al., 2010)

Integrins are heterodimers consisting of two subunits α and β. Researchers have found 18 α-subunits and 8 β-subunits that form into at least 24 combinations in vertebrate cells (Ruoslahti & Pierschbacher, 1987). In T cells, there are at least 12 combinations of these subunits expressed (Fig. 4).

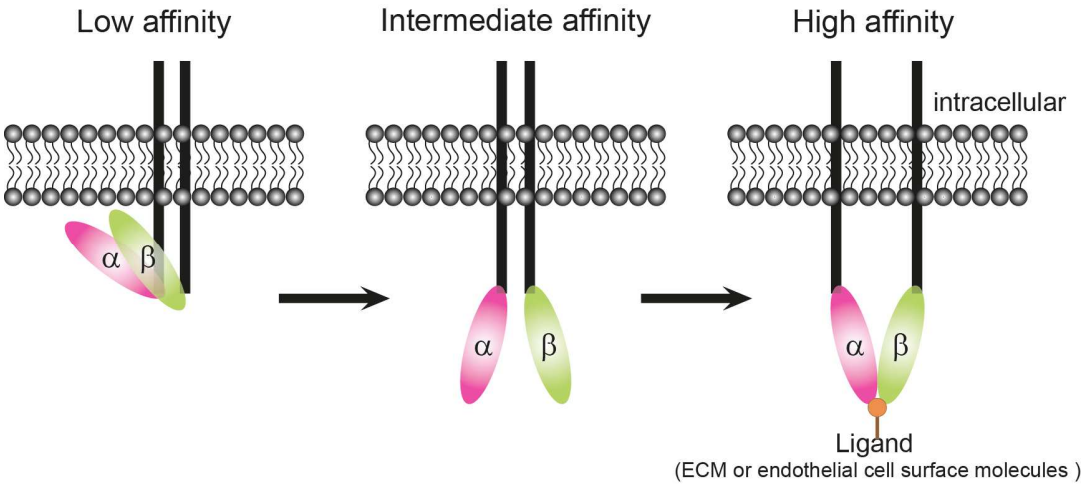

Fig. 5: Switching of different affinity states of integrin. In the low affinity state, the two subunits are very close to each other, the ectodomain of them are bent, in the intermediate affinity state, they are opened but not fully available for ligand binding, in the high affinity state, they are imparted further and are adequate for the ligand binding. The ligand can be a specific peptide of ECM or cell surface molecules of endothelial cells.

Integrins contain extracellular heads, which can bind to extracellular matrix or surface molecules of other cells, and short cytoplasmic tails as the transmitter. For efficient cell adhesion, integrins are converted into the activated (high-affinity) state from a natively inactivated state (low-affinity) with an intermediate state in between (Fig. 5, Luo et al., 2007; Springer & Dustin, 2012). The three states of integrins can be found in a dynamic situation, which can be altered by controlling the chelation with divalent cations Ca^{2+}, Mg^{2+} and Mn^{2+}. Meanwhile, it has been reported that in leukocytes, the fluctuation of the concentration of these divalent cations influences the state of cells from circulating to rolling and attaching (Zhang & Chen, 2012). Inside the fibroblast cells, integrins are able to organize the cytoskeleton and focal adhesions to bind with the extracellular matrix (Fig. 6). There are over 100 proteins that have been identified to localize into focal adhesions (Zamir & Geiger, 2001a), here just some of them are shown in the connection with actin filament in Fig. 6b. In T cells, similar adhesion structures have been brought up, which contains many components resemble those in the focal adhesion of adherent cells (Billadeau et al., 2007).

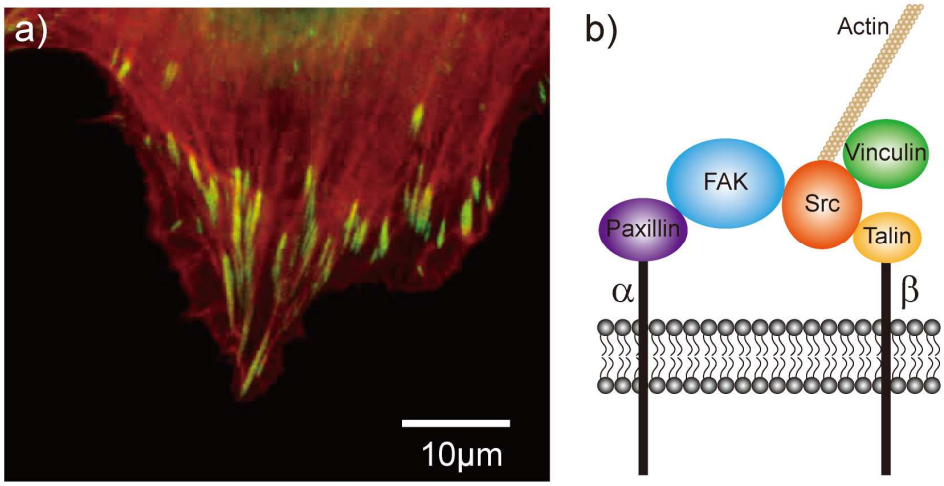

Fig. 6: Focal adhesion. (a) Focal adhesion in a Ref 52 YFP-Paxillin cell (rat embryonic fibroblast cell stably expressing YFP-Paxillin (green)) Actin (red) is stained with phalloidin-555. The merged sites (yellow) are focal adhesions. (b) Schematic structure of focal adhesion.

1.2.1 Role of Integrins in Inflammation

Integrins are not merely linkers between leukocyte and the blood vessel, they play key roles in the process of crossing the endothelial barrier, i.e., switching the state from rolling to adhesion,

which is dependent on $\alpha_4\beta_1$ and $\alpha_L\beta_2$ respectively (Hogg et al., 2003). The affinity state of integrins can balance inflammation (Herter & Zarbock, 2013). They can affect inflammatory diseases such as hypersensitivity and arthritis (de Fougerolles et al., 2000). There are two signaling pathways involved to modulate the function of integrins.

1.2.2 Outside-in & Inside-out Signaling Pathway

The outside-in signaling pathway is called when integrins first bind to extracellular ligands and initiate intracellular reaction of corresponding proteins. Numerous molecules presenting upon other cells or ligands in extracellular matrix can initiate this signaling pathway by catching holds with integrin. Upon TNF stimulation, it is reported that the expression of ICAM and VCAM in the endothelial cells is upregulated (Nourshargh & Alon, 2014). A primary activation occurs when the extracellular domain of integrins in leukocytes (i.e., $\alpha_4\beta_1$) binds with ICAM and VCAM, the activation signals are thus transported to the intracellular domain of integrins. Then adaptor proteins like vinculin, talin and paxillin can be recruited to the cytoplasmic domain of β_1 into adhesion structures which are able to connect with the cytoskeleton. This signaling pathway is shown in Fig. 7a. As well, Src-like tyrosine kinases are activated and integrins undergo clustering (Constantin & Laudanna, 2012).

In contrast, the activation of integrin mediated inside-out signaling pathway relies on the regulation through the binding between specific intracellular proteins and the cytoplasmic domains of integrin (Hynes, 2002; Fa et al., 2009). Generally, this interaction between intracellular proteins and integrins are triggered by external signals. In T cells, the transduction of the stimuli are usually transduced through G protein coupled receptor (GPCR) and T cell receptor (TCR), which thus induce a successive protein or kinases activation inside the cells. Especially in the TCR mediated inside-out signaling, ZAP70 (ζ-chain associated protein kinase) serves as the very early effector which binds to TCR complex and the RAP1-GTP (Ras-related protein 1-guanosine-5'-triphosphate) as the crucial protein to the intracellular chain of α integrins as well as talin and kindlin to β integrins (Brownlie & Zamoyska, 2013). Meanwhile, the phosphorylation of kinases is considered to reflect the occurrence of the signaling

transduction cascade in T cell. For instance, in neutrophils, it has been reported that TNF plays an important role in the integrin mediated inside-out signaling (Bouaouina et al., 2004), because the observation of activated p38 mitogen-activated protein kinase (MAPK) and Src kinases were involved in the engagement of β_2 integrin in neutrophils. Also in adaptive immune responses, T cells can possibly be activated via the same inside-out signaling pathway induced by TNF. As one possible enzyme in this pathway, the lipase neutral sphingomyelinase 2 (nSMase2) is found can be activated by TNF. As further components, TNF-R1-associated protein FAN (Factor Associated with Neutral sphingomyelinase activity), RACK1 (Receptor for Activated C Kinase 1) and EED (Embryonic Ectoderm Development protein) are also involved as signaling components (Philipp et al., 2010). *In vivo* study suggested that knockdown of FAN in zebrafish causes a defective recruitment of leukocytes to infected sites (Boecke et al., 2012). In addition, RACK1 and EED have been reported as partners directly interacting with the cytoplasmic domains of integrins (Liliental & Chang, 1998; Rietzler et al., 1998; Witte et al., 2004). Fig. 7b shows the hypothesis of inside-out signaling pathways in integrin-mediated T cell adhesion to the extracellular matrix in response to TNF stimulation. In detail, the T cells is initiated with the binding between TNF and TNFR, and then activated via the recruitment of intracellular effector proteins to the endodomain of integrins. The intracellular conformation change of integrins thus

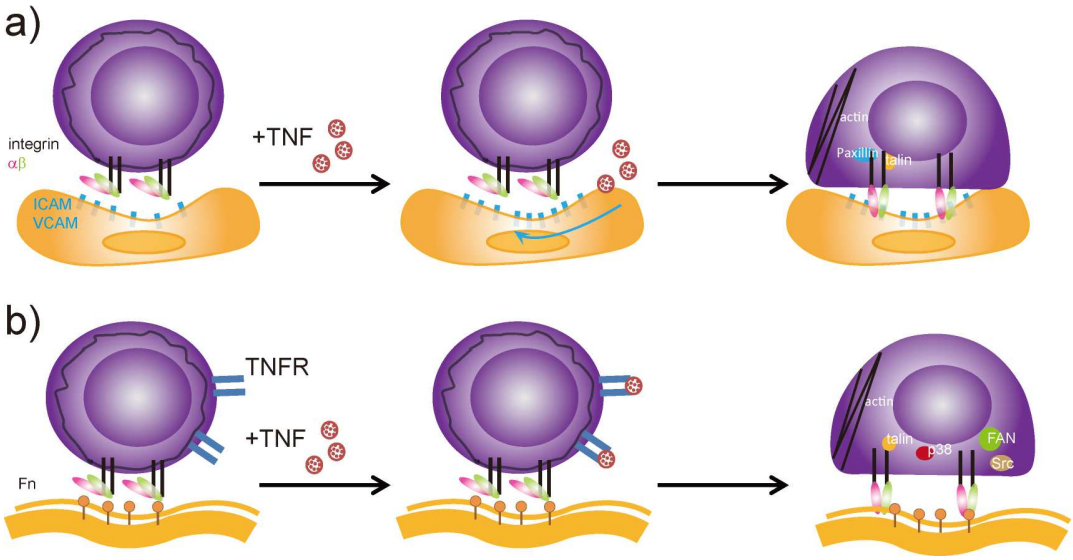

Fig. 7: Outside-in (a) and hypothesis of inside-out (b) signaling pathways in T cells. Integrin and ligands on FN are shown with same symbols as before (Fig. 5).

transports the signal to extracellular and might facilitate cell adhesion.

Outside-in and inside-out signaling pathways can occur simultaneously and depend on each other closely (Kinashi, 2005). For example, without β_2 mediation in outside-in signaling, neutrophils get detached under flow (Giagulli et al., 2006). Furthermore, neutrophils attachment can be enhanced via inside-out signaling pathway by facilitating the conformation changes of extracellular domains in LFA-1 (Lymphocyte Function-associated Antigen 1) and α_4 integrin (Kinashi, 2005). Meanwhile, the outside-in signaling acts as the amplifier following the inside-out signaling especially in lymphocytes (Abram & Lowell, 2009).

1.3 Mechanical Connection between Cells and the Microenvironment

Cell behavior is regulated by the induction of cytokines and recognition of signal molecules. However, cells *in vivo* are subjected in a 3D microenvironment coupled with mechanical forces, where cells can sense and relay the signals from extracellular matrix as well as actively respond in a way to modulate the surrounding environment. Numerous studies have described the interactions between cells and microenvironment in terms of biochemical signals. However, a few studies have been carried out on the effect of physical parameters to the cells. There are lots of questions remaining unclear, such as: How can cells transfer signals from the extracellular matrix? How do cells get into reconstructions? Which physical properties affect cells adhesion? Meanwhile, what are the active roles of cells for the construction of the microenvironment?

1.3.1 Microenvironment Modulates Cell Adhesion

1.3.1.1 Fibronectin (FN), an important protein in extracellular matrix (ECM)

In the organisms, a ubiquitously presenting protein structure surrounding cells is the extracellular matrix (ECM), which not only transduces biochemical signals but also provides physical cues. In ECM, FN performs as one of the most important component in the form of insoluble fibrils. It is a large glycoprotein with the molecular weight about 440 kD. Two identical monomers linked by a pair of disulfide bonds form into the basic protein dimers of FN (Pankov & Yamada, 2002). FN

has repeated units: FN type I repeats (FN1), FN type II repeats (FNII), FN type III repeats (FNIII) and a variable domain (V), which is connected with FNIII. These structures could bind with many kinds of integrins (Luo et al., 2014) and therefore mediating cell adhesion. Among these structures, the FNIII domain and the V domain are especially interesting in our study. The FNIII domain binds with $\alpha_v\beta_1$, $\alpha_v\beta_3$, $\alpha_v\beta_6$, $\alpha_{IIb}\beta_3$, $\alpha_8\beta_1$, $\alpha_5\beta_1$, and the V domain binds with $\alpha_4\beta_1$ (To & Midwood, 2011). It is known that many cell types such as fibroblast cells, endothelial cells, chondrocytes, myocytes and synovial cells can synthesize FN (Mao & Schwarzbauer, 2005). Meanwhile, FN localizes at different places, for example, that secreted by the endothelial cells stays on top of these source cells (Peters et al., 1990) and that produced by the surrounding fibroblast cells present in the local connective tissue (Yamada & Kennedy, 1979). Besides of the insoluble form, FN also exists in a soluble form and circulates in the plasma, which is crucial for the cell adhesion and wound healing as well. In this thesis, I used FN from human plasma to coat coverslips in order to generate a surface that mimics the *in vivo* situation, where FN is present naturally on endothelial cells (Peters et al., 1990).

1.3.1.2 Cell Structures Perform as Force Sensors in Adhesion

Mechanical forces such as shear stress, tension, and compression *in vivo* are considered as the major driving force to facilitate adhesion of most cells (except those in the resting state). In contact with the extracellular matrix, these cells not only deform their shapes but also capture and transduce mechanical forces to realize most functions of biological events such as proliferation, differentiation, etc. There are many proteins, molecules and subcellular structures that serve as mechanical sensors in the physical force transduction. As an important subcellular structure, a focal adhesion is a cluster connecting the cytoskeleton and the ECM (Chen et al., 2003). It is less than 15nm between the cytoskeleton and the ECM (Zaidel-Bar et al., 2004). The proteins in the focal adhesion are in a rapid association and dissociation dynamics in response to the physical change of ECM or the inside stress. Thus, through the focal adhesion, mechanical force can be distributed inside the cell in a manner to sense the microenvironment (Huang et al., 2004).

The elasticity change of the cytoskeleton is considered as the major response factor to the mechanical force as a result of stretching or bending of the cell (Fletcher & Mullins, 2010). As

shown in Fig. 8, microtubules and actin fibers are in conformation balance to control the shape of the cell. Inside an adherent cell, the microtubules are buckled intensively and the polymerized actins are tightly bundled along the binding sites (Ingber, 2006). In this case, the force initiated in specific regions of talin, would regulate the binding of F-actin and therefore regulate the anchoring of integrins (Calderwood et al., 2013).

Fig. 8: Schematic shows of the balance of microtubules (black) and actin fibers (white) in floating (left) and adherent (right) states.

Transmembrane proteins, such as integrins and cadherins, are the important connections between the cytoskeleton and the extracellular matrix. They are assumed to transmit the exterior and/or interior mechanical force through the cell membrane (Calderwood et al., 2013). Furthermore, such physical stimuli are usually conducted into chemical signals. The molecular dynamics of integrins is usually defined with affinity, valency and avidity. Affinity is usually related with the conformation change of the monomeric integrin, which increases the binding force between integrins and correspondingly reduces the rate of dissociation. Valency defines the diffusion and density of the integrins in the cell adhesion area and the number of adhesive bonds. Avidity illustrates the equilibrium of the integrin affinity conformation and the valency of a bulk integrins (Herter & Zarbock, 2013). From diffusion to adhesion, the dynamics of integrin has been brought up recently, as shown in Fig. 9 (Boettiger, 2012). The integrin binding is controlled by the rate-limiting step (Fig. 9b). It has been reported that the affinity of integrins for leukocyte adhesion is increased dramatically by the ligand binding, e.g., 500-1000 fold for LFA-1, which is more than 100 times than that for fibroblasts integrin (Shimaoka et al., 2003). The mobility of the ligand affects the stability of integrins, leading into a more unstable binding of integrin to a soluble ligand and a more fixed binding of integrin to immobilized ligands (Fig. 9c, d). The concentration of integrins in T cells, which differs from other cell surface receptors recognizing hormones or soluble molecules, can be 10-100 times higher on the cell surface. Their binding ability relies on the clustering of integrins, which looks like plaque across the cell

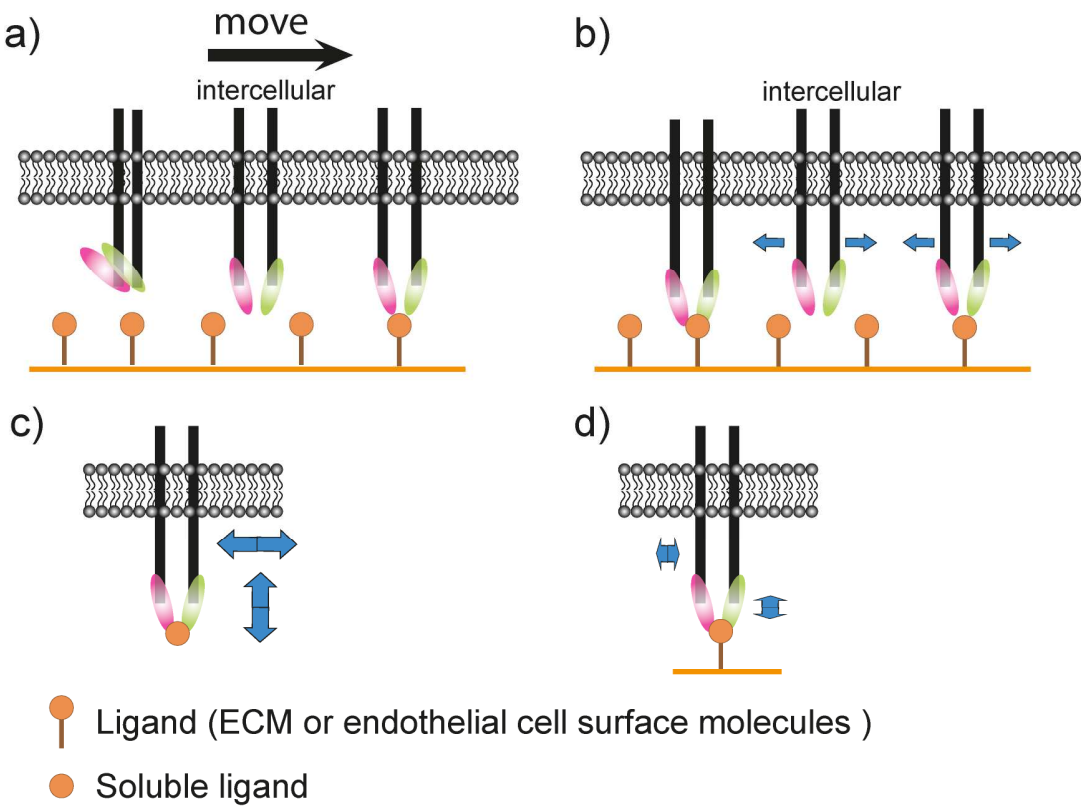

Fig. 9: Dynamics of integrin diffusion (modified from Boettiger, 2012). (a) Conformation of integrin in floating cells. (b) Diffusion of integrin is reduced when cells attach to some ligands presenting on the surface. (c) Integrin binds with a soluble ligand. (d) Integrin attached to the ligand stabilized on the surface. Blue arrows show the direction of the exerting force from integrins.

membrane (Alberts et al., 2007). Interestingly, the clustering itself does not enhance the strength Of the adhesive bonds, rather the machinery to generating and maintaining the integrity of the clusters administers bond strength considerably (Paszek et al., 2009). Furthermore, specific behaviors of cells, to a great extent, rely on the exquisite balance between the anchoring protein and the cytoskeleton. In the leukocyte adhesion cascade, such balance governs leukocytes sensing the endothelial cell layers as well as the transmigration via hydrodynamic forces from the chemoattractant source (Nourshargh & Alon, 2014).

Ion-channels are also believed to serve as sensors in the transport of mechanical stimuli into cytoplasm, which is dependent on integrin mediation (i.e., Ca^{2+} flow) (Janmey & McCulloch, 2007). In neutrophil migration, high affinity LFA-1 incorporated with calcium channel transmits the shear stress to facilitate cell polarization and subsequently transmigration (Dixit et al., 2011).

Besides the above modulations, other structures have been brought up also as force sensors, such as interface of membrane and phospholipid, elements of the nuclear matrix and lipid bilayers (Janmey & McCulloch, 2007).

1.3.1.3 Extracellular Properties Affect Cell Adhesion

Besides of the mechanical sensors in the cells, extracellular properties have been proved very important for influencing cell adhesion.

Many studies have shown that fibroblasts and endothelial cells increase their focal adhesion sizes, spreading areas as well as change their shapes on a stiffer substrate (Yeung et al., 2005; Califano & Reinhart-King, 2010). However, floating neutrophils do not adhere to the change of stiffness when the elastic modulus is in the range from 2Pa to higher than 2000Pa, and even in the adhesion condition, the cells are not sensitive to the large range of stiffness value (Yeung et al., 2005), as a reference, the elastic modulus of 10% gelatin is 241Pa (Leick, 1904). In contrast, a soft matrix supports muscle cell and neuron cell adhesion (Engler et al., 2004). Additionally, wettability and surface roughness have been found to affect the adhesion of fibroblasts and endothelial cells (Lampin et al., 1996). In recent years, nanostructured surfaces have been developed to mimic the extracellular matrix with defined distances.

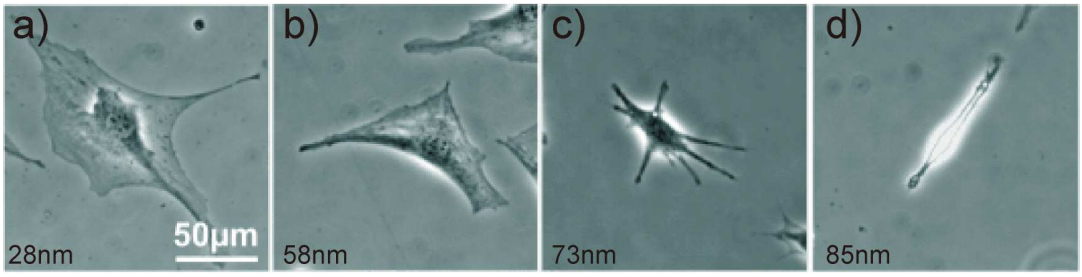

Fig. 10: Different fibroblast cell morphologies on varied distance of gold nanodots conjugated with peptides (Arnold et al., 2004)**.**

Through adjusting the distance of nanoparticles (e.g., gold dots) delicately, the cell adhesion, spreading and migration are revealed as a function of the ligand presentation. Cell morphology varies greatly over the distance of the gold nanodots, which are functionalized with c(RGDfK-) thiols. Fig. 10 shows that the best adhesion and spreading for fibroblast is at the distance of 28

nm between two adjacent gold nanodots. Cells also can spread fairly well at 58 nm. From 58 nm to 73 nm, cell spreading is diminished greatly. When the distance of the gold nanodots is larger than 85 nm, the binding of cells to the surface comes to the minimum. In osteoblast, detailed visualization shows that cells protrusions sensing the pattern of the functionalized gold dots at the distance of 80 nm and the binding sites are observed (Fig. 11).

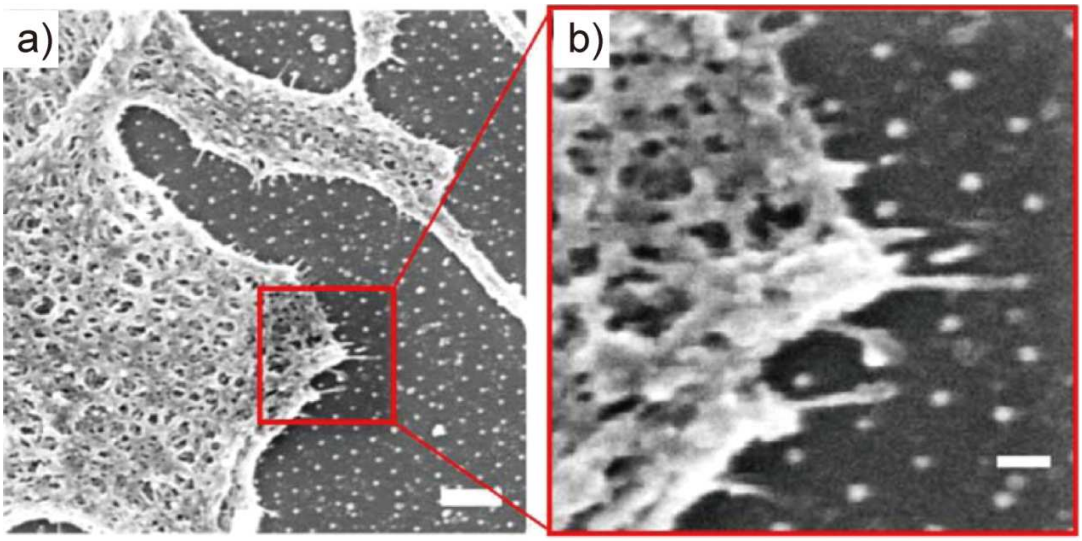

Fig. 11: Mc3t3 osteoblast in contact with a biofunctionalized 80-nm pattern and exhibiting cell protrusions sensing the pattern. Scale bar is 20μm (left) and 200nm (right) (Hirschfeld-Warneken et al., 2008)

1.3.2 Cell Adhesion Affects Microenvironment

It is already known that cell adhesion depends largely on the mechanical signals transmitted from the microenvironment to the cytoplasm. As active living units, cells are able to exert internal force and influence the microenvironment. Exerted within the interaction between actin and myosin, this internal force has been defined as traction force, which results in the deformation of the microenvironment (Wang et al., 2009). The first experiment to study the traction force was implemented in 1980 on observing the wrinkles on silicon rubber substrates coming from the force of adherent cells (Fig. 12a, (Harris et al., 1980)). This remarkable work detected the force in horizontal to the two-dimensional (2D) surface, where the force is exerted in parallel to the surface (Fig. 12b). However, *in vivo*, the extracellular matrix is in 3D environment. So the force distribution should be more complicated than that on 2D surface. On soft and stiff substrate, the

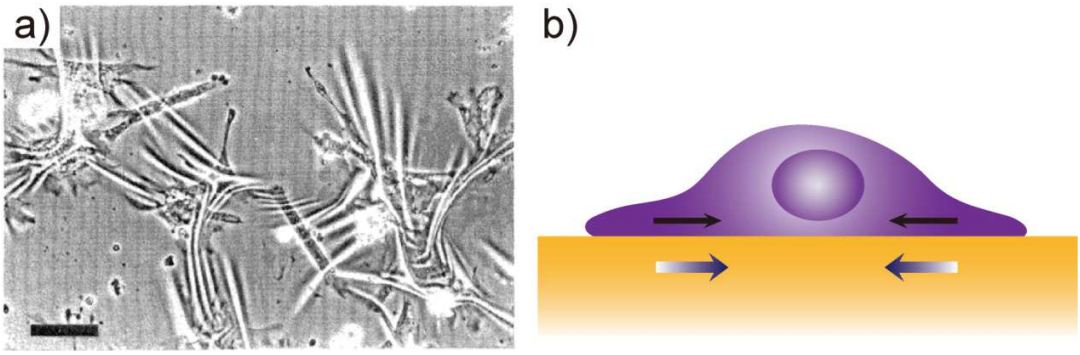

Fig. 12: Traction force exerted by cells to the ECM. (a) Wrinkles on the silicon rubber surface generated by chick hear fibroblasts (Harris et al., 1980). (b) Sketch of traction force at a cell-surface interface in 2D, parallel forces from cell pulling and substrate deformation are shown in arrows (modified from Hersen & Ladoux, 2011).

force distribution models were brought up by Delanoë-Ayari (Fig. 13). They found that the cells pushed the surface down towards the substrate, and as a response, the surface pulls the cells upwards (Delanoë-Ayari et al., 2010). Afterwards, the mechanism "push and pull" was brought up (Hersen & Ladoux, 2011). Similarly to the model in Fig. 13, a recent study assumed that leukocytes exert traction forces in response to TNF on the matrix, leading to a thinner endothelial cell basement membrane (Pober et al., 2012; Finsterbusch et al., 2014; Nourshargh & Alon, 2014).

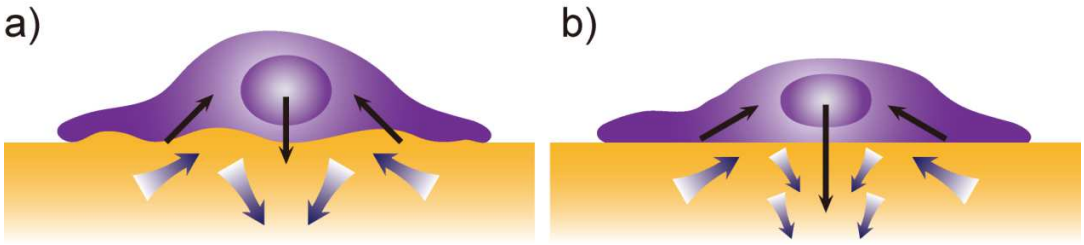

Fig. 13: Push-pull mechanism in 3D. (a) On a Soft surface, the cell exerts force (perpendicular to the substrate surface) in the interior of the substrate and pulls into the cytoplasm close to the binding area (Delanoë-Ayari et al., 2010). (b) On a stiffer surface, the cell spreads into a thinner shape. The pushing force is higher and also the counterpart pulling force makes nucleus bear higher pressure (modified from Hersen & Ladoux, 2011).

Although these 3D models or assumptions might be still simple to interpret the real mechanical force between cells and the surroundings with the fact that cell-cell interactions cannot be omitted, they still provide the preliminary approach in understanding the interactions between cells and the microenvironment on the premise that the cells already adhere on the surface.

The positive feedback loop between the cell interior dynamics and the variation of extracellular environment indicates that the contractility of the actin cytoskeleton with the enhanced interaction between integrin and ECM leads to the conformation change of FN, which enhances the mechanical effect from the matrix again (Rape et al., 2011). These reciprocal strengthening at both directions is also brought up as mechanical signals of outside-in and inside-out in adherent cell mechanics study (Provenzano & Keely, 2011) shown in Fig. 14, which therefore indicates the importance of the mechanical coupling and force transduction between the microenvironment and the cells in a bidirectional manner. Specially, in periphery blood system, lymphocytes are under shear stress in adaption with the blood flow as well as actively exert force to the other lymphocytes and endothelial cells during adhesion, migration and invasion for pathogen elimination and wound healing.

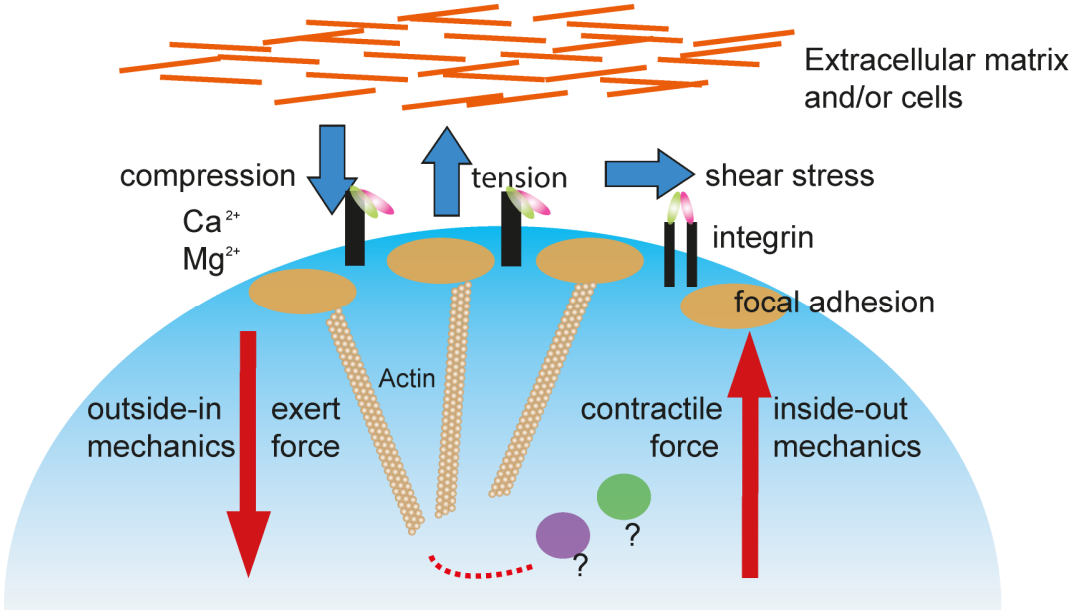

Fig. 14: Schematic mechanics of outside-in and inside-out signaling (reviewed from Provenzano & Keely, 2011).

1.4 Aims of the Study

The function of TNF as a trigger of integrin-mediated outside-in signaling pathway via upregulating the expression level of surface molecules on endothelial cells is well established. As well, it has been reported that the adhesion strength is increased of lymphocyte cells attaching to endothelial cells which were pre-stimulated with TNF (Zhang et al., 2006; Jaczewska et al., 2014). Recently, the other pathway of inside-out signaling has been brought up in response to TNF stimulation on biochemical level. However, it is still elusive how TNF interplays in this pathway on cell mechanics level, although we speculate that TNF may control the inflammatory recruitment and the binding of T cells to the endothelium by directly impacting the adhesiveness of T cell integrins via inside-out signaling.

In my project, I plan to employ a biomimetic surface coating based on FN and investigated the adhesion change as a fact of TNF stimulation. FN surface provides the constant binding sites for a broad range of integrins (Luo et al., 2014), which excludes the interference of the surface molecules on endothelial cells as the adhesion surface. I plan to investigate cell adhesion area and protrusions projected from cell membrane under optical imaging, check integrin expression on Jurkat E6-1 cells, measure cell adhesion force and dynamics of detachment with single-cell force microscopy, launch preliminary microfluidic tests by applying shear stress on cells to detect the cell velocity and percentage of adherent cells, and image proteins constructing adhesion structure on functionalized nanopatterned substrates. All these strategies have the aim to understand the very initial cell behavior at the time point a cell attaches to the surface and to examine if it is influenced by TNF. Meanwhile, we would like to bring up the models of the adhesion manner of integrins with the extracellular matrix in a very short cell-surface contact time scale.

The following questions should be addressed in the thesis:

- Can TNF influence cell adhesion by changing adhesion area/size and subcellular structures?
- Does TNF influence cell adhesion strength?
- What happened to the role of integrins during the cascade of ruptures from single molecule and/or molecular clusters?

1.5 State of the Art Strategies for Measuring Cell Adhesion

Cell adhesion can be studied with various strategies, such as optical microscopy for visualizing morphology changes of cells and organelles in stable or mobile states, force microscopy for measuring adhesion strength on single cell or even single molecule level. In the first part of this chapter, classical methods as well as advanced setups for cell imaging will be introduced. In the second part, leading-edge technologies for cell mechanics measurements will be demonstrated. All of the techniques were applied in my project.

1.5.1 Imaging Tools

1.5.1.1 Phase Contrast Microscopy, Fluorescence Microscopy

Phase contrast microscopy was first invented in 1932 by Frits Zernike and has been widely employed to image transparent samples as a standard method. The imaging principle is that there happens small phase shifts while light passes through the specimen, and this refracted light passes through a transparent phase-plate. Therefore, this light is increased to half a wavelength and leads to the change of brightness that can be visualized. As shown in Fig. 15a, the morphology of a typical Ref52 wt cell is clearly imaged. Meanwhile, fluorescence microscopy uses excitation filters to illuminate the specimen, the specific wavelength (s) absorbed by the conjugated fluorophores can be emitted with longer wavelength, after splitting by a dichroic mirror for reflection and a emission filter for excluding the weaker light, the dynes labeled

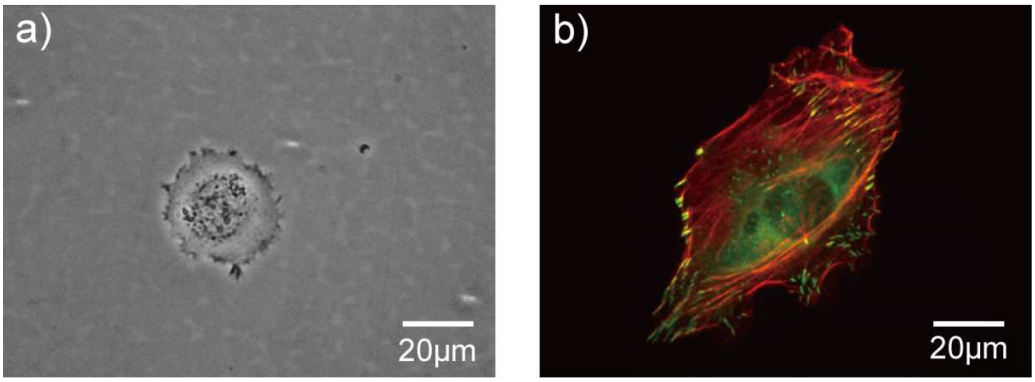

Fig. 15: Morphology of Rat embryonic fibroblast 52 (Ref52) cells. (a) Ref52 wild type cell (Ref52 wt cell) on tissue culture plastic surface using phase contrast microscopy. (b) Ref52-YFP-Paxillin using fluorescence microscopy. (Red: actin stained with phalloidin-555; green: YFP-paxillin).

specimen can be visualized. It performs well in the imaging of specific organelles and studies of colocalization of proteins. Here, Fig. 15b shows the position of actin and paxillin in Ref 52 cells, where actin was stained with phalloidin-555 and cells stably expressed YFP labeled paxillin protein.

1.5.1.2 Confocal Laser Scanning Microscopy (CLSM)

Confocal laser scanning microscopy (CLSM) was developed from confocal microscopy and became a standard imaging technique at the end of the 1980s (Pawley, 2006). The greatest advantage of CLSM is that it can provide images in 3D by focusing the laser beam on the varied depth of the objective at a precise position. The schematic setup of the CLSM conjugated with fluorescence filters is shown in Fig. 16.

The laser beam is passed through an aperture and focused on the position of the sample through an objective lens. A fluorescence filter is installed ahead of the objective to allow only a specific wavelength of light passing through. The sample or the particular areas of the sample, which is stained with fluorophore, are thereby excited. The transmission light is reflected back to the

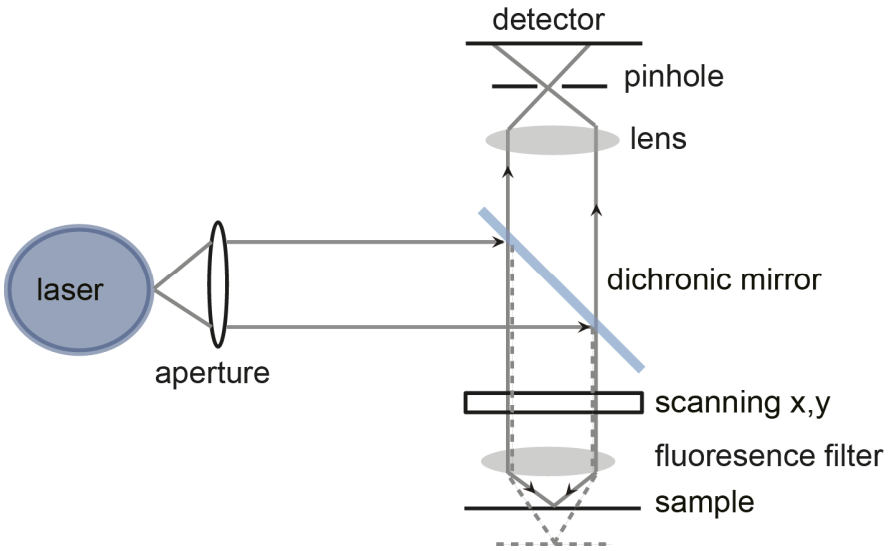

Fig. 16: Schematic setup of CLSM. Only the light reflected on the sample in focus passes through the lenses and can be detected (black line). The light not in focus (shown in dashed grey lines) is suppressed.

photodetection device and recorded there. Most of the out of focal point reflected light is blocked by the pinhole in order to increase the brightness and contrast of the images. In a scanning mode, the laser scans the surface or defined depth of the sample like “slicing” into a “Z-stack”, and by adjusting the signal-to noise ratio, the artificial fluorescence in the background can be decreased (Pawley, 2006). In this way, a minimum concentration of the staining in one sample can be imaged in high-resolution.

This technique has been widely applied in the biological studies with the advantages of not only allow imaging of the stained fixed cells but also enable the living cells that carry with fluorescent reporter protein.

1.5.1.3 Fluorescence-activated Cell Sorting (FACS)

Flow cytometry is a high-throughput technique. It can isolate single particles in a liquid condition with different parameters. As a special kind of flow cytometry, FACS sorts cells one by one and collects them into more than one container. The separation is based on the complexity and fluorescent staining, the schematic principle is shown in Fig. 17.

Under a vibration control, cell suspension is passing in a stream through a tube and the forward scattered light and side scattered light is recorded. The cells stream breaks into droplets, which

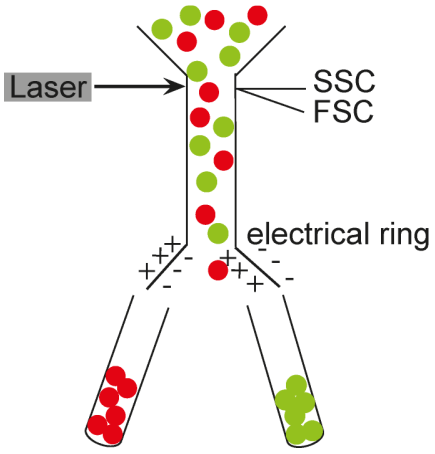

Fig. 17: Schematic of FACS. FSC: forward scattering; SSC: side scattering. Cells stained with different fluorescence dyes (red & green) can be classified.

encounter with an electrical ring placed exactly at the out comingmouth of the tube. Hence, a single cell can be charged and sorted into different containers. Similar as fluorescence microscopy, FACS has been widely applied in biological analysis where a wide range of up to 18 fluorophores can be distinguished (Ornatsky et al., 2010).

1.5.1.4 Photonic Crystal Slabs (PCS)

Biological imaging usually requires label-free methods and devices with high light intensity. Biosensors based on optical waveguides recently provide many possibilities to measure behaviour of the living cells on the whole cell body level (Ramsden & Horvath, 2009).

PCS, as one type of these biosensors, is based on a 2D photonic crystal, which was first described by Thomas Krauss in 1996 (Krauss et al., 1996). 3D light confinement is achieved by a periodic nanostructure in two dimensions and index guiding for light (Johnson et al. 1999) in the third dimension. In general, they are nanostructured thin films produced on transparent semiconductor or glass substrates. In my study, PCS with a linear periodic structure were employed. Polarized light couples to the quasi-guided mode (QGM) of the PCS, which are the origin of guided-mode resonances (GMRs) captured by the microscope objective after the second

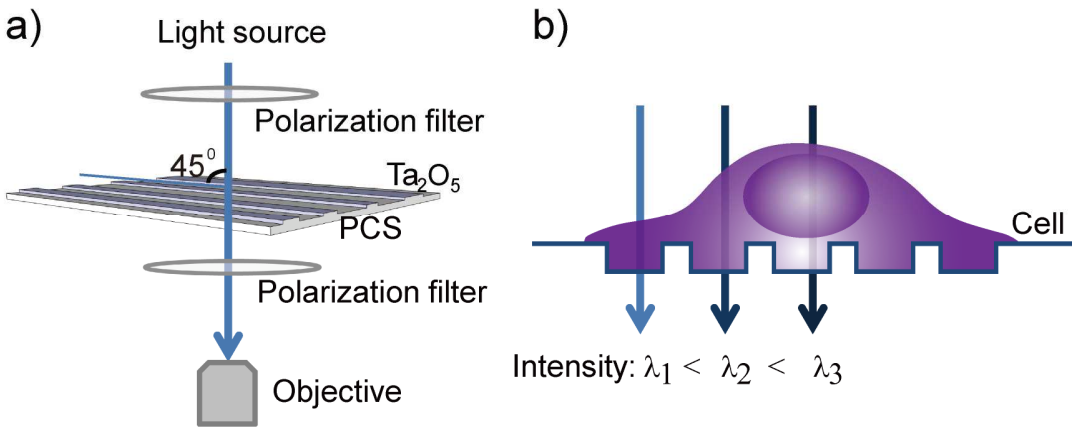

Fig. 18: Schematic image of the PCS setup and the height imaging principle. (a) Schematic imaging principle of PCS with a surface contrast microscopy. PCS has a glass substrate with a 300nm Ta_2O_5 layer, and the depth of the grating is 70 nm (modified from Nazirizadeh et al., 2012). (b) Measurement of the cell thickness based on the intensity of the wavelength (modified from Nazirizadeh et al., 2013).

crossed polarization filter (Fig. 18a). The crossed polarization filter setup suppresses the light from the light source not interacting with the QGM and only the GMR, which experiences a polarization rotation, can pass the second polarization filter. The optimized angle between the polarization of the light and the linear PCS is 45˚ (Nazirizadeh et al., 2008). The properties of GMRs such as the resonance position can be affected by the objects on the surface of PCS, resulting in the change of hue and intensity for the human eye. This strategy provides possibilities to image living organisms, i.e., cells (Nazirizadeh, et al., 2012). Moreover, it is possible to determine the thickness of cells, when the wavelength of GMRs is known (Nazirizadeh et al., 2013) (Fig. 18b). Fig. 19a, b show Jurkat E6-1 cells adhering on FN with phase contrast microscopy and surface contrast microscopy respectively. Where the cell shape is hard to determine with phase contrast microscopy due to halo formation, the PCS-based technique provides a sharp image of the cell edge.

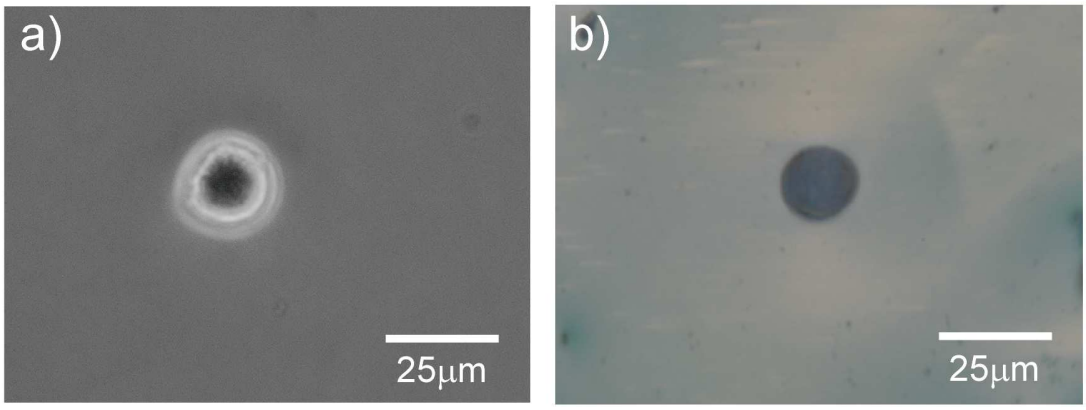

Fig. 19: Comparison of Jurkat E6-1 morphology on FN. (a) On a coverslip coated with FN, the cell was imaged using phase contrast microscopy. (b) On PCS coated with FN, the cell was imaged using surface contrast microscopy.

1.5.1.5 Reflection Interference Contrast Microscopy (RICM)

RICM is an interference-based optical method providing high surface sensitivity and contrast. It is an ideal tool to investigate the adhesion area of cells in detail.

Interference reflection microscopy (RIM) broadened its application from measuring thin films to its preliminary approach in biology in the early 1960s for cell-surface interaction study (Curtis, 1964). The interests had been diminished until the term “reflection interference contrast microscopy (RICM)” was brought up (Beck & Bereiter-Hahn, 1981). The advantage of it

compared to RIM is the antiflex technique (described in the next paragraph). By then, it was further applied in the quantitative measurement of the tiny distances between objects and the surface with the highly augmented contrast of images (Zilker et al., 1987). The measuring distance range from the surface in vertical and lateral direction can be as small as 1 nm to 10 nm (Schilling et al., 2004; Robert, et al., 2008).

The optical setup for RICM is shown in Fig. 20. Monochromatic light was achieved with a mercury lamp combined with a band-pass filter (λ=546 nm) and a field diaphragm system to adjust quasi-parallel illumination. Furthermore, the Antiflex technique enhances the contrast of the interference pattern (Ploem, 1975). This method includes cross polarizers and an oil immersion objective where a plane-parallel λ/4 wave plate is mounted in front of the final lens. Only light passing the objective twice can reach the camera, resulting in an enhanced contrast of light.

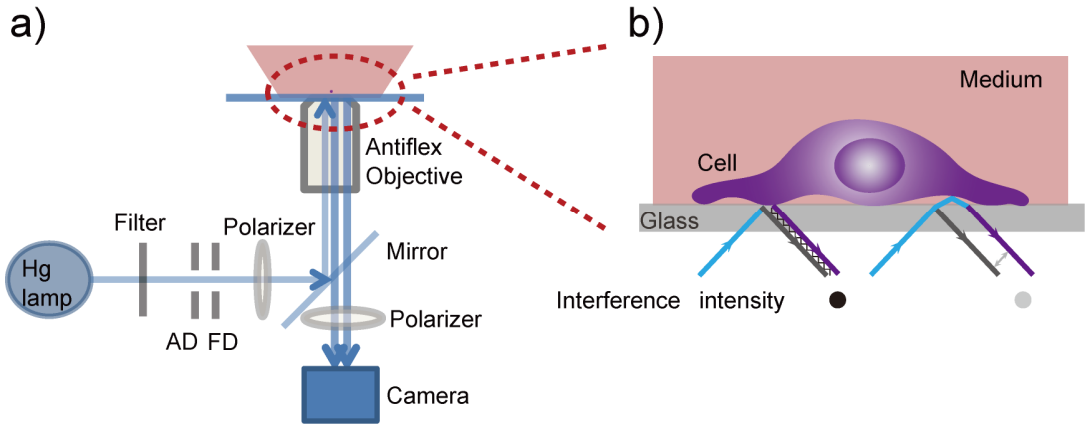

Fig. 20: Schematic principle of RICM. (a). Schematic setup of microscopy. AD: aperture diaphragm; FD: field diaphragm. (b). The principle of interference light between cell membrane and glass. When cell membrane is adhering to the glass, the interference between reflected light at glass surface and cell membrane is very intensive, in contrast, when the cell membrane is far away, interference is small.

Light (I) is reflected at glass-medium surface and medium-cell membrane surface. The interference intensity at the lateral position (x, y) is given by the following equation:

$$I = I_1 + I_2 + 2\sqrt{I_1 I_2}\cos\left(\frac{4\pi n}{\lambda}h(x,y) + \phi\right) \quad (1)$$

where I_1 and I_2 stand for the intensity of light reflected at the above two reflected surfaces. n is the refractive index of the medium (≈ 1.33), λ is the wavelength of the illuminating light, $h(x, y)$ is the position of the cell border relative to the glass surface at the (x, y) position, ϕ is the phase difference, which in this situation is equal to π. In case, of the cell membrane adhering to the surface (h=0), I become the smallest value, leading to a dark area in the image.

Cell behavior on the glass surface can be visualized and tracked. Fig. 21 shows Jurkat E6-1 cells adhering on FN with bright field (a) and RICM (b). Compared to bright field imaging, RICM has great advantages in observing the real adhesion area and protrusions from cell membrane as well as the machinery fluctuations, as both features are not visible in phase contrast microscopy images.

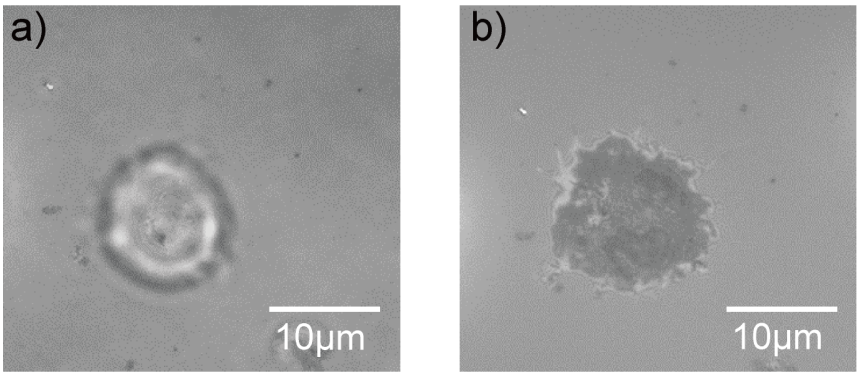

Fig. 21: Jurkat E6-1 morphology with bright field microscopy (a) and RICM (b).

1.5.2 Measurements for Quantifying Cell Adhesion

Since it is considered that the changes of physical properties of cells vitally regulate cell architecture and function, abundant interest has been drawn on the development of techniques to measure and define the responses of cells to extracellular or intracellular signals. Physical approaches are intended to decipher the tricks employed by cells with the introduction of external forces that mimic the force *in vivo* situation. Therefore, the properties such as viscosity, elasticity, adhesion force and dynamics can be determined. There are different ways to exerting forces on cells. In this chapter, AFM for measuring the force directly and microfluidics applying a force field employed in the project will be explained.

1.5.2.1 Atomic Force Microscopy (AFM)

Compared to traditional microscopy, AFM provides high precision and resolution in the measurement of surface topography as a novel strategy. It also shows advantages in studying adhesion forces between cells-cells, cell-matrix or even single molecules interactions in a close-physiological condition.

AFM (also called scanning force microscopy (SFM)) was developed from scanning tunneling microscopy (STM) invented by Binning and Rohrer in the beginning of the 1980s. The first approach of AFM was to measure the surface at single atomic scale with a super small force, where it was supervised with a cantilever beam (Binnig & Quate, 1986). Afterwards, Cappella and Dietler extensively explained the force-distance curve in 1999 for studying surface interaction (Cappella & Dietler, 1999). The general idea of AFM is the measurement of the attraction or repulsion force between the cantilever tip and the surface so that surface topographies can be imaged: the deflection of the cantilever corresponds to the reflection of an aligned laser beam, which is output into the voltage change with a position-sensitive photodiode (Fig. 22a). Cantilevers are normally made from silicon or silicon nitride. The backside of cantilevers it is often coated with gold to increase the efficiency of laser reflection. The measurement can be carried out in air, gas or liquid. Fig. 22a shows the principle of surface mapping with AFM.

In contact mode, the tip scans the surface in the x,y direction, the geometry of which is measured

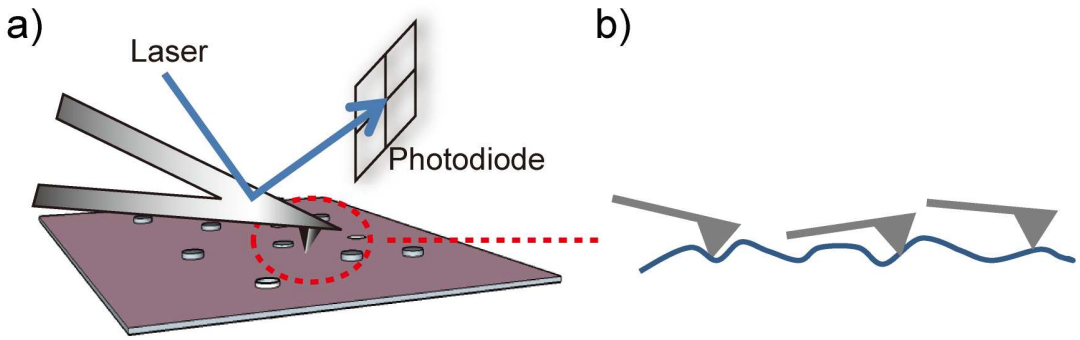

Fig. 22: Schematic illustration of surface imaging with AFM. (a) Surface topography is measured by screening a surface with a cantilever by the deflection of laser on the backside of the cantilever. (b) Contact mode.

by the deflection of cantilever probes with a feedback loop defining the method of the movement of cantilever (Fig. 22b). Another mode is intermittent contact mode (also called: tapping mode), in which the cantilever is oscillating close to its resonance frequency. The image is produced in a dynamic contact between the tip and the surface. The resolution of the surface imaging can be as small as 0.1 nm with the force smaller than 10^{-9} N (Cappella & Dietler, 1999).

Based on hook's law, the force (F) generated between the tip and the sample is:

$$F = kx \tag{2}$$

where k stands for the spring constant (N/m) and x is the deflection of the cantilever (m). To obtain correct images and the mechanical properties of the sample, it is essential to obtain the spring constant (so called: calibration) before launching a measurement. Although spring constant can be calculated with established equations from the shape of the cantilevers (Butt et al., 2005) and is provided from the manufacturer, considerable variations in the thickness of the

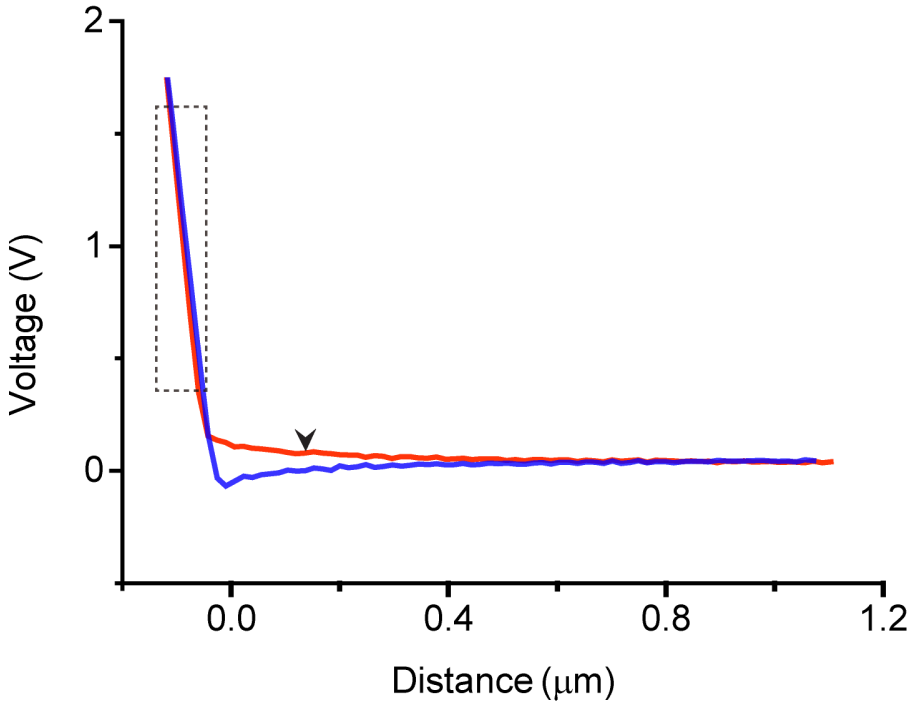

Fig. 23: A typical force-distance curve for a cantilever interacting with a Petri dish with approach curve (red) and retraction curve (blue). The cantilever get contact with the surface (arrow) followed by the elastic deformation on the surface. The linear part (in the grey dashed box) of the approach (usually) is fitted to obtain the sensitivity.

cantilevers make these values unreliable. Thus, spring constants of cantilevers must be calibrated prior to an experiment. Furthermore, sensitivity must be determined. Sensitivity is the conversion factor of voltage captured by the photodiode and the movement of the cantilever. This relationship is relatively linear over a wide range. From a calibration curve on a Petri dish in medium (RPMI), the proper sensitivity is easily obtained by fitting the linear part of the approach curve from a typical calibration curve (Fig. 23).

The thermal noise method was employed which was established before (Hutter & Bechhoefer, 1993) to obtain the spring constant with the corrected factor following the guide by the JPK software for the cantilevers (MLCT, with "V" shape). So the force comes out as

$$F = U * S * k \tag{3}$$

with: U is voltage in V, S is sensitivity in m/V and k is spring constant in N/m.

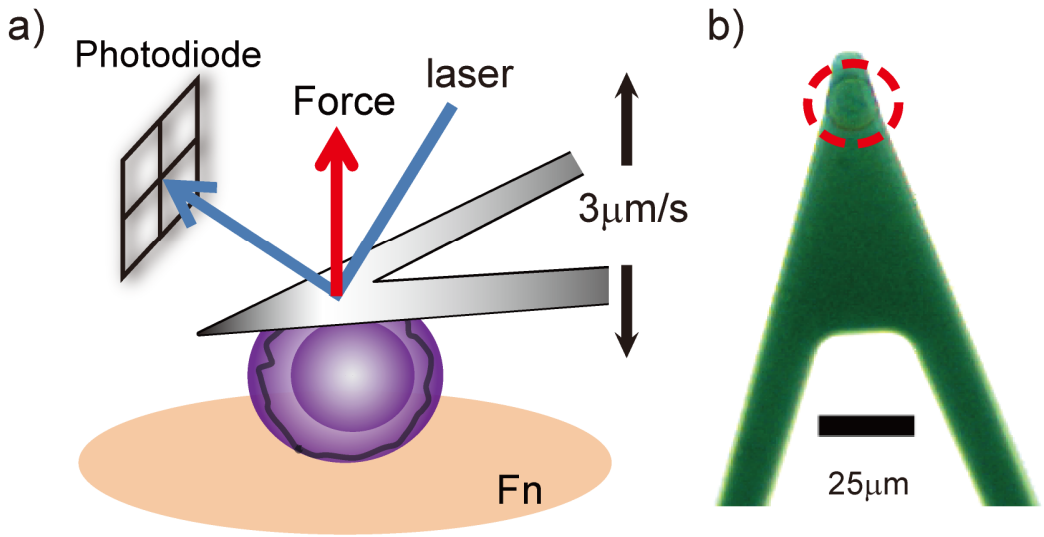

Fig. 24: (a) Principle for measuring cell adhesion force with AFM of a single cell to the FN surface with the constant speed of approaching and retracting. (b) A single Jurkat E6-1 cell is successfully attached to the top of the free end of a cantilever.

AFM based single-cell force spectroscopy is applied in measurement of cell adhesion force due to the very broad range of exerting force from about 5 pN to 100 nN (Helenius et al., 2008). Cell adhesion strength can be determined in the following way (Fig. 24a): a single living cell is

attached to a tipless cantilever (Fig. 24b) and pressed onto a fibronectin-functionalized surface using an atomic force microscope. After a certain time interval, the cell is detached from the surface with the cantilever. Meanwhile, a lot of parameters can be illustrated from a representative force-distance curve (details in 3.2.1).

1.5.2.2 Microfluidics

Biological studies often face the problem that the dynamic interactions of living cells or organisms with their surrounding environment are difficult to reproduce in static *in vitro* conditions. Microfluidics, as a technology with very broad applicability for situations where flow plays a role has proven to be a pragmatic approach to tackle such problems (Paguirigan & Beebe, 2008). It has many further advantages, i.e., very tiny volumes (several µl) of sample solutions, and is very sensitive, fast and cost effective as experiments can be carried out in parallel (Harrison et al., 1992).

Microfluidics are the devices containing channels from tens to hundreds micrometers in dimension, which allow the volume of flow from 10^{-18} to 10^{-9} liters to be analyzed (Whitesides, 2006). The first series of microfluidics setups emerged in the late 1970s for studies of ink-jet printers and in gas chromatography (Bassous er al., 1977; Petersen, 1979). Afterwards, modern devices were developed as versatile tools in interdisciplinary studies, mostly in physics, chemistry and biology. Representative examples in biological applications are macromolecular analysis for DNA (Taylor et al., 1997; Jacobson & Ramsey, 2006), enzyme, cellular analysis such as cytometry (Carlson et al., 1997; Li & Harrison, 1997; Fiedler et al., 1998) and cell-cell/environment interactions (Folch, 2000).

A variety of different structures of microfluidic setup are available commercially. In this study, single-channel microfluidic chambers were selected. The setup is explained schematically in Fig. 25: a pump system drives the cell suspension flow from a syringe to the chamber first through tubes and then through the microfluidic channel.

The laminar instead of turbulent dynamic inside the chamber enables that the liquid does not mix

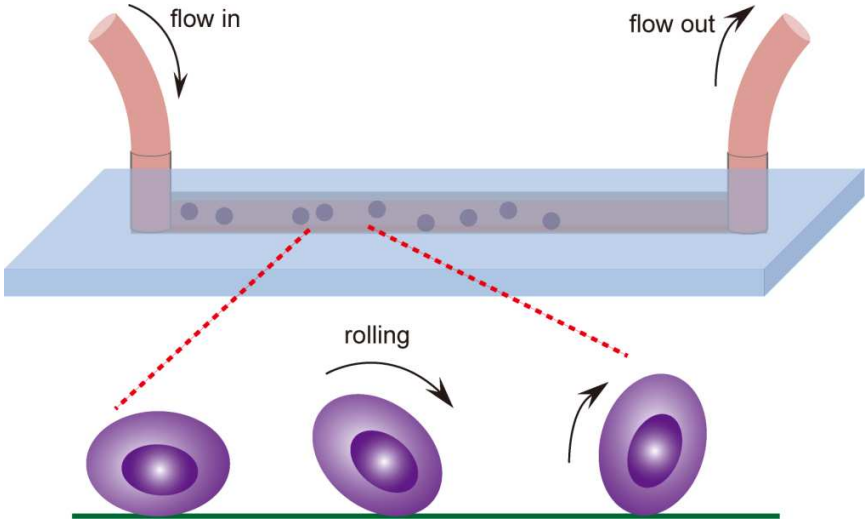

Fig. 25: Schematic illustration of the setup (above) and the rolling cells under a microfluidic chamber (below).

and cells are under the flow in one direction so that the diffusion is negligible, which simplifies the movement of cells and makes it unidirectional. A shear stress (τ) occurs while the fluids flow along the solid boundary and experience a velocity loss. Shear stress is defined as the product of the dynamic viscosity (η) and the shear rate (γ):

$$\tau\,(Pa) = \eta\,(Pa \cdot s) \times \gamma\left(^{1}/_{s}\right) \tag{4}$$

Shear rate describes the velocity change between two parallel fluid layers due to the resistance to the shear flow. Dynamic viscosity depends on the characteristics of the liquid and the surrounding temperature. The dynamic viscosity is a parameter commonly used for the characterization of fluids and is often expressed in Centimeter-gram-second system of units (CGS units) (Harrison et al., 1992):

$$[\eta] = 1\,\frac{dyn \cdot s}{cm^2} = 0.1\,Pa \cdot s \tag{5}$$

When a pump drives a small amount of living cells with external connections (syringe, silicon tube) under a constant flow, cell motion and transport can be recorded within a fast recording speed camera. For a flow in a rectangular section, according to Cornish (1928) and the chamber

used in this thesis (µ-Slide I 0.4, ibidi application), the shear stress is,

$$\tau\left(\frac{dyn}{cm^2}\right) = \eta\left(\frac{dyn \cdot s}{cm^2}\right) \cdot 131.6 \cdot \phi\left(\frac{ml}{min}\right) \quad (6)$$

ϕ is the flow speed. Based on this equation, it is possible to investigate the rolling and adhesion of cells.

1.5.3 Capabilities of the Measuring Strategies

Light microscopy usually aims at providing general information from the whole cell body to the specific molecules. Besides phase contrast microscopy, fluorescence microscopy is the most common method to visualize specific molecules, especially CLSM with an enhanced resolution. Moreover, 3D imaging with CLSM is appropriate to visualize cells and even the localization of single molecules. However, this technique relies highly on the binding efficiency of fluorophores to the molecules of interest. Moreover, autofluorescence presents in many cells (Monici, 2005), and in many cases, the fixation method restricts the application in the living conditions. FACS is adequate for high-throughput analysis, and provides information on protein fluctuations in a population rapidly. Nevertheless, the information of delicate protein dynamics is elusive and it also depends on the efficiency of fluorescence dyes.

Compared to phase contrast microscopy, PCS is a novel sensitive method that has the advantages to avoid “halo artifacts”. However, it is still limited in illustrating the fine structure and dynamics in the living condition because the specimen should be dried for imaging. Additionally, RICM has shown to be a potent tool in live cell studies on the dynamic interplay between cells and surfaces. Unfortunately, it requires a complex data evaluation (Limozin & Sengupta, 2009). Scanning electron microscopy (SEM), which is able to image details in structures with the dimension less than 1nm, requires extra preparation efforts for coating which might inevitably introduce artifacts (Wilson & Bacic, 2012). In a living cell, the protein folding and unfolding are in a rapid mode, how exactly and precisely cells interact with others and respond to the extracellular matrix is still an open question.

AFM based single-cell force spectroscopy is an appropriate method to study discrete adhesion with delicate controlling parameters and temporal visualization from cell to single molecule adhesion level at very short cell-surface contact time scale (Franz & Peuch, 2008). Compared to optical tweezers and magnetic tweezers, which are mainly used to detect the transport of mechanical stress inside the cells (Wang et al., 2005), AFM has many advantages such as not invasive to the cell, wide force range (up to 100 nN) to study strong adhesions as well as forces associated with single molecular bonds. Further improvements of this setup are required for cell experiments, especially an aqueous condition to reduce limitations such as electronic signal-to-noise ratio, acoustic and the hydrodynamic artifact. Furthermore, elaborate data processing and development of biomodels are crucial for explaining molecular dynamic events in certainty. Interdisciplinary devices such as AFM integrated with CLSM (Adams & Czymmek, 2007), fluorescence resonance energy (FRET) (Vickery & Dunn, 2001) or other advanced microscopic methods would expand the spectrum for bringing research data on the accurate localization of proteins or molecules at nanoscales in future.

Microfluidics, which mimics the *in vivo* movement of floating cells, can be fully exploited with high-speed cameras and fast analyzing programs. In comparison with AFM and microfluidic methods, AFM can only produce up/down movement while microfluidic generates a more natural environment for blood vessel experiments; AFM needs cantilever as handle which potentially influencing the cell but microfluidics does not need it; AFM works at single-cell level, microfluidics rather gives ensemble average data. Therefore, the future development of microfluidics in cell biology is more prone in the cooperation between sophisticated design of the chamber structure and molecular recognition together with AFM force-distance curves.

2. Results & Discussion

2.1 T-lymphocyte Adhesion on Fibronectin (FN) as A Function of TNF Stimulation

In my project, I compared the adhesion of TNF treated and untreated T-lymphocytes on FN-coated surfaces. This setup is a fairly straightforward and simplified system without interference from the surface molecules of endothelial cells. The initial bulk assays were implemented for unraveling effects of TNF on cells size in phase contrast microscopy and PCS based surface contrast microscopy, and the cell adhesion area as well as the length of the cell microspikes with RICM. Most importantly, AFM-based single-cell spectroscopy was applied to study cell adhesion strength and strength of single rupture events within short cell-surface contact time scales. With a microfluidic setup, cell behavior was studied under shear stress, mimicking the *in vivo* situation of lymphocyte adhesion in the blood vessel.

2.1.1 Light Microscopy Studies of Cell Adhesion Area

2.1.1.1 Studies of Cell Size under Phase Contrast Microscopy and on PCSs

As a preliminary test, I tried different methods for making FN coated surfaces. Coverslips

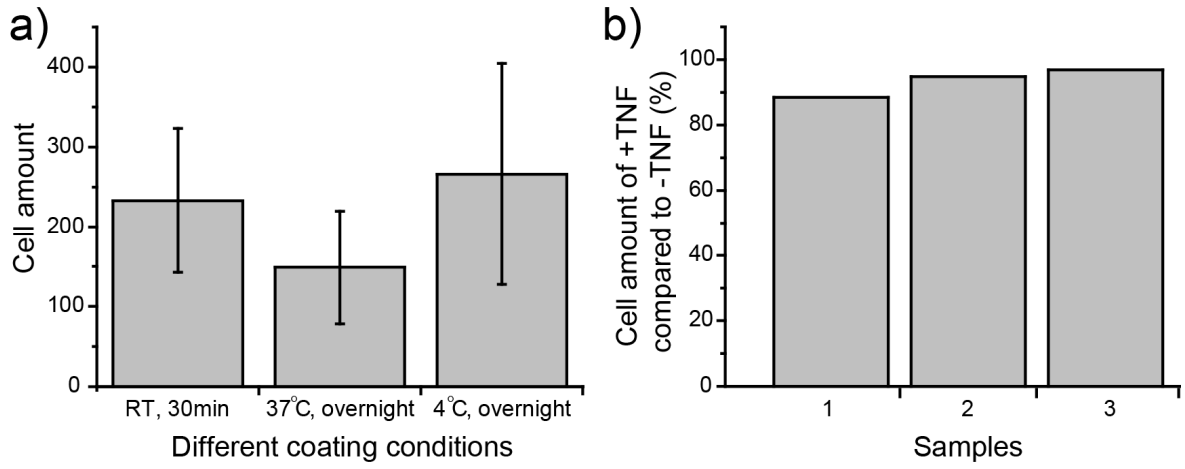

Fig. 26: Adherent Jurkat E6-1 cell amounts on FN coated surfaces. (a) Different methods of coating. There are 2 repeats for each coating method. Error bars show the standard deviation. (b) Adherent cell amount comparison of TNF treated to TNF untreated on FN surface. FN is coated at 4 ^{o}C overnight. The result shows the 3 independent experiments.

(diameter: 24mm) were incubated with a concentration of 15µg/cm^2 at room temperature (RT), 30min; at 37 ºC overnight and 4 ºC overnight, respectively, in order to obtain the best coated surfaces for the adhesion of Jurkat E6-1 cells in later experiments. As shown in Fig. 26a, it is

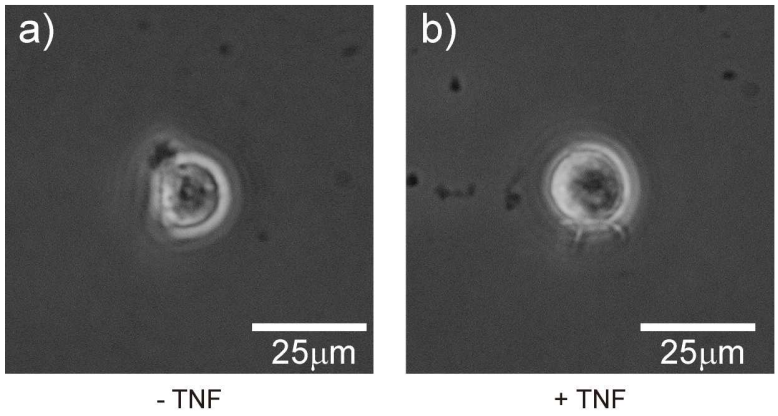

Fig. 27: Adhering Jurkat E6-1 cells morphology studied with phase contrast microscopy. (a) A cell not treated with TNF. (b) A TNF-treated cell.

obvious that the highest average amount of cells presents on FN coated surface treated at 4 ºC overnight. So in the following experiments, all FN-coated surfaces were prepared with this method. Afterwards, the amounts of adhering TNF-treated and untreated Jurkat E6-1 cells were counted on FN surfaces after the incubation time of 1h with phase contrast microscopy. The result is shown in Fig. 26b. Fig. 27 shows the morphologies of TNF treated and untreated cells after fixation on FN surfaces. No significant difference in cell amount analysis was found in

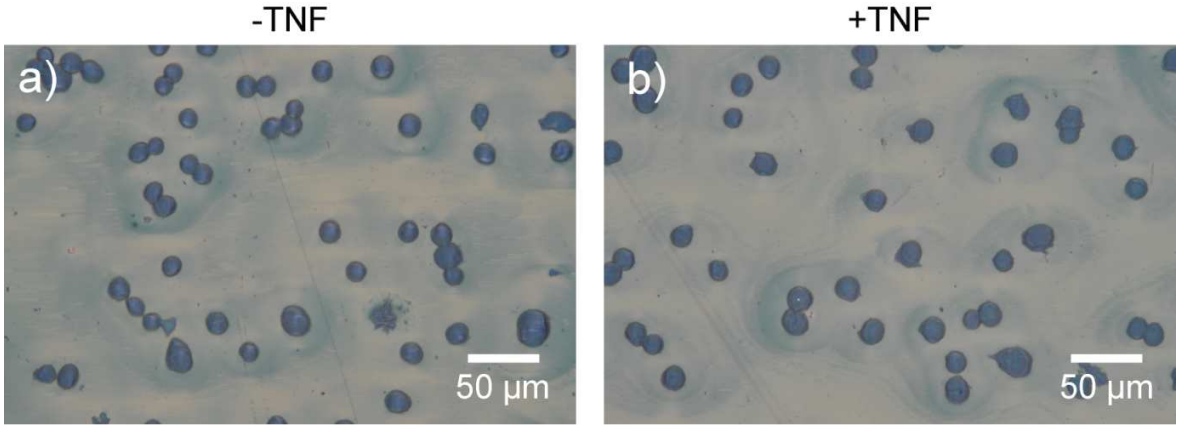

Fig. 28: Adherent Jurkat E6-1 cells on FN-coated PCS. (a) Cells without TNF treatment. (b) Cells pre-treated with TNF.

response to TNF stimulation. As well, the morphologies of cells in each situation are the same. Apparently, this method was not ideal for analyzing cell adhesion area, since the cell was surrounded by a bright halo. To address this problem, we tried to use PCSs as adhesion substrates rather than normal glass coverslips. The principle and advantages of the PCS have been described in section 2.1.2 and the surface is coated with FN as well.

On the PCS surface, we analyzed the cell adhesion area for about 400 cells on each sample. Cell morphologies are shown in Fig. 28. Only single cells with clear border were included in the analysis. This experiment was done twice in triplicate. However, no difference between cell treated and not untreated with TNF was found (Fig. 29). Anneke Möhring supported the analysis under my supervision.

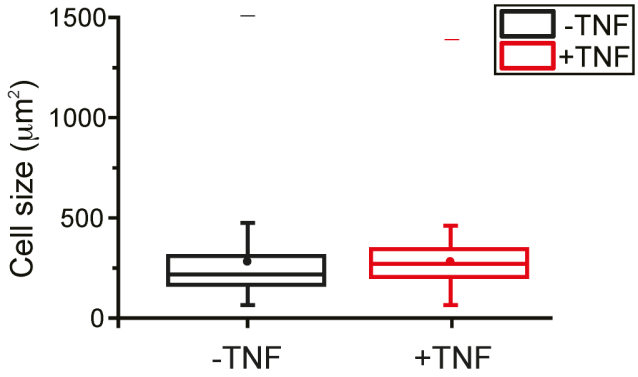

Fig. 29: Comparison of Jurkat E6-1 cell adhesion area on PCS. Cells not treated with TNF (black) and cells treated with TNF (red). Box plots were applied for the analysis. (Box: interquartile range; line in each box: median; dot: mean; whiskers: coefficient factor at 1.5). This experiment was repeated twice in triplicate.

However, there are still drawbacks rising from the technique itself in our experimental condition. Firstly, it is hard to obtain a convincing cells amount by manual counting, because of the inevitable variations during cell seeding and the inhomogeneous distribution. For PCS experiments, the cells need to be fixed and dried on FN. (1): The incubation time is long (1h); (2): the whole cell membrane was displayed, which perhaps covered the unattached parts below the cell body; (3): the dynamics of the cell adhesion cannot be acknowledged.

2.1.1.2 Cell Adhesion Area and Length of Microspikes under RICM

As soon as we realized the limitations from phase contrast and surface contrast microscopy, we employed RICM to study the exact adhesion zone below the whole cell body in living cells. Meanwhile, since the setup is coupled with a high-resolution camera, we can even detect dynamic protrusions from the adhesion area and observe their motion during migration behavior.

In the leading edge of a migrating cell, two dynamic components are exploring space: lamellipodia and filopodia, which both rely on actin polymerization. As schematic structures shown in Fig. 30, filopodia are the pioneering parts to explore the environment and decide the direction of locomotion (Mattila & Lappalainen, 2008).

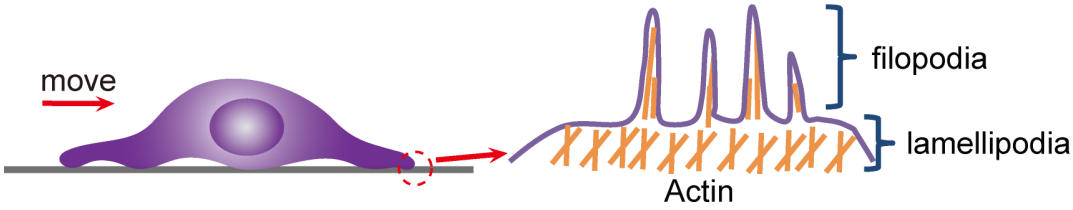

Fig. 30: Schematic structure of filopodia and lamellipodia.

Lamellipodia contain quasi-two-dimensional actin projections and have been reported to contain all machinery necessary for cell motility. Although they are lack microtubules within cell membrane, lamellipodia are capable to migrate normally (Alberts et al., 2007). Filopodia enclose cell adhesion molecules such as integrins and cadherin (Galbraith et al., 2006; Partridge & Marcantonio, 2006), which exist in many cells. Microspikes usually describe very short filopodia almost fully embedded to the front edge of cell contour (Svitkina et al., 2003; Mattila & Lappalainen, 2008). Besides of mediating cell migration inside the lamellipodia, microspikes also play important roles, e.g. in neuron growth (Azari et al., 2011) and in cell-cell interactions (Millard & Martin, 2008). Lamellipodia and filapodia are reported as sensors for optimized path finding during the intraluminal crawling (Song et al., 2014).

The intention of investigating adhesion area and microspikes was to confirm whether TNF affects the cell adhesion machinery and the true cell adhesion area, which is supposed to cause changes of cell adhesion area and/or the length of subcellular structures like protrusions.

As surface controls, we measured the adhesion of the Jurkat E6-1 cells on normal glass and PLL-g-PEG (Poly-L-lysine-graft-poly-ethylene-glycol) coated glass. The PLL-g-PEG is known to repel protein absorption of the cell membrane. It is observed that on normal not functionalized glass, cells just physically precipitated, as shown in a small unclear dark area under RICM (Fig. 31a). Neither "cell adhesion area" nor microspikes can be observed. For the PLL-g-PEG sample, cells were just hovering over the PLL-g-PEG coated glass, searching for the possibilities to bind. The cell is only a blurry bright shadow which indicates that it is far away from the surface (Fig. 31b). In contrast, on FN-coated glass surface, different cellular features can be detected at the border of cells (Fig. 31c). Filopodia are longer than microspikes (longer and shorter white line shown in Fig. 31d, respectively), radially shaped lamellipodia (Fig. 31e) and further elongated filopodia (Fig. 31f).

A real time camera was used to track the fluctuation of the Jurkat E6-1 cell adhesion area on a

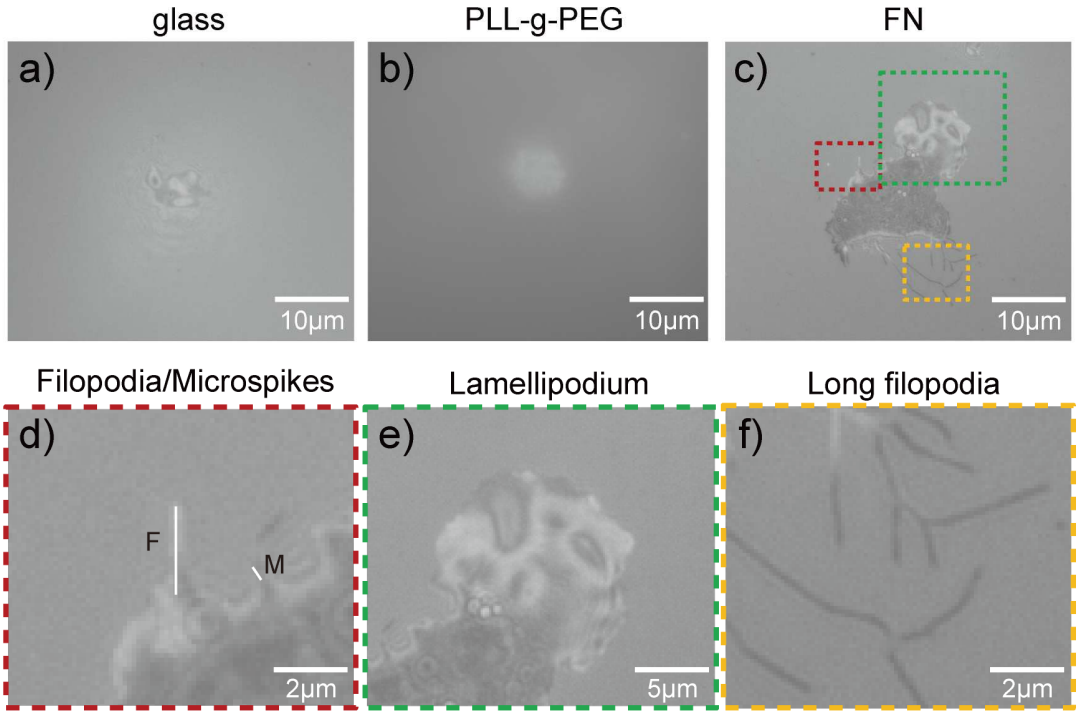

Fig. 31: Morphology of Jurkat E6-1 cells on different surfaces (a-c) and enlarged images parts in RICM (d-f). (a-c) Cell adhesion morphologies on different surfaces (left to right): clean glass (a), and PLL-g-PEG-coated glass (b) and FN-coated glass (c). (d-f) Different subcellular structures of the adhesion cell on FN-coated glass in RICM: the filopodium (F) is much longer than the microspike (M) (white lines were drawn along the projected direction) (d), lamellipodium (e) and long filopodia (f). The images are enlarged parts from Fig. 31c.

FN-coated glass surface with RICM. Fig. 32 shows the development of the adhesion area (i.e., at different time points). At the very initial stage, the cell found a "desirable" spot and prepared to "land". Afterwards, the cell attached to the surface and within a couple of seconds, it spread to make a tiny area, and extended preliminary protrusions into the environment. After some time, the expansion of cell adhesion area and protrusions seemed to be stopped, which is probably coming from the retrograde flow, where the actin polymerization at the fast growing end (barbed end) is much faster than the speed of cell protrusions, and this leads the flow back of the actin filaments to the center (Mattila & Lappalainen, 2008). It has been reported that microspikes and filopodia in the initial development phase can only last for less than 1 min. But when they transited into the status of retraction fibers, the sustaining time can be more than 2 min (Svitkina et al., 2003).

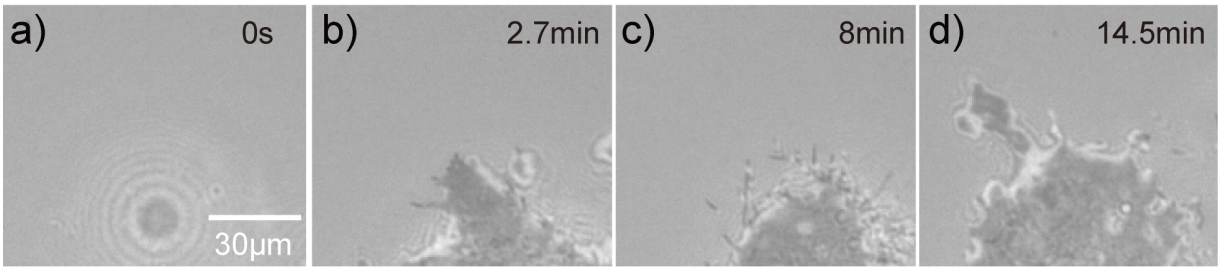

Fig. 32: Fluctuation of Jurkat E6-1 cell adhesion area under RICM. (a) Initial attaching (t=0 s). (b) Filopodia were formed (t=2.7 min). (c) Lots of elongated filopodia were observed (t=8 min). (d) The cell adhesion area was expanded continuously (t=14.5 min). Scale bar is 30 µm for all images.

In this study, it is found that most of the cells are able to reach a stable adhesion area size after 20 min adhesion on the surface, which was also the time scale all images were saved in RICM for analysis. Adhesion area was segmented manually. Microspikes were measured following finger or line-shape like protrusions out of the cell border. Afterwards, we plotted all data and defined the filopodia and microspikes in accordance with previous definition: those with a length smaller than 10 µm we call microspikes and those higher than this value are filopodia with significant projections (Selhuber-Unkel, 2006).

Fig. 33 shows that the distribution of cell adhesion area is in the range of 38 μm^2 to 337 μm^2, and that the majority length of protrusions falls in the range below 10 µm, which are considered as microspikes playing the main role in the adhesion dynamics within measured time.

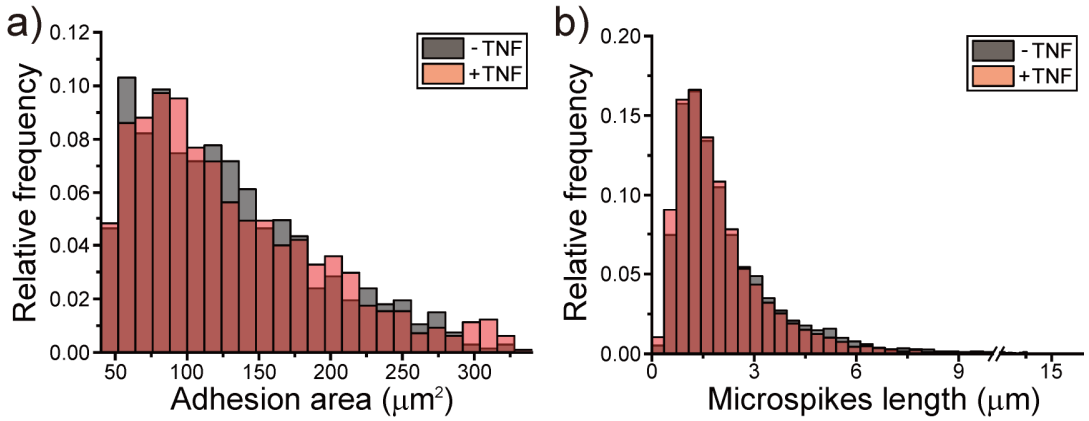

Fig. 33: Comparison of relative frequency of Jurkat E6-1 cell adhesion area (a) and microspike length (b) for TNF untreated (-TNF, black) and TNF treated (+TNF, red) cells in RICM. The columns in -/+TNF represent bins of same size are in the same size of bins, and columns are merged with a colour transparency of 50%.

Clearly, there is no significant difference in the adhesion area and microspikes length of cells treated with TNF or not. Relative frequency represents the probability distribution of the measured parameter, which does not rely on the total number of the data. There were 7-10 cells and 50 microspikes per image and about 20 images analyzed for cells treated with TNF or not experiment situation. This experiment was repeated four times in duplicate.

2.1.1.3 Discussion

In this part of the experiments, cells were visualized using phase contrast microscopy and size of cells adhering on PCS was analyzed with surface contrast microscopy, the latter of which served as a better substitute surface to exclude halo artifacts, but the result was not reproducible. In RICM, we successfully imaged and tracked the fluctuations of the true cell adhesion area and the protrusions projected from the cell membrane. In our experiment, the most adhesion areas of Jurkat E6-1 cell were above 50 μm^2 within 20min. This is in agreement with a previous study, where Jurkat E6-1 cell adhesion area reached about 52 μm^2 within a similar same adhesion time scale, and increased to a stable size after 40 min at about 65 μm^2 (Zhu et al., 2007). My result is quite convincing, because comparing to their adhesion molecule (CD58) coated surface, the FN coated surface has a huge additional receptor binding sites for Jurkat E6-1 cells.

In previous studies, it has been reported that in response to TNF, the actin filament density can

be increased in epithelial cells (Koukouritaki et al., 1999). Furthermore, cytoskeleton in fibroblast cells can be reorganized (Puls et al., 1999) as well as in endothelial cells (Lee et al., 2011) and neutrophils (Lokuta & Huttenlocher, 2005), but there is not yet information about the direct relationship between TNF and the cell adhesion area. As well, my result came out that no difference between TNF untreated and treated cells was found for both cell adhesion area and length of microspikes.

The possible explanations could be that the dynamics of the proteins and kinetics inside the cell is very rapid. Even one can assume that TNF activation, serves as a chemical gradient flow, can modify the recognition of the ligand-receptors, changes conformation of the anchoring proteins, and/or changes cell rigidity on the level of the whole cellular architecture. This hypothesis can still not necessarily reflect into expanded adhesion area, especially the cell starts to migrate as soon as it is stabilized on the surface. Meanwhile, 20 min is reasonable to enable most of the cells (except about 10% of cells in apoptosis situation or already broken) adhering on the FN surface in a stable state. (2) It was observed in the video (Supplementary Video 1) that the filopodia were in the process of a balance “elongate-retract-reelongate” that the movement of the whole cell body was approaching to the sites with probable higher local density of FN in micro-scale or neighboring cells for the “cross-talk”. The polymerization and depolymerization of actin filaments is not easy to be measured by the bulk assay for cell dimension.

2.1.2 Expression of Integrins Measured with CLSM and FACS

Considering integrin as crucial adhesion structure and force transmitter, I checked the expression of alpha integrins in our cell line for confirmation, although the subunit combinations in T cells have been reported (see 1.2). In this experiment, both CLSM and FACS were applied as two complimentary techniques. The glass surface was coated with PLL, which was washed extensively prior to cells seeding. This thin layer of PLL provided an adhesive layer since Jurkat E6-1 cells are suspension in native state. We did not use FN-coated surfaces, even the extensive wash with PBS still cannot avoid the small fragment of FN sticking on the surface. After fixation, these remaining fragments would form into crystal-like structures, which would introduce high amounts of staining artifacts and could ruin the fluorescence imaging.

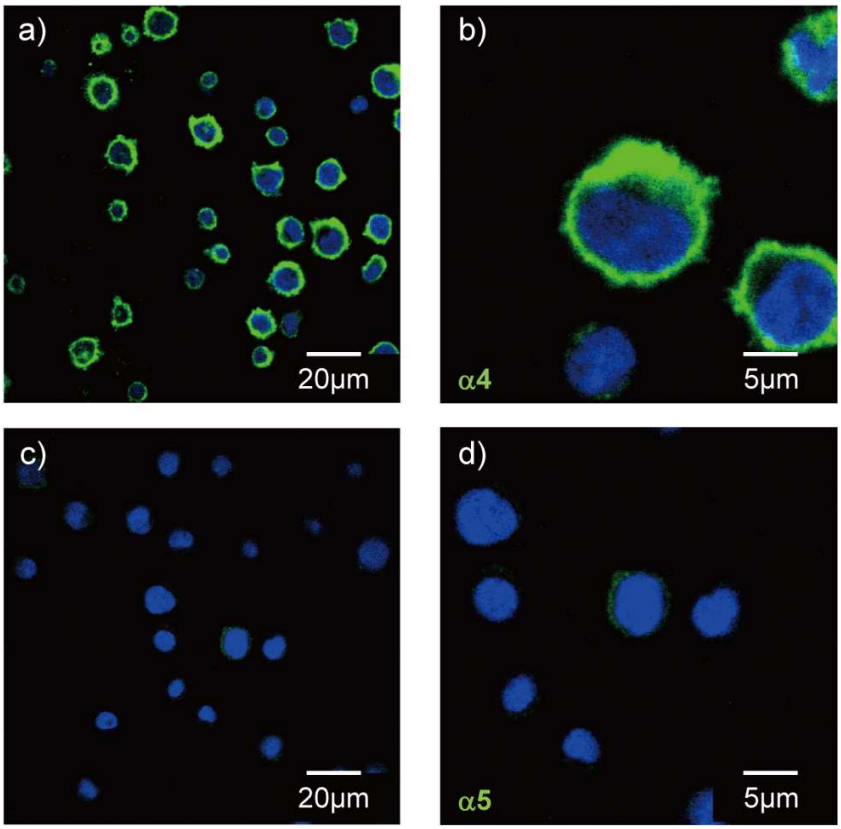

Fig. 34: Integrin expression in Jurkat E6-1 cells checked with CLSM. Expression of α_4 in (a) & (b) and expression of α_5 in (c) & (d) were checked on individual samples. Nuclei were stained with DAPI (in blue). Integrins (in green) were stained by mouse primary antibody and goat anti-mouse secondary antibody conjugated with FITC.

Fig. 34 shows the expression of α_4 and α_5 with immunofluorescence staining method, and nuclei in Jurkat E6-1 cells were stained by DAPI. The expression of both α_4 and α_5 were observed. These two integrin subunits are located close to the cell membrane but expression levels of them differed to a great extent. On the surface, most of the cells express high level of α_4 apart from those are very small and look like undergoing apoptosis. In some cases, a thicker ring of cells is observed with small spikes protruding from the cell membrane (Fig. 34b). These might be integrin clusters containing individual integrin heterodimers. For a convincing imaging, two controls are required for equilibrating the background fluorescence signals: one is the unstained sample and the other one is only fluorophore-conjugated sample (in this staining only secondary antibody is linked with fluorophore rather than primary antibody).

As another method, FACS was applied for quantitatively check for integrin expression levels. Fig. 35 shows the results of untreated unstained cells as negative control and cells only stained with secondary antibody as positive control for equilibrating the fluorescence signal. The "untreated unstained" means native cells, where no staining were applied. The geometric mean is expected to be more accurate in signals than mean in such a log-normal fit distribution. The fluorescence signal for geometric mean in the negative control is 2.12 and that in the positive

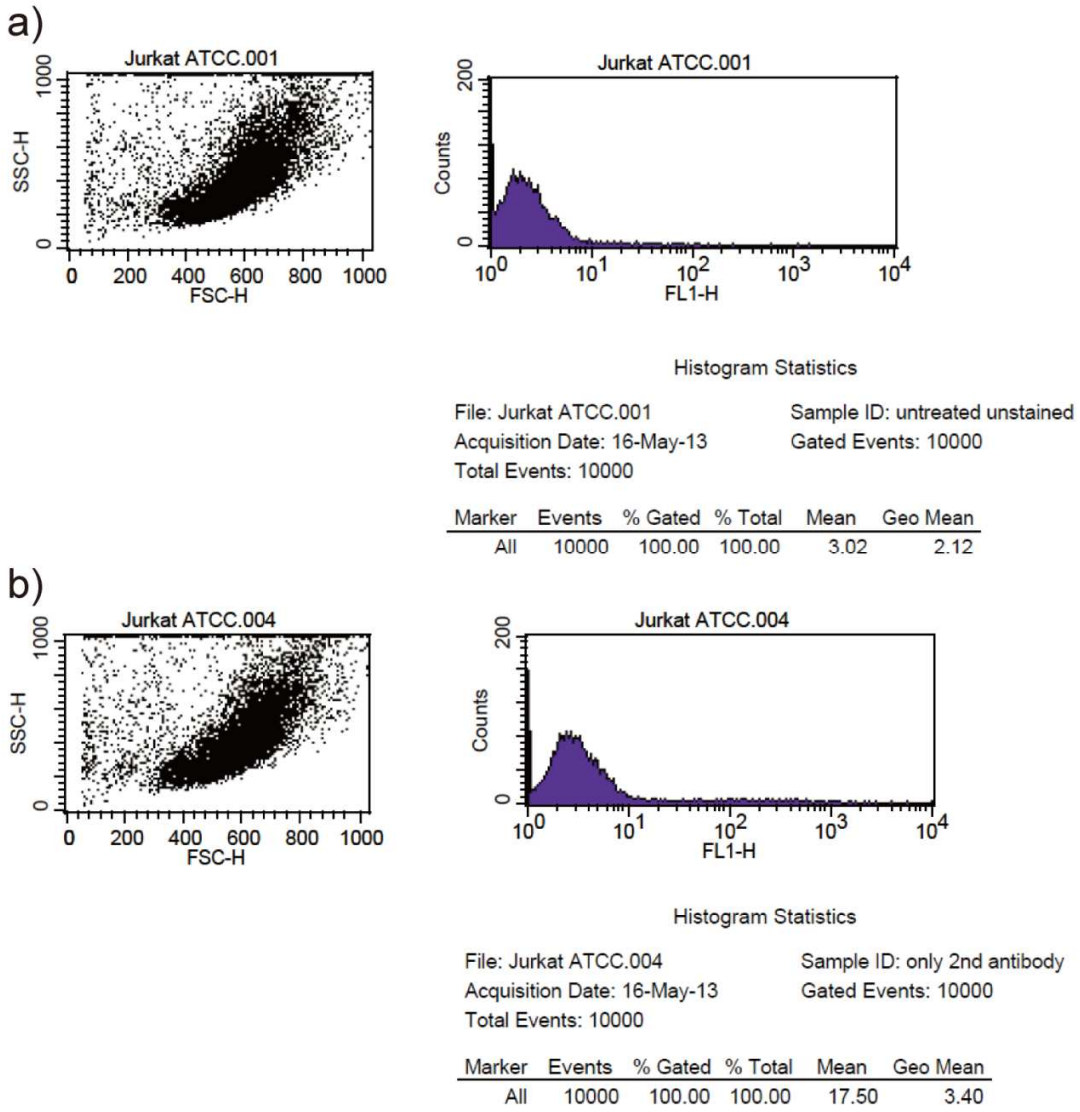

Fig. 35: Equalibration of fluorescence signals with untreated unstained Jurkat E6-1 cells (a) and only secondary antibody stained cells (b). SSC-H: Side scatter pulse height is a measurement for the complexity of the particles inside cells. FSC-H: Forward scatter pulse height, presenting the volume of the particles. FL1-H shows the fluoresence intensity.

control is 3.4, which is consistent with this cell line (Fig. 35). Fig. 36 shows the result of alpha integrins expression with FACS. Again, we found that the signal for α_4 is higher than α_5. In detail, the fluorescence signal of α_4 is about 500 and that it is around 50 for α_5. This 10 times difference of intensity is consistent with what we observe in fluorescence images. In this FACS experiment, we detected the expression of both α_4 and α_5 and the difference of the fluorescence intensity indicates their distinct expression level. Therefore, for integrin expression check, both immunostaining and FACS methods present the expression of α_4 and α_5 and especially, the expression level of α_4 is much higher than that of α_5 in our cell line.

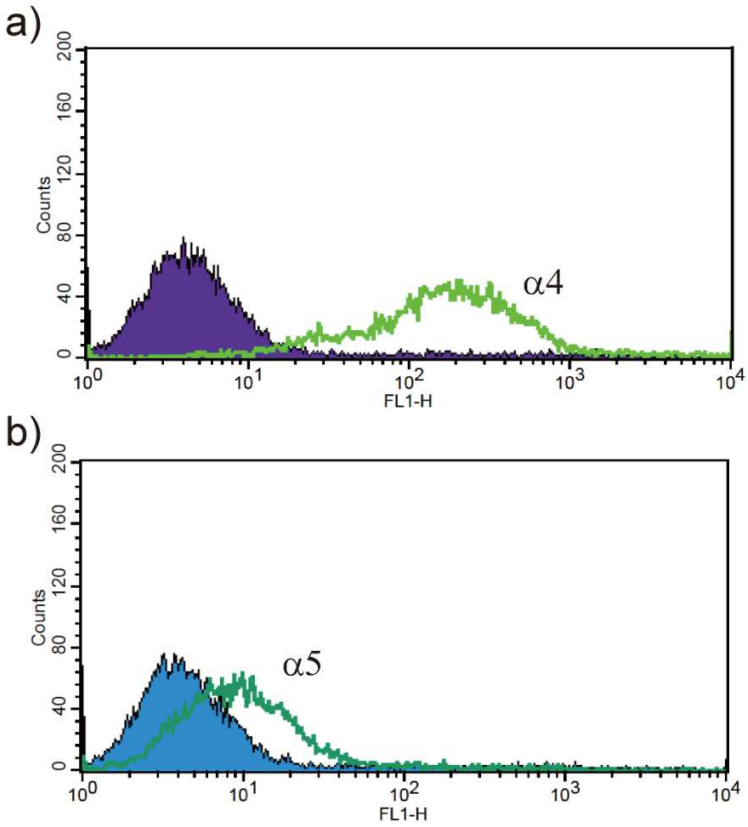

Fig. 36: Fluorescence signals for α_4 (a) and α_5 (b) in Jurkat E6-1 cells examined by FACS. In (a), the purple peak shows the signal for only secondary antibody stained cells (positive control) and bright green line shows the signal of α_4. In (b), the blue peak shows the positive control in this group and grass green line shows the signal of α_5. These two secondary antibodies are comparable with those for sample staining antibodies.

2.1.3 Quantification of Jurkat Cell Adhesion

2.1.3.1 AFM Studies

In order to measure if TNF stimulation affects the cell adhesion strength at the cellular and sub-cellular level, I approached Jurkat E6-1 cells to the FN-coated glass surface with defined contact time in a serum-free medium at 37 ˚C with AFM-based single-cell force spectroscopy (SCFC). These measurements were carried out for very initial contact times (no longer than 10 sec cell-surface contact time), in order to mimic the very rapid attachment of leukocytes *in vivo*.

2.1.3.1.1 Interpretation of Representative Force-Distance Curves

A representative force-distance (F-D) curve for approaching and detaching a Jurkat cell from a fibronectin-coated surface is shown in Fig. 37a. The cell-surface contact time is 0 sec, which usually requires a bit long time (i.e., about 0.2 sec) to reach the maximum contact force. From the approach curve, the cell deformation properties can be measured. The elastic modulus of Jurkat cells is 0.51±0.06 kPa reported previously and the value of them is about 50% compared to normal lymphocytes (Cai et al., 2010). Here we did not measure it again.

We analyzed the retraction curve to understand how strong Jurkat E6-1 cells adhere on the Fn coated surface and the dissociation strength of cell anchoring molecules. We set the contact force at 500 pN for all experiment situations as a small force (less than 2 nN) allows the cell to establish contacts on the adhesive surface without applying too much pressure which might induce apoptosis. Since the cell can be treated as viscoelastic body. The deformation of the cell can be considered as the viscoelastic relaxation with the increasing approaching force. Following the preset contact force, the relaxation of the cell reduces the actual force exerted on the cell by 30-90% in the first several seconds contact time (Franz & Taubenberger, 2012) and drags the cantilever towards the surface as presenting in the curve in Fig. 37a. It thus leads an absolute decrease of the force till the maximum negative value. This value is also called as cell detachment force, which initiates cell detachment and is associated with successive single rupture events. The grey area between the baseline and the retraction curve is detachment energy. Noteworthy, this parameter reflects the sum of the energy dissipated during the detachment process and the viscoelastic compliance of the cell.

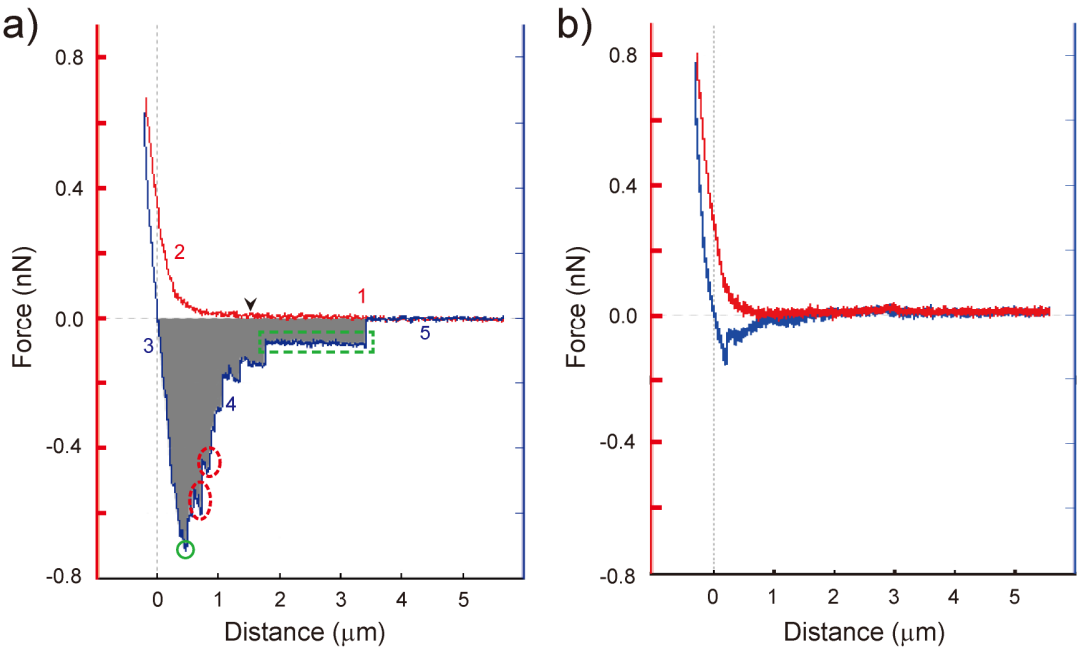

Fig. 37: (a) A representative F-D curve of a single Jurkat E6-1 cell approached to the FN-coated surface and detach again. (b) An F-D curve obtained when approaching and detaching a single cell from an uncoated Petri dish, clearly showing non-specific background adhesion. For both curves, the red curve shows the approach phase. The blue curve shows the retraction phase.

In Fig. 37a, at the minimum contact time of 0.2 sec, the maximum adhesion force already reached up to about 0.7 nN, which indicates a strong interaction between Jurkat E6-1 cells and FN coated surface. This result is in full agreement with the extremely short reaction time of immune cells that is required for making contacts inside the blood vessels under flow. Maximum adhesion force in the curve is negative, which shows the direction of the cantilever deflection. In contrast, as the control surface, maximum adhesion force is very small for cell binding to a non-coated Petri dish and also no single rupture events are observed (Fig. 37b).

Fig. 38 shows in detail the different phases of an F-D curve and the processes happening at the cell. The dynamic deformation of a cell and the ruptures of molecules are corresponding to Fig. 37. There were 11-15 individual cells and about 250 curves analyzed for each experiment situation, I tried 0, 5, and 10 sec cell-surface contact time and cells without and with TNF treatment were compared. Each cell represents an independent experiment, that is to say, for example, cells without TNF treatment at 0, 5 and 10 sec were not identical. Furthermore, if the same cells were used at these three contact times, the duration for measurement would be too long for single cells to survive force experiments without damage. Meanwhile, it should be more

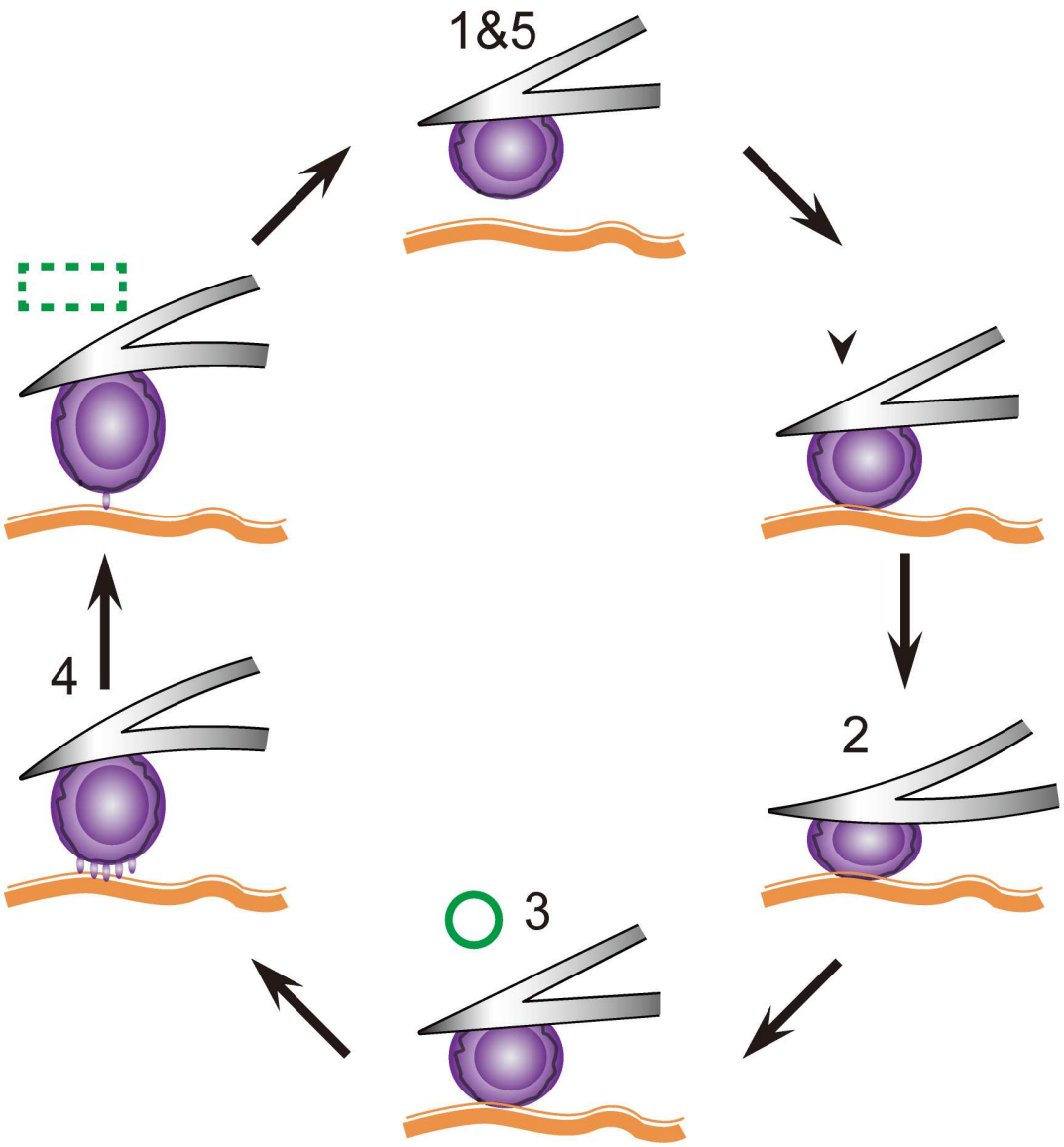

Fig. 38: Dynamics of a single cell during the F-D curve. The numbers or symbols above the cantilever are consistent with Fig. 37a. (1) The cell is still far away from the surface, no deflection of the cantilever exists. The very initial cell-surface contact is labeled with an arrow (black); (2) the cell undergoes deformation until the force reaches the preset maximum value of contact force (in this experiment 500 pN); (3) the cell is pulled up until the maximum adhesion force (i.e. the force applied by the cantilever to initiate cell detachment) is reached (green circle); (4) afterwards, successive ruptures follow; and the last tether-connected rupture is shown (dashed green box); (5) finally, the cantilever deformation returns to the baseline.

convincing in the experiment to first measure a single cell at untreated condition for about 15 curves and then after incubating this cell for 25 min with TNF in the Petri dish heater (the container for the F-D measurement, details in 6.8.3), it is measured again at the post-treatment condition. The strategy was tried but failed in the practical work, an obvious “tardy” reaction was

observed from the F-D curve.

The loading rate (also called slope prior to the rupture) is defined as the relation between force and time for the coming single rupture: $r = dF/dt$. This parameter is very important for the force measurement because it can explain the cytoskeleton/membrane anchorage. In the curves, both so-called jump (J) events (Fig. 37a. red dashed circle) and tether (T) events (Fig. 37a, green box) are found in the force curves of my experiments. A zoomed in explanation is shown in Fig. 39. In J events, a significant negative loading rate is observed, indicating an involvement of cytoskeletal fibers in the intracellular binding of the adhesion molecules.

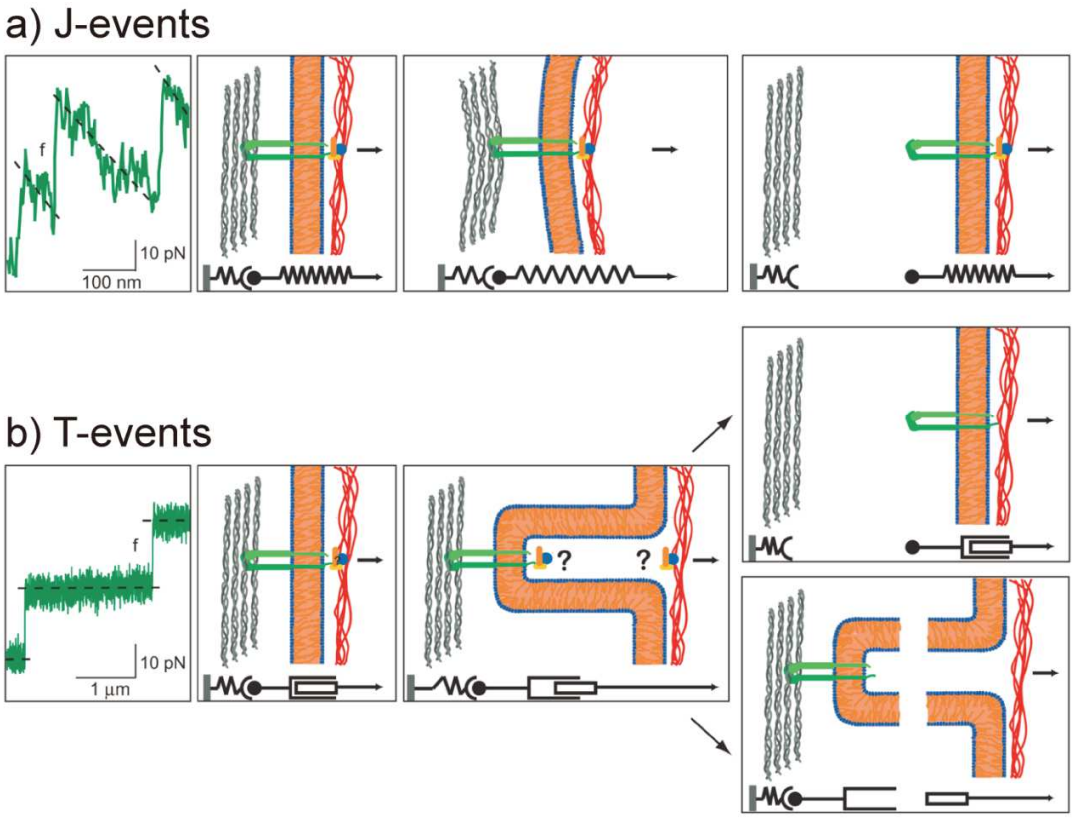

Fig. 39: J events and T events in the retraction curve (Taubenberger, 2009). The loading rate was fitted to the length of the tether in dashed black. In J events, the rupture is connected with cytoskeleton. In a T event, two assumptions of the tether rupture were brought up.

In T events, the loading rate is close to zero and tethers up to several µm in length are pulled out from the cell membrane, so that probably no cytoskeletal anchorage is involved. For T events, there are two possible explanations: The first is that the tube-like structure is intact after bond

rupture. In the second model, the membrane tube structure was damaged itself. Till now, there is no information indicating that tethers themselves are damaged. Curves with at least two ruptures in the retraction curve were analyzed, and they amounted to more than 90% of the whole curves.

In all AFM experiments, the “closed-loop” mode was chosen in the feedback system, which can adjust the piezo extension with the measured height and also avoid the possible force increase at the contact position. In addition, we applied “contact height” in the delay mode, where the height of the cantilever was maintained during the whole contact time and was not affected by the deflection, e.g. the thermal drift. Another delay mode would be “contact force”, where the force exerted on the cell was stable.

The measurement was carried out in the medium, which has properties such as viscous, leading to a hydrodynamic drag force exerting on the cantilever in the opposite direction with the movement of the cantilever. The relationship between hydrodynamic drag force and speed of the cantilever movement is fairly linear (Fig. 40), as a high speed can introduce a very high hydrodynamic drag force, which can even reach up to the single molecule rupture force. In this study, the speed was set to 3µm/s. For such a small velocity, the hydrodynamic drag should be negligible (Fig. 40).

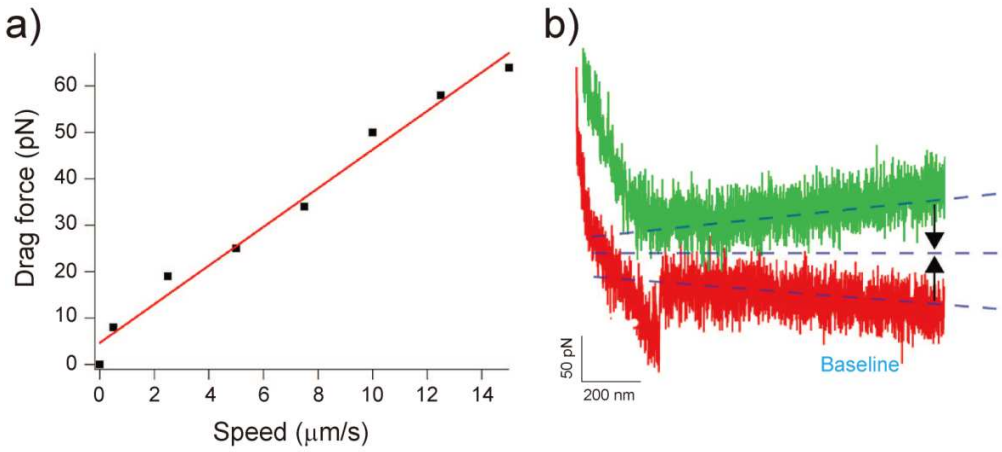

Fig. 40: Hydrodynamic drag force versus pulling speed. (a) The relationship between hydrodynamic drag force and the pulling speed. (b) The dynamic drag force makes the difference of the baseline between the approach (green) and retraction curves (red) (Franz et al., 2007).

2.1.3.1.2 TNF and Contact Time Increased Detachment Forces and Detachment Energy

To study the cell adhesion strength, I successfully measured cell detachment force and detachment energy within great ranges at different cell-surface contact times. In detail, the cell detachment force ranges from about 200 pN to 2 nN and the detachment energy ranges from about 2×10^{-16} J to as much as 85×10^{-16} J (Fig. 41). 10 sec is the maximum time length because cells were very easily got lost from the top of the cantilever after long time contacted with FN coated surface. In addition, the measured highest force in all even reaches up to 2 nN (Fig. 42a), which is close to the binding force between cell and concanavalinA for cantilever functionalization (Zhang et al., 2006).

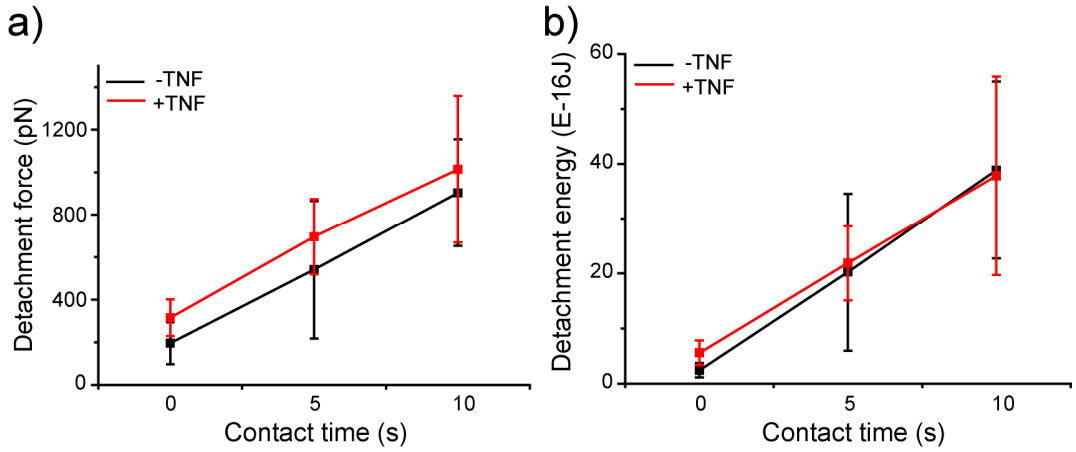

Fig. 41: Comparison of cell detachment force (a) and detachment energy (b) of the Jurkat E6-1 cells detached from FN coated surface after different contact times. Untreated (-TNF, black) and TNF-treated (+TNF, red) Jurkat E6-1 cells. Square shows the average value of the cells in each experiment situation, error bars represent standard deviations.

The average value of maximum adhesion force roughly increases in a linear and rapid mode with contact time (Fig. 41a): from 0 sec to 5 sec and to 10 sec, about 1.5 fold and 3 fold increases (average value) are observed for TNF untreated cells. A greater raise is present in detachment energy, where the increase of the average value is about 8 fold and 18 fold for TNF untreated cells (Fig. 41b). For TNF-treated cells, the increases for both cell detachment force and detachment energy follow a similar trend as for cells not treated with TNF. After TNF stimulation, the maximum adhesion force compared to TNF untreated cells is dramatically increased at cell-surface contact times of 0, 5 and 10 sec for evaluating the mean value for each experiment situation (Fig. 42a). Similarly, this reinforcement is also found in the cell detachment

energy (Fig. 42b). In both parameters, the significance level is smaller than 0.001 with Mann-Whitney *U* test. This test is used for evaluate the significance of the data which do not present a normalized distribution. Especially, with shortest cell-surface contact time of 0 sec, the TNF-induced enhancement of adhesion forces and detachment energies shows the strongest effect. In detail, the mean value of maximum adhesion force increases by 60.8% (manual calculation) in TNF treated cells for 0 sec cell-surface contact time, whereas the reinforcement is much less pronounced at 10 sec cell-surface contact time, only 12.2% increase is found. Meanwhile, for the cell detachment energies at 0 sec, the increase is 130.4%, but again not very strong for 10 sec contact time. These results clearly show that TNF enhances T-lymphocyte adhesion strength to fibronectin layers. Since in such a short experiment time frame (maximum total time including

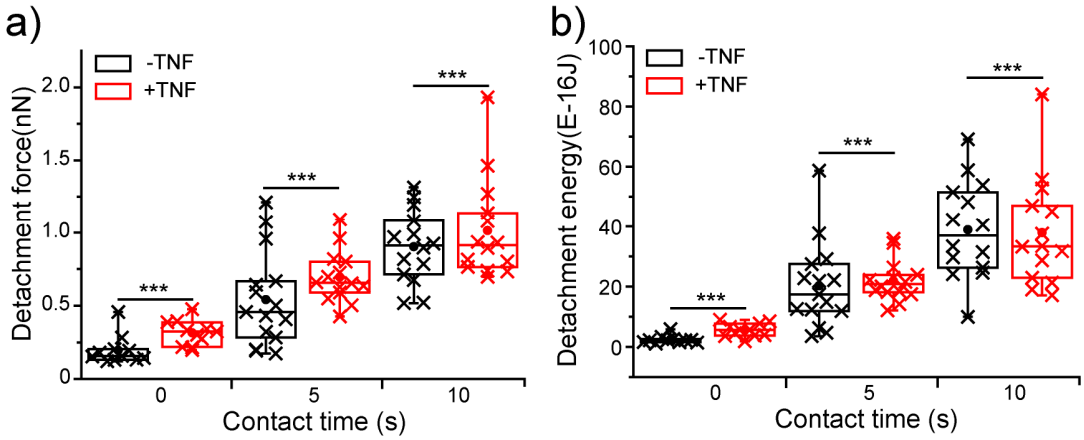

Fig. 42: Influence of TNF on cell mechanics of the Jurkat E6-1 cells detached from FN coated surface after different contact times. Untreated (-TNF, black) and TNF-treated (+TNF, red) cells. Each cross shows the average value of a single cell. Line among the crosses shows the median value. (a) Determination of the maximum adhesion force. (b) Measurement of detachment energy. Statistical significance was tested by a Mann-Whitney *U* test. * $p<0.05$, *** $p<0.001$.

the incubation and the measurement was 1h), there is no *de novo* protein synthesis, TNF should probably interplay in the inside-out signaling pathway and increase cell adhesion strength in a short cell-surface contact time.

2.1.3.1.3 TNF and Contact Time Increased the Number of Single Rupture Events in a Force Curve

To further investigate if the TNF-induced reinforcement of Jurkat adhesion observed in the cell

detachment forces can be explained by changes in molecular binding processes, a detailed analysis of cell detachment force-distance curves was carried. An increase in the number of bonds present in the end of the adhesion phase could be such a first parameter responsible for increased detachment forces. The number of successive single rupture events during the cell detachment process as a function of TNF stimulation was therefore analyzed.

Again, it is observed that the increase of ruptures number with the increasing of contact time, from 0 sec to 5 sec and to 10 sec. The rupture number increases in TNF untreated cells are about 60% and 230% when the contact time is increased from 0 sec to 5 sec and from 0 sec to10sec, respectively. As well, for TNF treated cells, 1 fold and 2 fold increases are observed at 5 sec and 10 sec comparing to the rupture number at 0 sec, respectively (Fig. 43a). The overall value of rupture number for TNF treated cells is higher than those of untreated ones.

To get the idea if the number of binding sites was one reason for the increasing adhesion strength by TNF, I analyzed the number of the rupture for all individual Jurkat E6-1 cells treated with TNF and untreated ones after contacting with FN-coated surface for certain contact times.

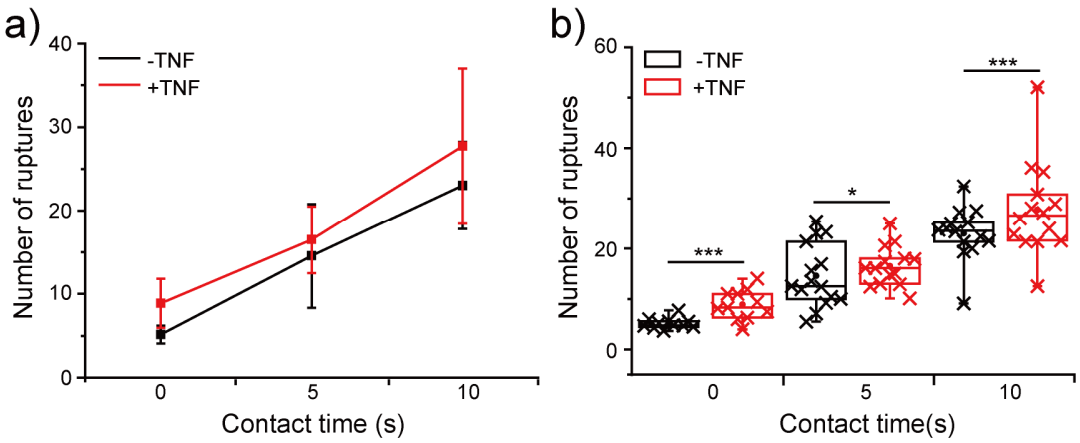

Fig. 43: Determination of the number of ruptures that Jurkat E6-1 cells detached from FN coated surface after different contact times. (a) An overview of the number of ruptures between -/+TNF cells (black and red respectively). (b) The distribution of individual cells. Each cross shows the average value of a single cell. Line among the crosses shows the median value. Significance was tested by student's t-test. * $p<0.05$, *** $p<0.001$.

Notably, for all three investigated contact times, TNF stimulation significantly increased the number of rupture events that cells needed to completely detach from the surface (Fig. 43b). The

significance is smaller than p is 0.001 as reveal by a student's t-test, which is normally used to evaluate the significance for normalized distributed data. This dramatic increase of number of ruptures (between -/+TNF) further confirmed our hypothesis that TNF should play as a positive role in the inside-out signaling pathway across the whole cell body.

2.1.3.1.4 TNF and Contact Time Increased All Rupture Forces

To investigate whether the increased binding force of single molecules contributed to the adhesion enhancement, forces associated with all single rupture events in the force curves were analyzed. Since the numbers of ruptures for each experiment situation were not the same, relative frequency was plotted for forces released after single rupture events for cells treated with and

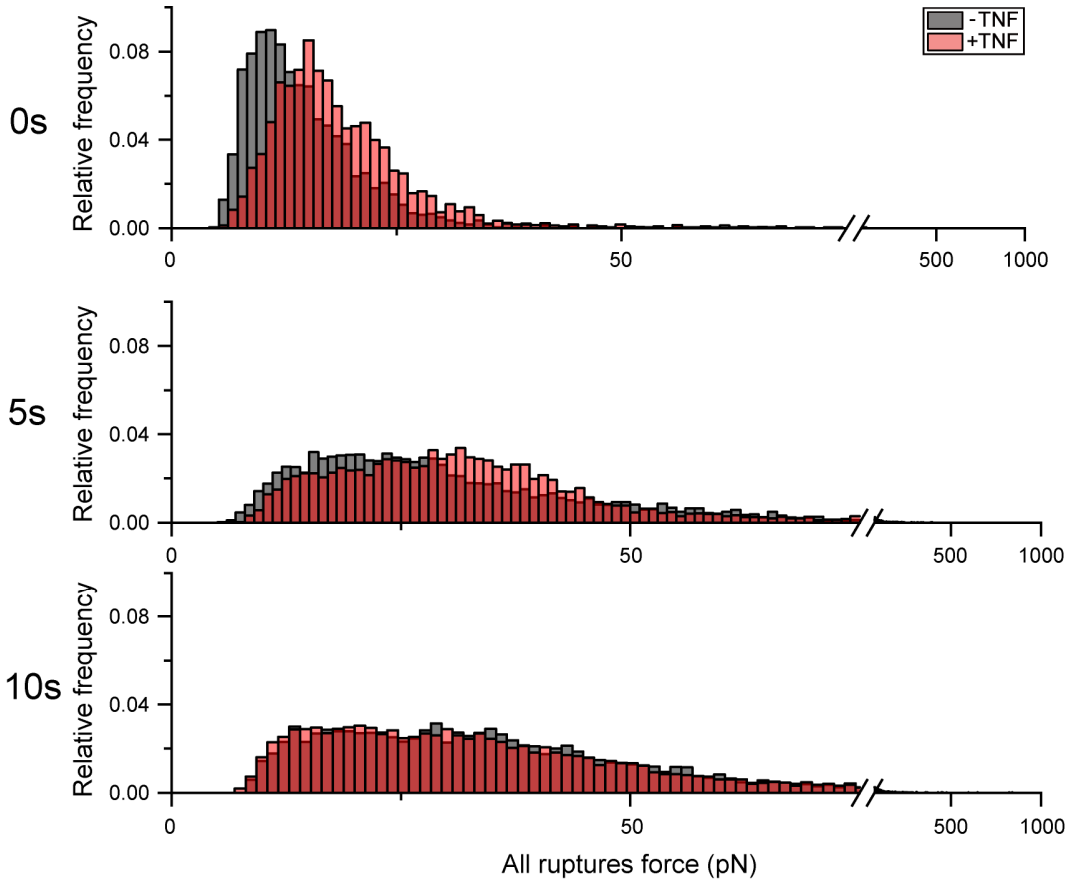

Fig. 44: Force associated with the last rupture event before complete cell detachment at cell-surface contact times 0, 5 and 10 sec. The columns in -/+TNF (black and red respectively) are in the same size of bins, the overlaid columns are merged with the colour transparency of 50%.

without TNF in Fig. 44. This relative frequency presents the distribution probability of the measured force. It is found that the distributions of forces are very broad for all three contact times, and notably, TNF stimulation clearly shifts the distribution of single molecule rupture forces towards higher force values (Fig. 44). In detail, at 0 sec cell-surface contact time, the force at the first main peak increases by 38% from 11.025 pN to 15.225 pN. Interestingly, TNF treated cells also have a tiny second peak at around 22.5 pN. Since single rupture events are often identified with the rupture of single molecules or tiny clusters (Müller & Engel, 2007), this second peak might be a hint for cluster dissociation, where several molecule bindings rupture simultaneously. At 5 sec cell-surface contact time, a slighter increase of 21.3% from 23.5 pN to 28.5 pN (the force at the highest relative frequency was compared) is observed. However, no impose from TNF stimulation is found at 10 sec cell-surface contact time. This can be concluded as with increasing cell-surface contact time, the reinforcement of single rupture forces, also here the effect from TNF decreases at 0 sec cell-surface contact time.

It is assumed that besides of strengthening adhesion on the level of the whole cell, TNF can influence the strength of cell adhesion molecules (i.e., integrins) by recruiting the bonds into clusters than single bonds. As the reinforcement of binding forces disappeared for 10 sec cell-surface contact time, it is supposed that the effect of TNF-modulated adhesion is in an extremely short-term mechanism.

When compare the effect coming from different contact time, it is find that for both TNF untreated cells and TNF treated cells, the prolonged contact time (from 0 sec to 5 sec) makes the value of all rupture forces doubled. However, when the contact time increases another 5 sec to 10 sec, no obvious increase of rupture forces can be detected.

To confirm that the analysis was not biased by systematic errors in cantilever calibration, a comparison of single rupture forces was carried out in each cell. The result is shown in Fig. 45. This is very important to acknowledge whether there occur systematic errors, e.g., due to cantilever calibration. Here, all data points for each individual cell with different colors were plotted. Convincingly, it is shown that the distributions of different cells were quite homogeneous.

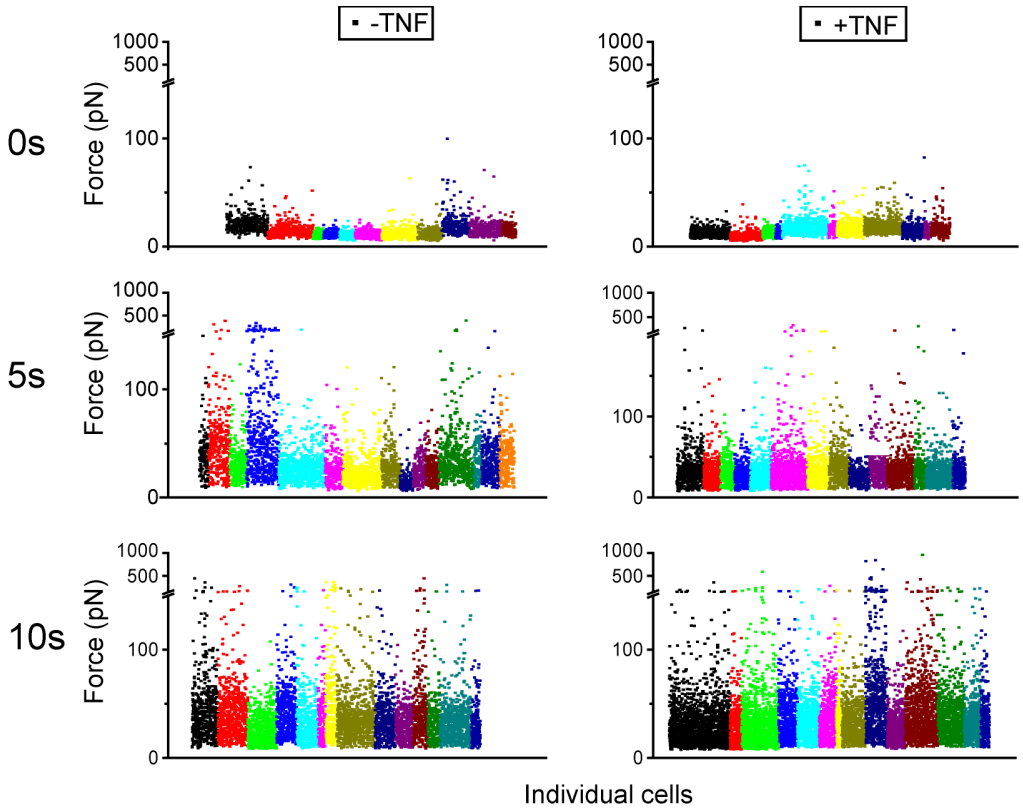

Fig. 45: Distribution of all rupture forces of individual cells. Cell-surface contact time: 0 sec (first row); 5 sec (second row); 10 sec (last row). Cells untreated with TNF (left column) and cells treated with TNF (right column). Each color represents data from a single cell. The same color data in these plots show distinct cells.

2.1.3.1.5 TNF and Contact Time Increased Last Rupture Forces

With AFM, it is not possible to determine the order in which molecules detach. Probably, those adhesion sites at the edge of a cell are first uncoupled, but as the force distributions in the cell-surface contact zone are very complex, it is also possible that the molecules just rupture in a very random way (Fig. 46) (Erdmann & Schwarz, 2006).

Therefore, the last rupture in a force curve is considered to be an important parameter to convey exactly the molecular rupture information and exclude a possible influence from other bonds. Hence, data were plotted in Fig. 47 to examine the forces associated with the last rupture events.

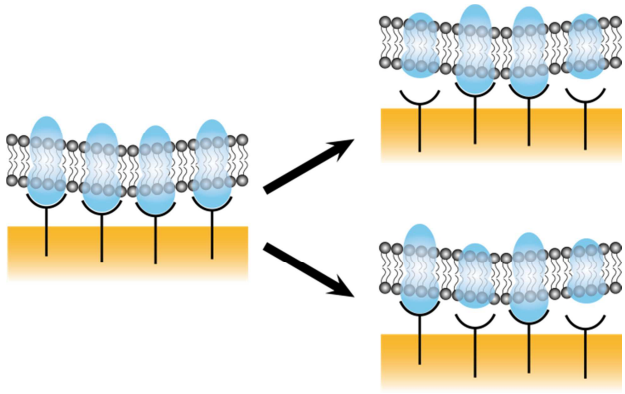

Fig. 46: Sketch of possible rupture orders for all molecules. The order of rupture of the binding between integrin (blue, translocate at phospholipid bilayer) and the surface molecules (black) on the surface (yellow) are still implicit.

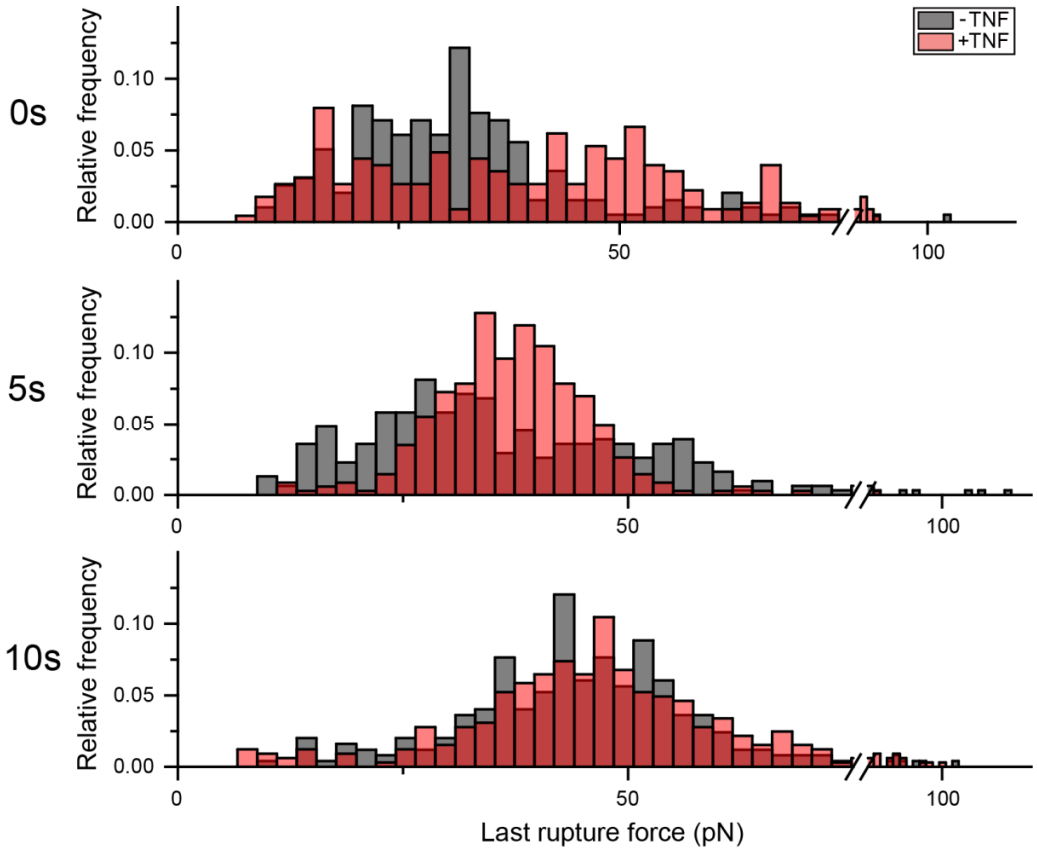

Fig. 47: Force associated with the last rupture event before complete cell detachment at cell-surface contact times 0, 5 and 10 sec. The columns in -/+TNF (black and red respectively) are in the same size of bins, the overlaid columns are merged with the colour transparency of 50%.

This effect is particularly evident at short cell-surface contact times of 0 and 5 sec. Consistent with the result shown in Fig. 44, it is also found that for these final rupture events, TNF shifts the probability distribution of forces towards higher values (Fig. 47) for 0 sec contact time. However, here it is not observed the increase of last rupture force in the first 5 sec prolonged time for TNF untreated cells, and it seems that for TNF treated cells, higher probability of forces appeared at around 35 pN compared to fairly homogeneously distributed force values at 0 sec. From 5 sec to 10 sec, increase of about 15 pN for last rupture forces was observed. Such phenomenon is convincing because in the all ruptures, one rupture is usually accompanied with the "healing" from other bindings and the force measured is smaller than the actual value (Benoit & Selhuber-unkel, 2011).

Again, to check if there is a change in calibration or AFM-associated parameters of the last rupture events, forces within a single cell were plotted (Fig. 48). No significant variation for this parameter was observed.

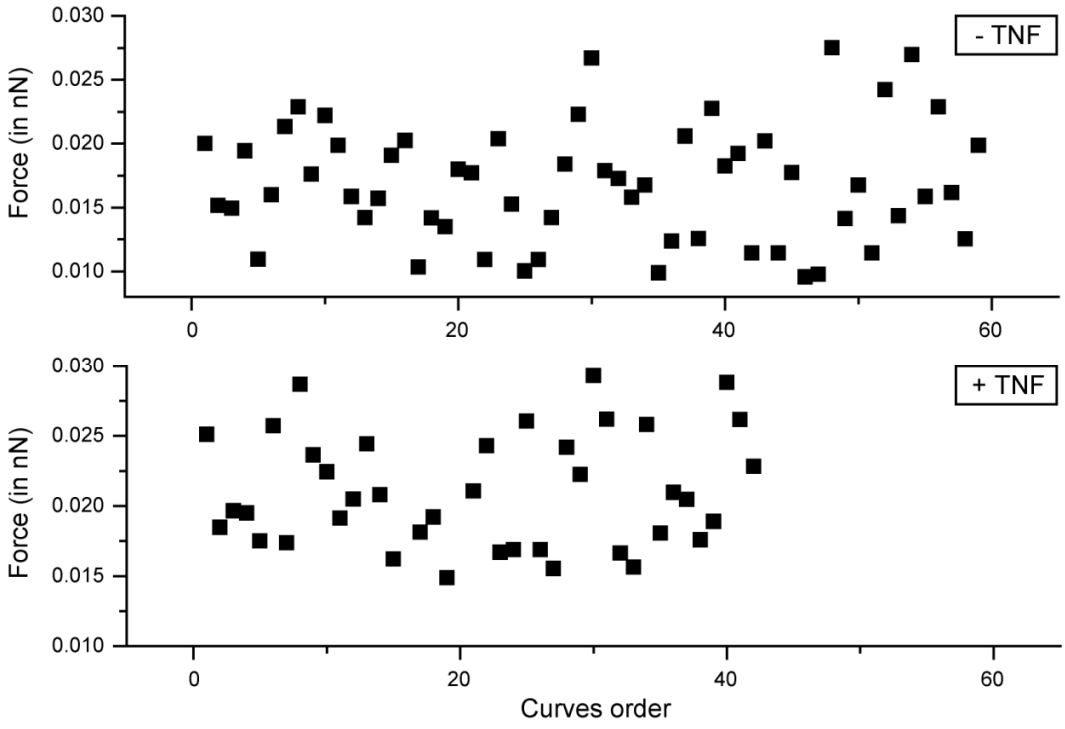

Fig. 48: Distribution of last rupture forces of two individual cells in without TNF treatment and with TNF treatment situation. Cell-surface contact time is 0 sec.

2.1.3.1.6 Cell-Surface Contact Time rather than TNF Increased the length of the Last Tether

Normally, prior to a sudden rupture, the bonds between the cell membrane and the surface undergo stretching by a force. To understand the length of last tether, this parameter was analyzed by manually determining the whole length of the tethers (ranges from 20 nm to several μm). The relative frequency of its distribution was plotted (Fig. 49). Since tether acts as force clamp, only length of last tether was carried out otherwise it is hard to know how many bonds are loaded.

It is found that at 0 sec contact time, although the maximum tether length is close to 7 μm, tethers longer than 3 μm become very rare. Meanwhile, at 5 sec and 10 sec contact time, tethers

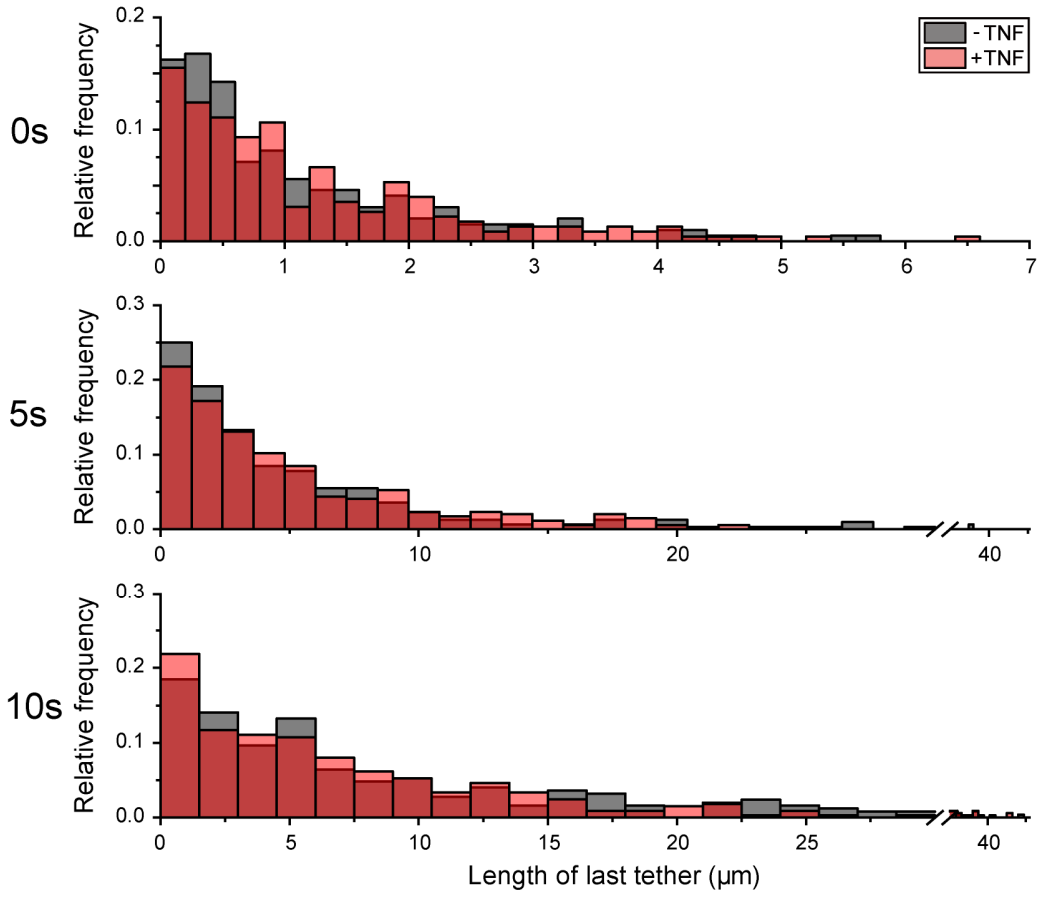

Fig. 49: Relative frequency of length of last tether. The columns in -/+TNF (black and red respectively) are in the same size of bins, the overlaid columns are merged with the colour transparency of 50%.

with tens of micrometers in length are observed, of which the longest ones can reach up to length of 50 µm. Compared to 5 sec, more long tethers (>10 µm) are present for 10 sec contact time. So it is very clear that with longer cell-surface contact time, longer tethers can be formed. This tether length is usually useful to evaluate the lifetime of the bonds, because the speed of the tether during the elongation is the same as the retraction speed set in our measurement (3 µm/s). Therefore, the lifetime t= tether length (µm)/ speed (3 µm/s). Therefore, it is also found that with increasing contact time, the lifetime of the bonds increased, which could be due to the binding between cell and the surface is tightened.

In response to TNF stimulation, no obvious significance of length of tether was found between TNF untreated and treated cells for all three contact times applied with both Mann-Whitney U

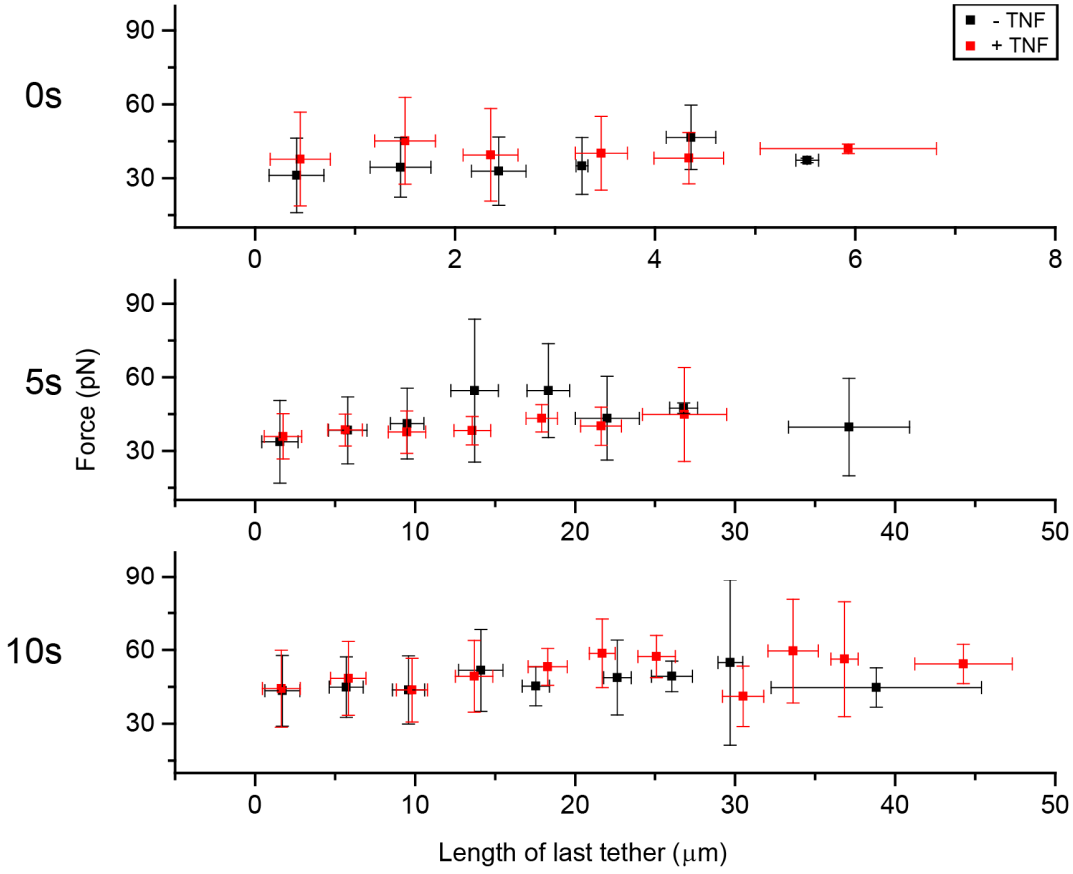

Fig. 50: Length of last tether versus last rupture force. Untreated cells (black) and treated with TNF cells (red). Data in 0s are plotted every 1µm and data in 5s and 10s are plotted every 4 µm, single data in the end are combined with the last range. Error bars present the standard deviation.

test and student's t-test. To understand the relationship between the length of the last tether and the last rupture force, the plot shown in Fig. 50 was made. Little difference was found after TNF stimulation.

2.1.3.1.7 Cell-Surface Contact Time rather than TNF Decreased the Absolute Value of Loading Rate of the Last Rupture

Through fitting the length of the last tethers, also the loading rate can be determined. Loading rate describes the mechanical coupling of a bond/cluster before its rupture, as it occurs during the elongation of the tether. Usually this value is an evaluation criterion to acknowledge whether there is cytoskeleton involved in the intracellular anchorage of the bond/cluster.

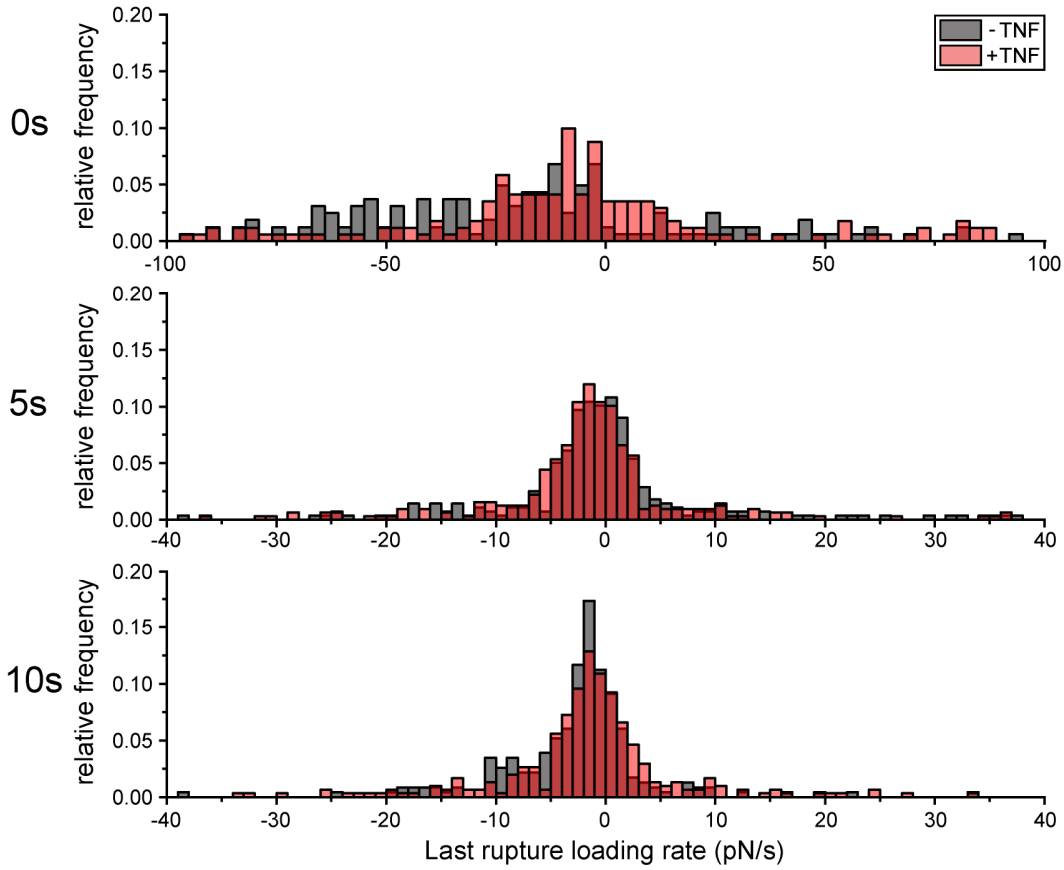

Fig. 51: Relative distribution of last rupture loading rate. The columns in -/+TNF (black and red respectively) are in the same size of bins, the overlaid columns are merged with the colour transparency of 50%.

Typical understanding about loading rate is that when cantilever retracts the cell up to release the last binding from the surface, although the whole body of the cell is deformed and complied with the cantilever, the binding itself should exert a repelling force or be kept in a stable force referring to the direction of the cantilever movement. This value of loading rate should be negative or very close to 0 in the origin value. Interestingly, in our study, both negative and positive values are found in all three contact times (Fig. 51), and the amount of the two groups is fairly similar. About 99% of the data fall in the range shown in x-axis (Fig. 51), and those varied

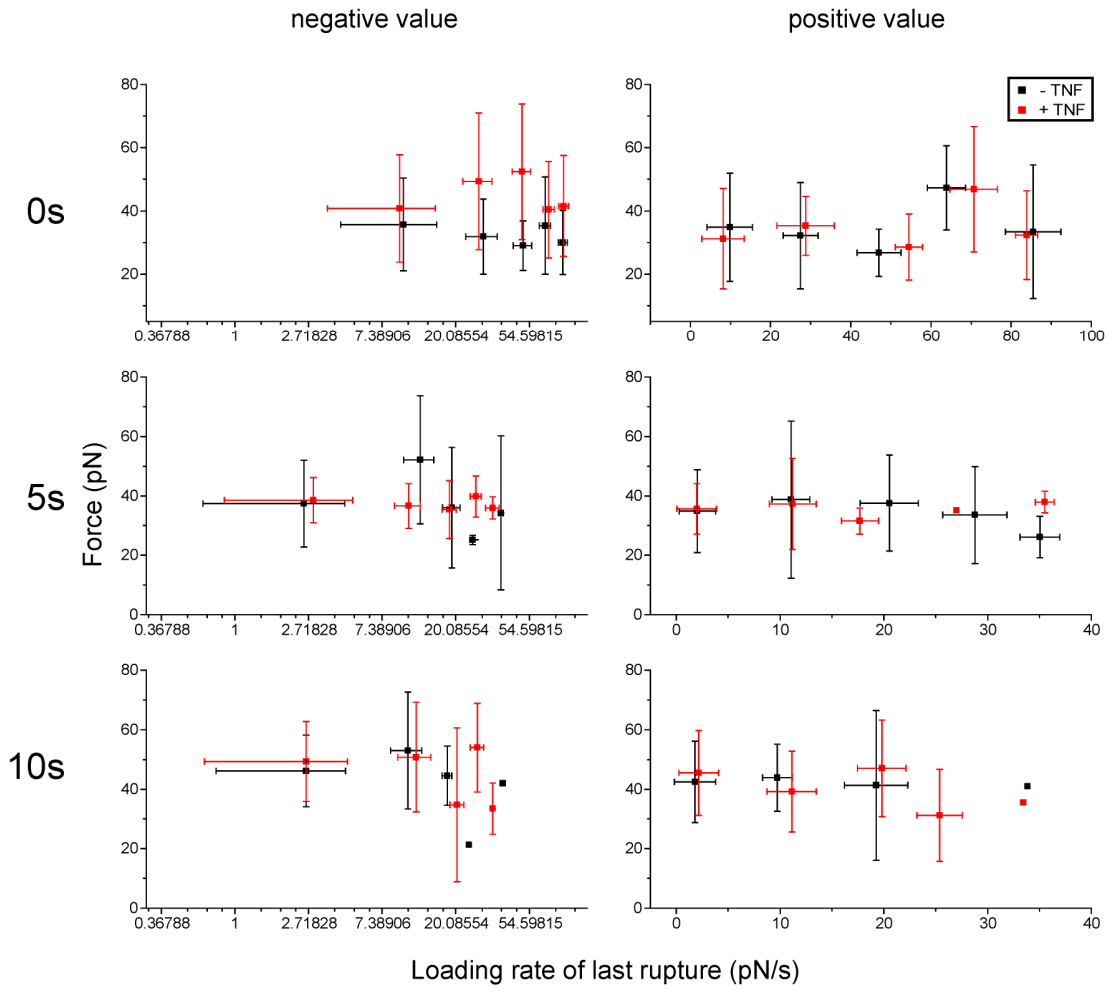

Fig. 52: Last rupture loading rate versus last rupture force. Untreated cells (black) and treated with TNF cells (red). Data in "negative value" column present the value which are negative from the result, and those in "positive value" column present the positive ones. Data in 0 s are plotted every 20 pN/s and data in 5 s and 10 s are plotted every 8 pN/s. The x axes in the "nagative value" column are in logrithmatic function of e (Ln). The x axes in the "positive value" column are in linear function. Error bars present the standard deviations.

too much (up to several hundreds of pN/s) were deleted from the dominant population. For 0 sec contact time, the distribution of the detect loading rate is very broad ranging from -100 pN/s to 100 pN/s, whereas those for the 5 sec and 10 sec contact time are mainly found within -40 pN/s to 40 pN/s. In detail, the highest peak for 0sec contact time is from -25 pN to 25 pN, and for 5 sec and 10 sec contact time, the peak correspondingly shrinks, presenting from -5 pN/s to 5 pN/s. It is assumed that the positive value might be that the binding site complies with the retraction of the cantilever or some phenomenon similar to retrograde flow of actin fibers at the binding site. Although no difference was found between TNF not treated cells and TNF treated cells, it is observed that with longer cell-surface contact time, the absolute value of loading rate decreased. To obtain detailed information of the distribution of the loading rate with rupture force, data in negative values and positive values are plotted in Fig. 52. In the negative value, the dissociation rate (k) of the receptor-ligand binding depends on the force (F) pulling them apart, which is described with Bell model (Bell, 1978) as

$$k = k_0 e^{-\frac{x_u F}{k_B T}} \tag{7}$$

where k_0 is the dissociation rate when no force is applied, x_u is the distance of the binding molecules is required to separated, $k_B T$ is the thermal energy. Based on Evans model (Evans & Ritchie, 1997), the most probable rupture force is derived as

$$F = F_B * \ln(\frac{r}{F_B k_0}) \tag{8}$$

where $F_B = {k_B T}/{x_u}$, r is the loading rate prior to the rupture. However, the slopes between the force and the loading rate for all experiment situations are close to 1, which is in Fig. 52 (negative value column). Therefore, the Bell-Evans model does not fit to my system. From the negative value, a possible boundary to define T and J events can be enacted in this measurement. Those higher than -30 pN/s are defined as the T events and smaller than -50 pN/s are defined as the J events. Since it is not easy to confine these two events from -50 pN/s to -30 pN/s in certainty. Therefore, if the positive values are put aside, it comes out that the percentages of T

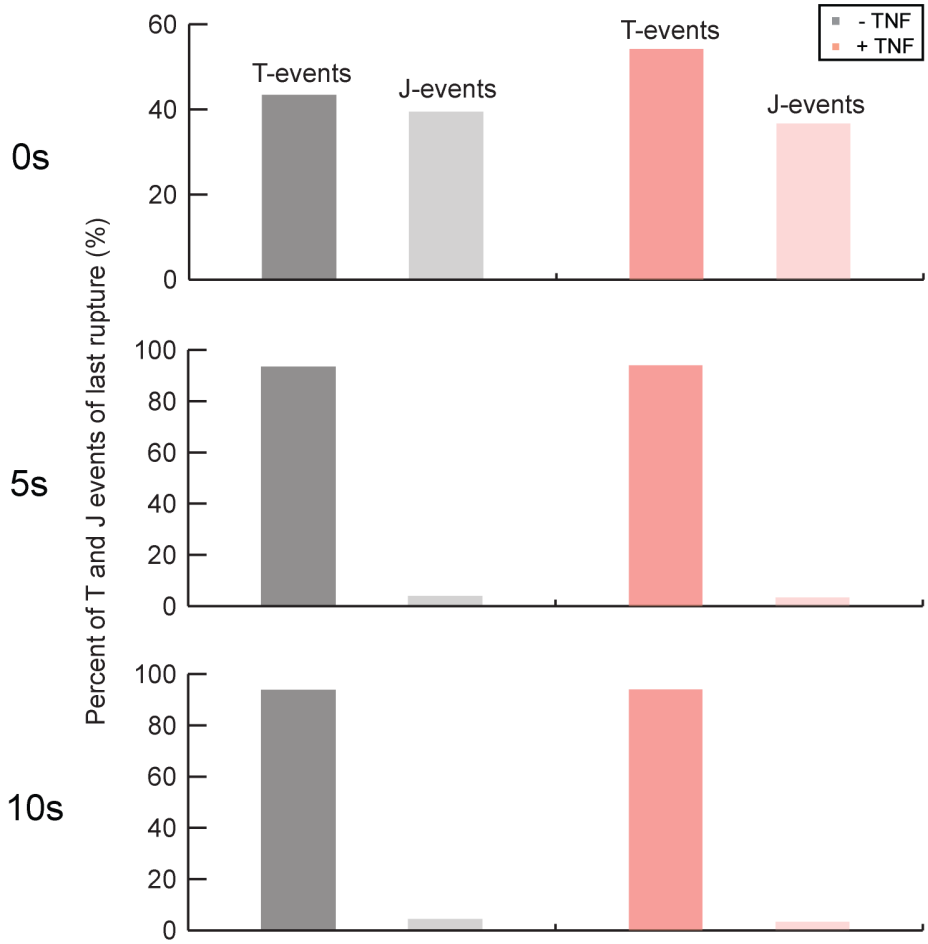

Fig. 53: Percent of T and J events of last rupture (%). Untreated cells (grey) and treated with TNF cells (reddish).

and J events (Fig. 53) for cells not treated with TNF present the similar value of 43.33% and 39.33% respectively at the cell-surface contact time of 0 sec. In response to TNF stimulation, T-events (54.17%) show a slight higher percent than J events (36.67%) at the shortest contact time. When the cell- surface contact time is increased to 5 sec and 10 sec, T events present the predominant events for the last tethers, about 95% compared to about 4% of J events. No difference of the percentages of these two events between TNF untreated cells and treated ones.

2.1.3.1.8 Cell-Surface Contact Time and TNF Increases the Viscosity of the Cell Body

The initial retraction force (the top force point at the retraction curve) demonstrates how the cell responds to the initial retract from the cantilever. This parameter is closely related to the

viscosity property of the cell. Viscosity defines the deformation of the cell membrane without extracting of the cell-surface bonds. Here, a plot of the initial retraction force and the detachment force is shown in Fig. 54 (negative value as the raw output from the software).

For 0 sec, all initial retract forces were above 200 pN, whereas for 5 sec and 10 sec, a large population of forces was below 200 pN. For 5 sec contact time, a small amount of data was even smaller than 0 pN. Negative values show that the direction of the force is opposite to the direction of retraction movement of cantilever, which can be considered as the membrane

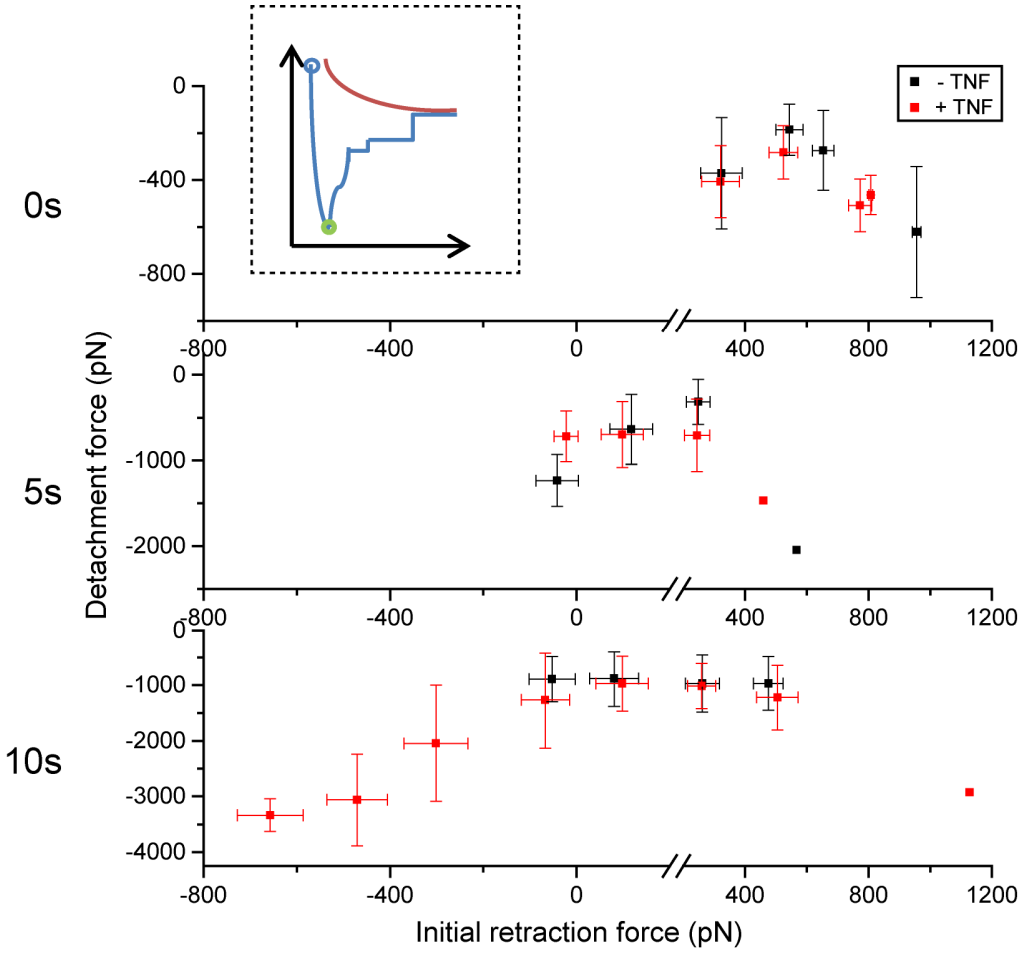

Fig. 54: Initial retraction force versus detachment force. Approach curve (red) and retraction curve (blue). Initial retraction force (blue circle) and detachment force (green circle). The values higher than the break are enlarged to show the data intensive area. Untreated cells (black) and treated with TNF cells (red). Data are plotted every 200 pN. A break is made at 200pN. Error bars present the standard deviation.

deformation of the cells and/or resistant force of the cell to the surface. When compared to the data below 0 pN, more forces fall in this range for 10 sec than those for 5 sec. Thus, it is assumed that at 5 sec and 10 sec, cells underwent higher viscous deformation than at 0 sec contact time, cells exerted pulling force to the surface, making the initial retract force increased (absolute value). Between -/+TNF for 0 and 5 sec contact time, no significant difference of the initial retract force was observed. However compared cell-surface contact times of 10 sec, more data in TNF treated cells were observed below 0 pN and even up to about 800 pN compared to those without TNF treatment.

This result shows that longer contact time increases the initial retract force by promoting the rigidity of bonds in the entire cell body. Meanwhile, a slight increase from TNF stimulation is found only for long contact times (10 sec) rather than for the shorter contact time.

2.1.3.2 Microfluidic Studies

It is known that *in vivo*, the formation of nascent contact between the leukocyte and the endothelial cells induces the leukocyte to slow down its speed and it can then be captured in blood vessel. To get a further understanding of the TNF effect in this initial phase of rolling and adhesion, we used microfluidics to study the dynamics of Jurkat E6-1 cells by mainly characterizing the properties of local velocity in different behaviors of cells (rolling/tethering and adhering). The local velocity of a cell defines the velocity of the cell itself, which is different from the global velocity of the cell (also the flow velocity). The method is based on the adhesion analysis, which is more proper in our study than the other assay called detachment analysis, which fits better in the analysis of detachment behavior after a defined adhesion time.

The value of dynamic viscosity was used from literature (0.7097×10^{-3} Pa · s) with the similar medium (RPMI) used before (Folger et al., 1978). Varied shear stresses and temperatures were carried out in our measurement. With the shear stresses of 0.08, 0.06 dyn/cm^2, adherent cells (untreated and treated cells) were counted at 30 ˚C and 21 ˚C. Obviously, higher shear stress decreased the adherent cell percent. In detail, At 30 ˚C, cells untreated with TNF show an adhesion percent of 1.8% and 5.8% at the shear stress of 0.08 dyn/cm^2 and 0.06 dyn/cm^2, whereas cells treated with TNF show an adhesion percent of 4.7 % and 7.9 % respectively (Fig.

55a). An increase percent of adherent cells is found in response to TNF stimulation, that at the shear stress of 0.08 dyn/cm^2, it is 2.9% and at 0.06 dyn/cm^2, it is 2.1%. For each experiment situation, the recording time for the video is around 3 min (supplementary video 2).

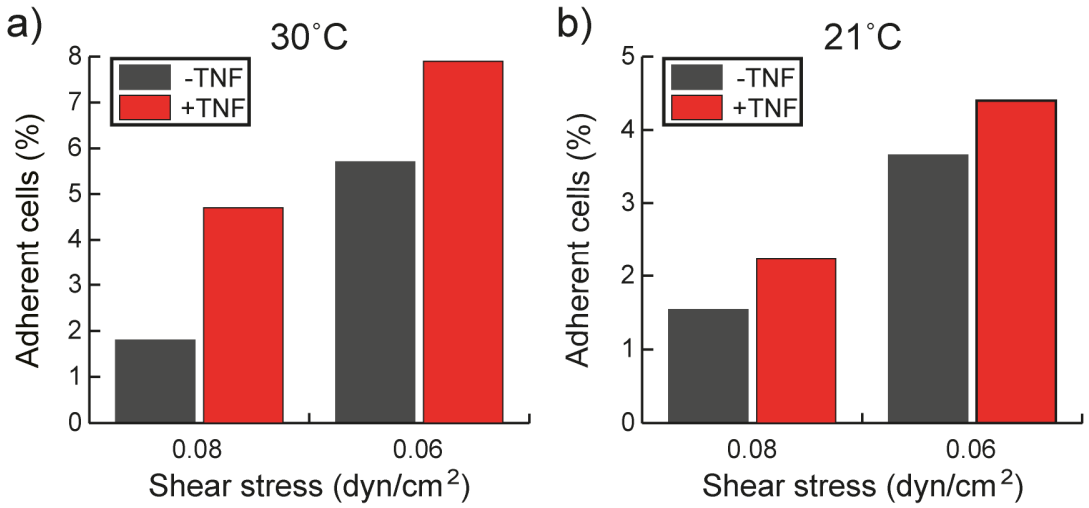

Fig. 55: Percentage of adherent cells at shear stress of 0.08 and 0.06 dyn/cm^2 at 30 ˚C (a) and 21 ˚C (b). Cell untreated with TNF (black) and treated with TNF (red). The experiment was done once.

Since lacking of sufficient facilities to keep the temperature at 30˚C, we afterwards did the experiments at 21˚C (measured with a thermometer, Fig. 55b). It is observed that the general adherent cell percent shows a decrease about compared to 30 ˚C at the shear stress of 0.08 and 0.06 dyn/cm^2, which is relevant to the reduced cell mechanism at lower temperature based on thermal energy (E) defined as

$$E = k_B T \tag{7}$$

Where k_B is the Boltzmann constant and T is the absolute temperature.

Meanwhile, it is found that at the shear stress of 0.04 dyn/cm^2 and the temperature at 22±1 ˚C, the percent of adherent cells is almost the same (Fig. 56a). The velocity of rolling cells at the shear stress of 0.04 dyn/cm^2 was also analyzed and shown in Fig. 56b. The result shows that TNF stimulation slowed down speed of rolling cells by about 15% from 50.97 μm/s to 44.47 μm/s, but the difference is not significant (by Mann-Whitney U test). Therefore, although TNF

stimulation slightly reduced the rolling velocity of the cells, the percent of adherent cells was not influenced as a function of TNF stimulation. Benjamin Spetzler did the microfluidics experiment under my supervision, and parts of these results are also work of his Bachelor thesis.

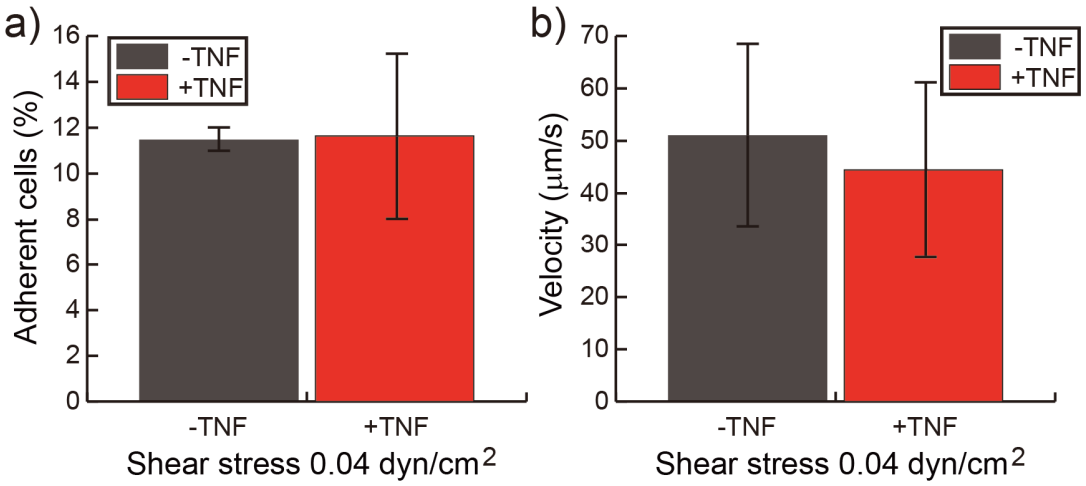

Fig. 56: Percent of adherent cells (a) and velocity of rolling cells (b) at shear stress of 0.04 dyn/cm^2 and temperature at 22±1 ˚C. Cell untreated with TNF (black) and treated with TNF (red). (a) was done twice in duplicate and (b) was done once and for each experiment situation there were 20-30 cells analyzed.

2.1.3.3 Discussion

2.1.3.3.1 Sub-second Contact Time is enough to Initiate Early Stage Cell-surface Adhesion

In the AFM measurement, I tried the shortest contact time, of which the actual time to arrive the pre-set contact force is about 0.2 sec. Surprisingly, a high adhesion force was observed at this shortest time. This is consistent with the rapid arrest of leukocyte cells on blood vessels, showing that single bond formation within less than 0.2 sec contact time is sufficient for establishing firm adhesion (Rinker et al., 2001). Such high adhesion force in very short contact time is not only found in T cells (Zhang et al., 2006), but also exists in other types of cells, such as fibroblast on nanostructured surface (Selhuber-Unkel et al., 2008), red blood cells on laminin (Maciaszek et al., 2014), prostate cancer cells on collagen and other cells (Sariisik et al., 2013) as well as for two bacteria adhering to each other (Benoit et al., 2000).

2.1.3.3.2 Contact Time largely Influences Cell Adhesion Strength

My results show that the cell adhesion strength including detachment force, detachment energy, and number of ruptures was clearly increased when the cell-surface contact time was prolonged for cells regarding of TNF treatment. This is in agreement with literature (Selhuber-Unkel et al., 2008) and can easily be explained by the number of adhesive bonds is increased over time, so

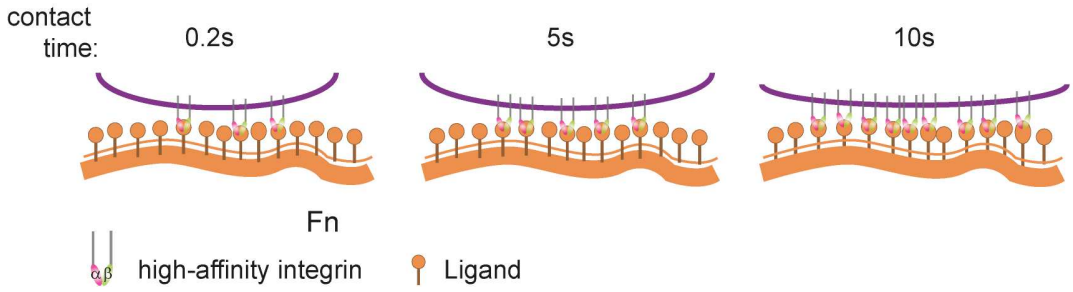

Fig. 57: Increase in bond number with contact time in the adhesion of a cell to on FN. Only integrins with high affinity are shown here.

that cell adhesion area expands over time (Fig. 57). A similar increase (10 fold after 1 min contact) is also found for Chinese hamster ovary cells (CHO) on collagen I, where the cells can be switched to an activated state, and correspondingly, the probability of cooperation among receptors is higher (Franz et al., 2007). In T cells, an even greater increase (up to 30 fold) of adhesion force can happen when they attach with antigen presenting cells (APCs) after 30 min contact (Hoffmann et al., 2011). However, due to the high migration of T cells, as long as 2 min contact time to the surface is very difficult to measure (Hosseini et al., 2009), in our case, 10 sec started to be not easy for Jurkat E6-1 cells.

What also contributed to the adhesion strength is the cell viscosit. The initial retraction force could be a direct reflection that with longer contact time, cells are more prone to pull the cantilever to the surface and stabilize the local adhesion sites. Similar to it, in less motile fibroblast, the viscoelasticity shows a higher value than a more motile one (Park et al., 2005). Cooperation effects between cell surface molecules within a relative larger adhesion area are assumed to contribute to the enhanced adhesion strength over time, which reflects into quite homogeneous increasing of all rupture forces. Among the integrins expressed on Jurkat cells, it has been reported that $\alpha_4\beta_1$ and $\alpha_5\beta_1$ are very important ones and contribute equally in mediating the adhesion to FN (Seminario et al., 1998; Bearz et al., 1999; Shimizu et al., 1990), as well the

expressions of β_2, β_5 and β_7 are found in Jurkat cells (Malte Puchert did it). Hence, it is assumed that there are positive collaborations between these integrins in the relatively long-term contact.
In addition, one can speculate that this enlarged adhesion area affects the last rupture events. It is found that in the AFM study, the last tether length increases consistently with the prolonged contact time. Similar to this, it is found that in an temperature increased condition, tether length is increased by about one fold from 16 ˚C to 37 ˚C (Rico et al., 2010). Upon the value set for classifying T and J events in the loading rate of the last rupture, it is found that longer cell-surface contact time contributes into higher possibilities of the T events, which have more higher loading rates (>-30 pN/s) at 5 sec and 10 sec cell-surface contact time in my result. This phenomenon is opposite to our original expectation that longer contact time builds into stronger actomyosin architecture. However, this result might indicate a weaker interaction between cell membrane and cytoskeleton due to a higher compliance of the cells to maintain longer time on the surface. Another hypothesis of the cells more prone to present T events is that the cells had higher migration during the measurement or simply because cells consume most of the forces and energy in segregating the connection to cytoskeletons in longer contact time. Hence, higher percent of cells shows the smaller loading rate. A similar criterion for defining the T and J events has been brought up in different type of cells and surface system, where the loading rates smaller than 27 pN/s are T events and those above 40 pN/s are J events (Sariisik et al., 2013).

2.1.3.3.3 The Interplay of TNF in the Inside-out Signaling Pathway can be measured in the Short Contact Time Independent of *de novo* Protein Synthesis

Although lymphocyte adhesion strength to endothelial cells has been reported, for the up-regulated surface molecule expression of ICAM and VCAM after TNF stimulation, such stimulation usually requires a long time (i.e., 6h) (Jaczewska et al., 2014) and obviously indicates the interplay of TNF in the outside-in signaling pathway. To the contrary, in this thesis, no endothelial cell surface molecules are present, and moreover, cells were pre-treated with TNF in the suspension state only for 25 min, since lacking of proper ligands, no activation of extracellular domain of integrins occurs. In addition, added with the time for force distance curve measurement, the total time is no longer than 1h. Thus, in such short times, we could consider there is no *de novo* corresponding proteins translation happened. Meanwhile, it is considered that

the inside-out pathway predominates the signaling in TNF triggered Jurkat cell adhesion, especially the significant increase of detachment strength in this immediate contact time.

Although no signaling cascade was studied in this project, it is assumed that it occurred and mediated cell adhesion due to short incubation with TNF as following reports. It is revealed that an even shorter time (only 1.5 min) of TNF incubation can facilitate protein transportation and protein complex formation (Philipp et al., 2010). Such a short-term activation also exists in other cells. In neutrophils, Src kinases, especially p38 MAPK, are involved in the initial activation of β_2 integrins (Bouaouina et al., 2004) through the inside-out signaling pathway by incubation with TNF for 10 min. Similarly, protein kinase C has been reported to activate the $\alpha_2\beta_1$ mediated inside-out signaling pathway within short time (Tulla et al., 2008).

Furthermore, it is found that TNF also slightly increases the viscosity at contact time longer than 5 sec. Maybe strong bonds with cytoskeleton incorporation participated during the initial retract process, and directly increases the rigidity of the cells. This enhancement is supported by experiments in other type of cells, e.g., endothelial cells, where the mechanical stiffness is increased as much as 50% after TNF treatment as well as the aggregation of F-actin filaments (Lee et al., 2011). Hence, it is assumed that TNF pre-incubation with cells augments the viscosity of the Jurkat cells prior to the force measurement, which can be considered as a factor contributing to the increased adhesion strength within as short as 25 min stimulation.

Although it is still elusive of the detailed dynamics of the protein cascade and the final binding with cytoplasmic domain of integrins on the T cells, it is known that the function of TNF through the inside-out signaling pathway is really rapid, which has also been proved on the different measured physical parameters of cell adhesion.

2.1.3.3.4 TNF Activation Influences the Properties of Integrin including Affinity, Valency and Avidity

From the detachment force and detachment energy to the number of ruptures on the whole cells level, significant increases in response to TNF stimulation are observed. Since the switch of

inactive to active state of the integrins is thought to be the final protein to transduce the signals interior to exterior, it is highly convincing that within the cell-surface contact area, the probability of activated integrins is increased. In detail, the available binding ligands presenting on the FN surface are stable, whereas more integrins are probably exerting force at the close adhesion area and the total amount of integrins distributing on the cell surface is constant. Therefore, it is assumed that integrins become more mobile and form into clusters (also higher valency) at the cell-surface contact area with a higher density in the TNF treated cells compared to the untreated ones. This phenomenon is similar to the clustering of LFA-1 in a rapid response to stimuli, which is also proved especially important for relocalization of LFA-1 in T and B cells (Carrasco et al., 2004; Abram & Lowell, 2009). Meanwhile, the clustering of integrins is probably also affected by the diffusion motion induced by TNF, which might be related with the modulation of ion channels reported before (Czeschik et al., 2008). As well, since TNF can rapidly activate tyrosine phosphorylation of paxillin and focal adhesion kinase, other components close to the cell membrane should also contribute to clustering of integrins.

Besides the internalization and recycling of $\alpha_5\beta_1$ suggested in endothelial cells (Gao et al., 2000), it is also reported that there occurs the switch between α_1 and α_2 integrin in cerebral pericyte from adhesion to migration (Tigges et al., 2013). Therefore, adding with clustering of integrins, redistribution of the different type of integrins is assumed to be another factor in response to TNF stimulation. In my AFM study, maybe the cross-talk between α_4 and α_5 led to the rearranged distribution of them. Closely associated with this probability are the specific compartments in cell membrane, i.e. lipid rafts. They are microdomains containing glycosphingolipids, gangliosides and cholesterols (Head et al., 2014). It has been reported that activated $\alpha_L\beta_2$ preferentially locate in the lipid rafts and afterwards they facilitate the recruitment of $\alpha_4\beta_1$ into the structures (Leitinger & Hogg, 2002). On the level of physical properties, since lipid rafts are usually stiffer than the surrounding lipid bilayer membrane (Roduit et al., 2008), how some of these integrins overcome the energy barrier to the lipid rafts is still elusive. Meanwhile, how the individual integrin heterodimers cross talk and divide the task for cell performance is also not yet clear. Maybe the redistribution of integrins also affects the lipid bilayer membrane, which is similar to the condensation of the glycocalyx layer during the conformation switch of integrins with low-affinity to high-affinity in a physical experiment

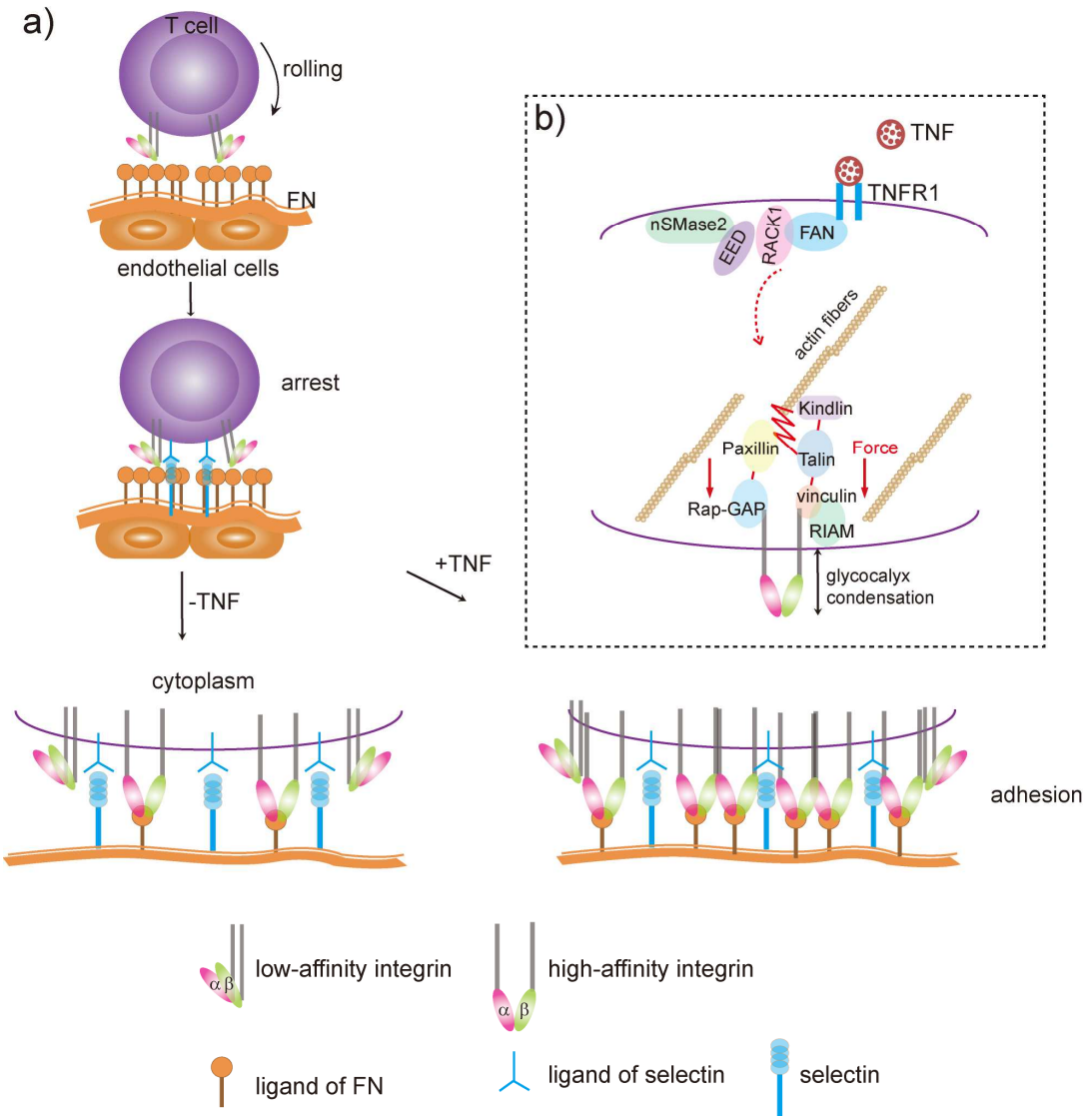

Fig. 58: (a) Assumption of T cell adhesion model between cells stimulated with TNF (+TNF) and without TNF (-TNF) *in vivo*. Fibronectin covers the endothelial cells layer. When T cells are rolling and arrested, integrins on the membrane of T cells are in a low affinity conformation. Arrest occurs mainly via selectins on the endothelial cells and their respective ligands on T cells. When cells are stimulated with TNF, a higher proportion of activated integrins is recruited to the adhesion site and binding clusters are formed in comparison to the situation without TNF stimulation. In the whole adhesion process, the amount of the available binding ligands on the fibronectin surface is constant. More bonds are present after TNF stimulation as the probability of bond rupture is decreased. **(b) Assumption of protein recruitment and force transmission of a cell stimulated with TNF.** TNF stimulation induces the formation of the FAN·RACK1·EED·nSMase2 complex. The following polymerization of actin fibers exert physical forces (red saw) to the proteins that are binding with the cytoplasmic domain of integrins. These proteins are assumed linked with strong bonds (red lines) in a "well-aligned" order. The forces are transmitted to the extracellular domain of integrins. The condensation of glycocalyx surrounding integrins with high affinity occurs. An individual integrin heterodimers is present.

model (Boettiger, 2012).

Furthermore, since the single rupture force is observed to increase as a function of TNF stimulation, it is considered as a direct reflection of higher probability of the affinity switch (from low affinity to high affinity) of individual integrin heterodimers in TNF treated cells. Regarding that the observed all ruptures can either originate from single molecule ruptures or from the ruptures of molecular clusters, we assume that at the short cell-surface interaction time of 0 sec, the ruptures of molecular clusters should be negligible. However, at longer contact times (5 sec and 10 sec), they should be considered. To acknowledge clearly about the single and cluster binding is still not easy. Only recently, the individual integrin affinity was found on epithelial cells (Patterson et al., 2013).

Therefore, according to these results, it is supposed that TNF influences the avidity of integrins in a way to increase both affinity and valency of integrins, since the significance level for detachment force, detachment energy and number of ruptures is high, we assume that the effect in strengthening the cell adhesion force from TNF is dramatic. Fig. 58 shows our assumption of physical mechanisms that TNF triggers the Jurkat cells binding, which is noteworthy mediated by the changes of physical features of integrins *in vivo* after the initial arrest of T cells. Although it has been reported that in the continuum conformation changes of integrins, the three states with low, intermediate and high affinity are discrete (Ley et al., 2007), to simplify the system, we here only present integrins in low and high affinity state. Importantly, we hypothesis that the formation of proteins complex (FAN·RACK1·EED·nSMase2) initiates the intracellular physical arrangement of the proteins. In detail, forces exerted by the actin fibers mediate the delicate alignment of adhesion structures (e.g., paxillin, vinculin, talin), therefore the strong bonds are formed among the proteins and the mechanical forces are transmitted through the cytoplasmic domain of integrins to the extracellular domains.

2.1.3.3.5 The Shortest Cell-surface Contact time reflects the most Dramatic Increase of Adhesion Strength in response to TNF

In this study, it is found that, for the first time, the most significant difference of cell detachment force and detachment energy between cells without and with TNF treatment for the shortest

contact time (0.2 sec). Also changes in forces associated with single ruptures and last ruptures occur only for contact times less than 10 sec. Although there are no reports proving or indicating the fluctuation of adhesion strength in such short contact time is due to the cytokine stimulation in the inside-out signaling pathway, it is considered that this relationship between most significant difference and the shortest contact time might be related with the fluctuation of kinases' phosphorylation inside cells. In neutrophils, the phosphorylation of p38 can be detected after 10 min incubation with TNF, and the level of the phosphorylation was reduced after 1h (Bouaouina et al., 2004). In our study, it cost about 20 min for 10 sec contact time to obtain all force curves for a single cell, which added with the pre-incubation 25 min probably makes the cells close to the end of the "efficient" react time (1h). Another possibility is that TNF-treated cells are more adhesive at the beginning, but that the interaction with FN additionally activates integrins independent from TNF, resulting in an equal level of interaction in TNF treated and untreated cells after 10 sec.

2.1.3.3.6 TNF Does Not Affect the Rigidity of Last Tether

Interestingly, although TNF increases cell adhesion strength as well as the force associated with the last ruptures, there is no difference of the last tether length or the loading rate prior to the last rupture as a function of TNF stimulation. The fairly similar amount of loading rate with positive and negative values might indicate the random direction of the exerting force of tiny bonds close to the cell membrane. The predominant presence of T-events indicates that cells did not highly rely on cytoskeleton for substantial anchoring on the surface. It is still not clear why there is no difference of the loading rate or the length of tethers due to TNF stimulation, however, one could hypothesis that the cells have already lost the bulk of force, energy and/or the well-constructed cytoskeleton network had been disrupted completely at the last rupture.

2.1.3.3.7 TNF Stimulation in the Shear Flow Condition Indicates the Positive Role of TNF through Inside-out Signaling Pathway

In our study, it is found that cells which were pre-incubated with TNF showed higher percent of adherent cells at shear stress of 0.08 dyn/cm^2 and 0.04 dyn/cm^2 at temperatures of 30 ˚C and 21±1 ˚C, although at shear stress of 0.04 dyn/cm^2 the percent of adherent cells presented similar.

These results should indicate the positive role of TNF to cells in the adhesion phase *in vitro*, which we consider the truth of the interplay of TNF in the inside-out signaling pathway.

The mechanisms of integrin-mediated outside-in signaling pathway under shear flow condition have been reported. In the system where TNF was used to pre-activate endothelial cells on several adhesive surfaces, clustering of integrins is reported at subsecond time scale, but it seems that the affinity of integrins is not enhanced (Grabovsky et al., 2000). In addition, LFA-1 mediated firm adhesion is highly dependent on ion-channel and cytoskeleton involvement (San Lek et al., 2013).

Besides the outside-in signaling pathway, in the inside-out signaling pathway, it is first reported that shear force is an indispensable factor in the chemokine-triggered integrins into a complete activated state (Woolf et al., 2007). The clustering of integrins also responds to shear forces through the signals transduced from the GPCRs (Alon & Dustin, 2007).

2.1.3.3.8 TNF Stimulation Facilitating Slower Rolling of Cells due to the Activation of Selectins besides Integrins

Prior to the integrin-mediated firm adhesion, it is known that T cells adhere and transmigrate through endothelial cells and that this process requires tethering with transient attachment mediated by selectins.

Meanwhile, considering the high level of other molecules expressed on T cells, activations from stimuli could be relayed from L-selectins to integrins. This assumption is supported by a previous report that the ligand for L-selectin initiates the activation of integrin and thus enables adhesion of lymphocytes to FN (Giblin et al., 1997). In addition, high amounts of TNF can up-regulate L-selectin on polymorphonuclear neutrophils (PMN) *in vivo* (Kiersnowska-Rogowska et al., 2006). The interactions among the surface molecules can also be considered as the regulator for adhesion under flow, e.g. P-selectin glycoprotein ligand-1 (PSG-1) and L-selectin form into the complex PSG-1-L-selectin (Stadtmann et al., 2013). In the tethering phase, subcellular structures also play important role, e.g., microvilli. They are proved more prone to be deformed during the rolling of the cells with higher probability of tethering, in order to enhance adhesion

(Caputo & Hammer, 2005). Furthermore, since the surface molecules habitat with microvilli, the stimulation due to TNF should be the synergic function of the surface molecules and subcellular structures.

2.1.3.3.9 TNF Stimulation Interferences the Bonds Formation

In the flow condition, the observed dynamics of rolling is due to the association and dissociation rate of the bonds. TNF in our study probably decreased the dissociation of the bonds and prolonged the tether lifetime due to the slower rolling rates and higher percent of adherent cells under flow. In detail, ligand binding makes a stronger loading force, which is able to facilitate selectins undergo conformation switch. As well, association rate of the bonds is increased and the dissociation rate is decreased. Such kind of bonds are called “catch bonds” (Marshall et al., 2003). In response to TNF stimulation, the association rate is assumed strongly increased while the dissociation rate is decreased slightly, therefore, the rates of association and dissociation are not in a balance, which might be in agreement with the similar effect of magnesium (Schmitz et al., 2009). If the microfluidics results are related with our AFM result, we can assume that in the shear flow condition, more bonds are formed and stabilized through the connection with cytoskeleton in the tethering phase (Erdmann & Schwarz, 2004).

2.2 T-lymphocyte Adhesion on Nanostructured Surfaces

The above studies of AFM and microfluidics investigated how cells respond to external force when they were allowed to attach to an ECM protein coated surface (FN) surface for different contact times. To obtain further and detailed information about the distribution of integrins, I launched initial experiment on cell adhesion on nanopatterned structures with defined distance. The nanodots were functionalized with peptides to provide specific recognition with integrins expressed on Jurkat E6-1 cells.

2.2.1 Fabrication of Nanopatterned Structures

The preparation of nanopatterned structures is based on the method of micelle nanolithography (Arnold et al., 2004). The principle is that when diblock copolymers with amphiphilic polarity

are dissolved in solvents, they can form into micelles above the so-called critical micelle concentration (cmc). In this study, two components of the diblock copolymer are polystyrene (PS) and poly-2-vinylpyridine (P2VP), the former one is hydrophobic and the latter one is hydrophilic. The solvent used here is toluene, and the principle of nanostructure fabrication is shown is Fig. 59. The outer part of the micelle is PS while the inner part is P2VP. After the formation of the micelle, hydrogen tetrachloroaurate (III) trihydrate is added into the solution and accumulates in the center. Hydrogen plasma with argon gas was applied to etch away the polymer micelle and to expose the gold nanodots on the surface. Afterwards, the gold nanodots were covalently coated with peptide. Choosing polymers with different molecule weight and adjusting the speed of dip or spin coating during the preparation can achieve the different distances between the gold nanodots. One of the samples was imaged with SEM (Laith Kadem provided the images) shown in Fig. 60, where it can be observed that the gold nanodots form into a hexagonal pattern, and the distance between single gold nanodots is 50±5 nm.

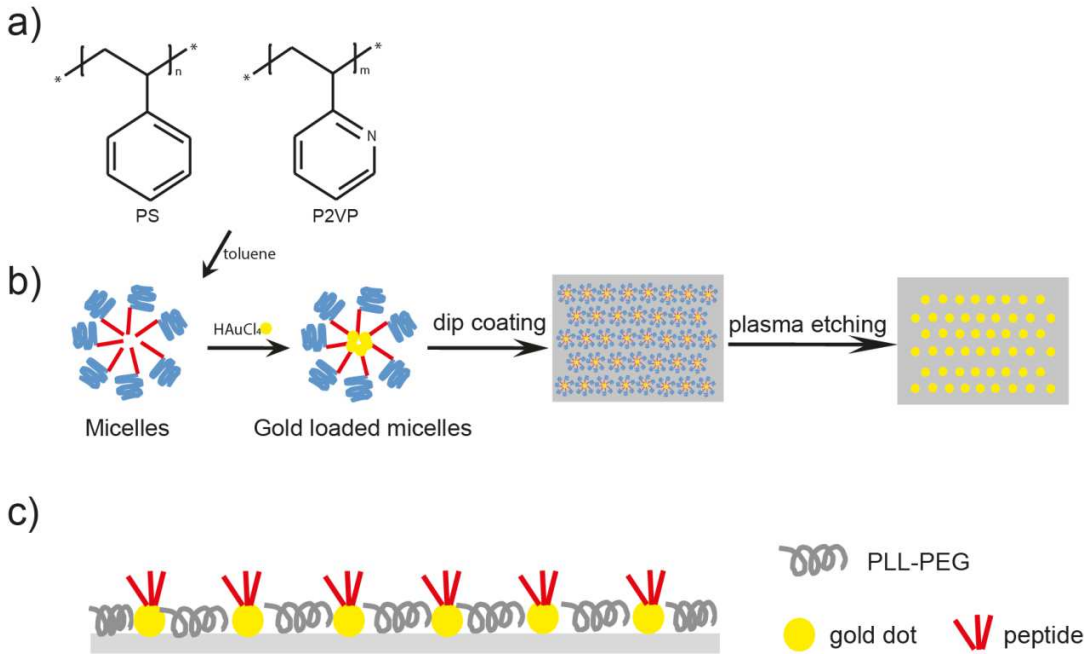

Fig. 59: Principle of the production of gold nanostructures and the functionalization. (a) Chemical structures of PS and P2VP. (b) The preparation of the nanopatterned structure. (c) Functionalization on the surface.

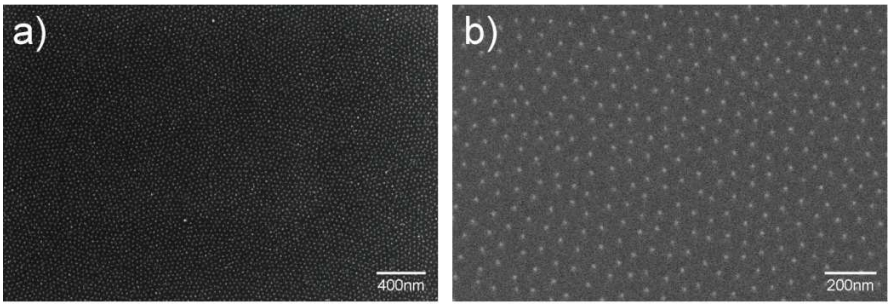

Fig. 60: Images of nanopatterned structure under SEM with lower magnification (a) and higher magnification (b).

2.2.2 Cell Adhesion on Gold Nanostructures Functionalized by cRGD and cLDV

Prior to the functionalization, PLL-g-PEG was applied to passivate the surface. PLL-g-PEG is

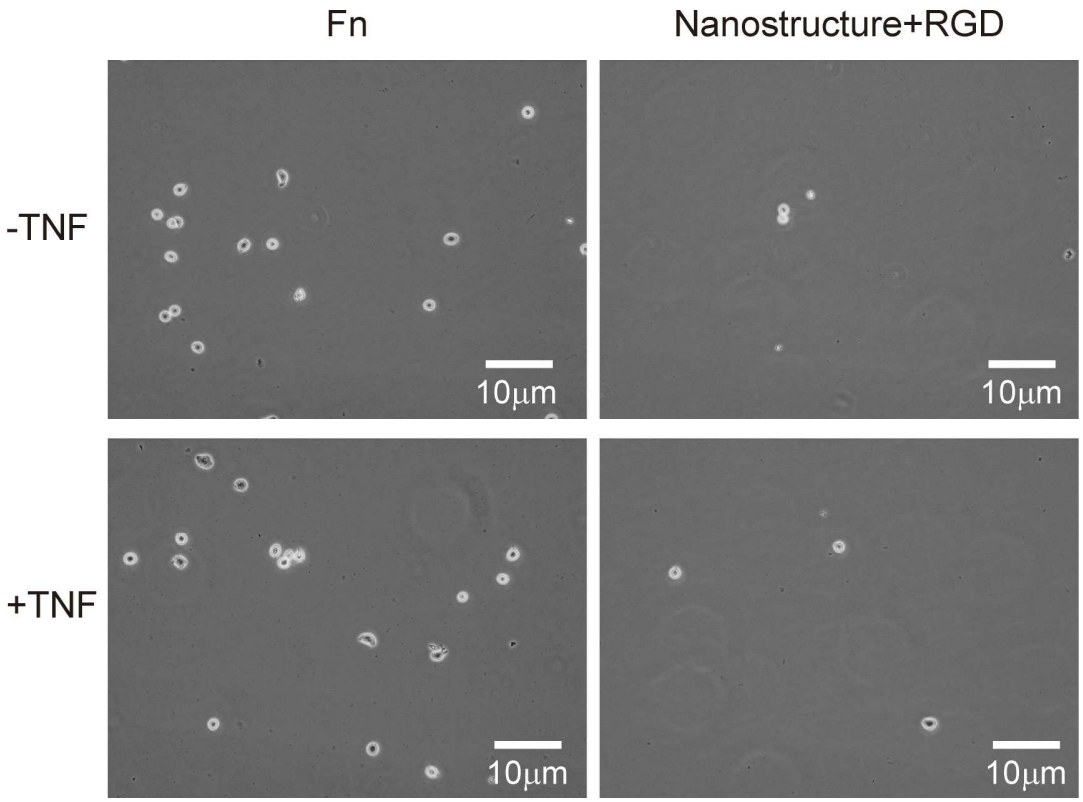

Fig. 61: Jurkat E6-1 cells on FN coated surface and cRGD functionalized nanostructures. The cell adhesion time is 1h.

capable to repel protein adsorption (Lee & Spencer, 2008) and to make sure that cells are able to attach on the nanopatterned sites. In 3.2, the expressions of both α_4 and α_5 were detected on Jurkat E6-1 cells. The ligands which can bind specifically with these two integrins were examined before, that cRGD in the FN III region can bind with $\alpha_v\beta_3$ and $\alpha_5\beta_1$ (Haubner & Finsinger, 1997) and cLDV in the FN V region binds with $\alpha_4\beta_1$ (Vanderslice et al., 1997). In the beginning of this study, cell adhesion studies on nanostructures functionalized with cRGD were carried out. The distance of the gold nanodots was 50±5 nm, samples were provided by Laith Kadem. Compared to many cells adhering on FN coated samples, there are few cells adhering on the cRGD-functionalized nanostructured surface no matter if there is TNF treatment or not (Fig. 61). Since the total number of cells adhering on the nanostructured surfaces was very small and the morphology of the cells did not change much due to TNF stimulation, which is probably due to absence of the expression of $\alpha_v\beta_3$ and the low expression level of α_5, the data were not quantified.

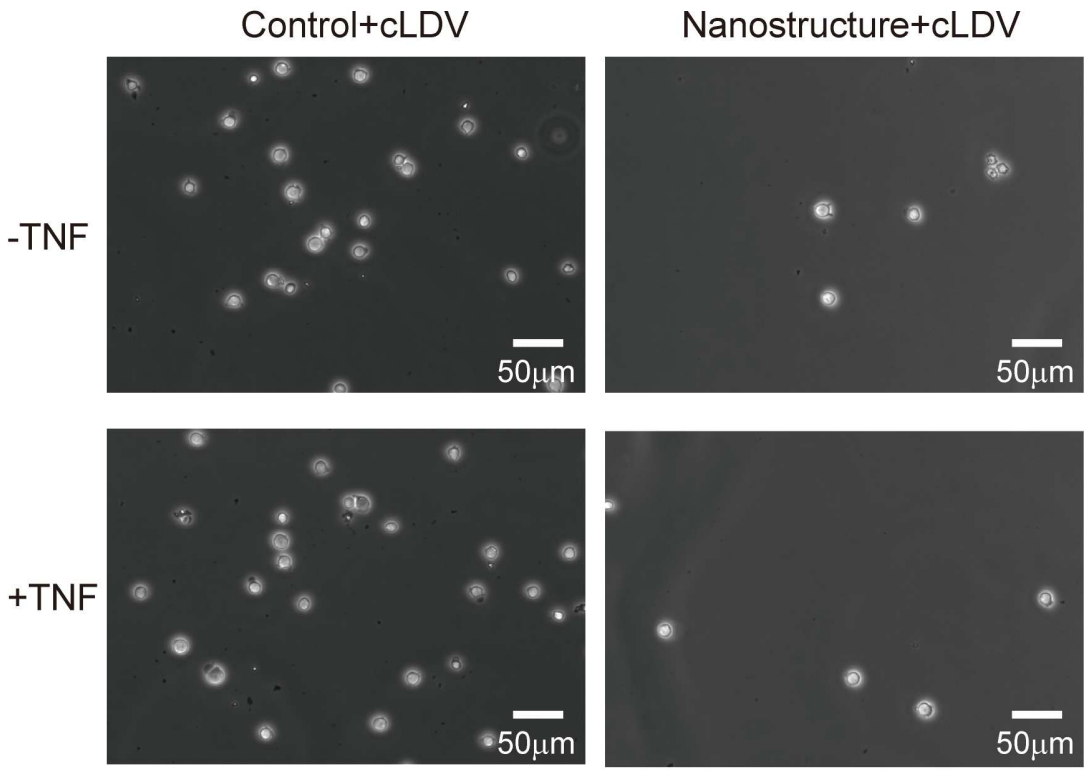

Fig. 62: Jurkat E6-1 cells on cLDV coated control samples and cLDV functionalized nanostructures. The cell adhesion time is 1h.

Due to the lower expression level of α_5 compared to α_4 in Jurkat E6-1 cells, cLDV was used to examine if there were more adherent cells compared to cRGD and/or the change of cell morphology in response to TNF stimulation. As a reference, coverslips physisorbed with cLDV (control+cLDV) were prepared. I observed many cells adhering and they had normal shape and formed protrusions (Fig. 62). Whereas on cLDV functionalized nanostructures, only a few cells adhered, many cells formed clusters and looked are dead, some cells were like "hanging" on the surface while moving during the imaging. Cell amount from 10 pictures was quantified. There were about 250 cells on the "control+cLDV" samples, no difference was found between TNF untreated cells and TNF treated cells. On the "nanostructure+cLDV" samples, only about 20

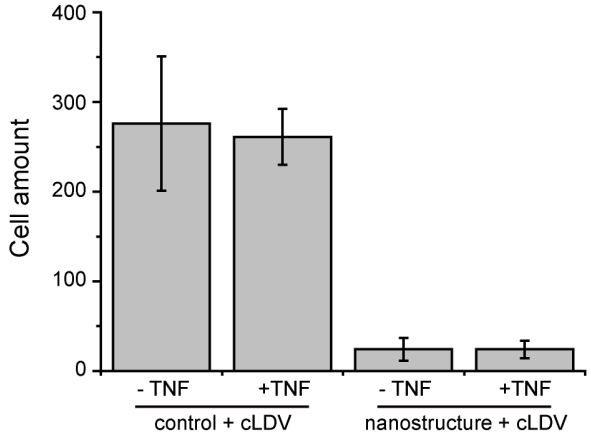

Fig. 63: Cell amount on different coated-surfaces. Control+cLDV: glasses homogeneously coated with cLDV. Error bar: standard deviation. The experiment was done once in duplicates.

cells were adhering on the surface. Compared to the "control+cLDV" samples, this amount is obviously too small (Fig. 63). To visualize the localization of the cytoskeleton and the component of adhesion complex, actin and vinculin were imaged with immunofluorescence after the cell counting on "control+cLDV" samples. The actin (green) locates at the cortex of the cells, and it forms into the protrusions of the cell membrane. Vinculin localizes quite homogeneously in the adhesion area and a condensed expression is observed in the cell membrane. Colocalization between actin and vinculin is observed (Fig. 64). No quantification study of expression of these proteins due to TNF stimulation was carried out. Chengqi Xu provided these "control+cLDV" samples and "nanostructure+cLDV" samples under my supervision.

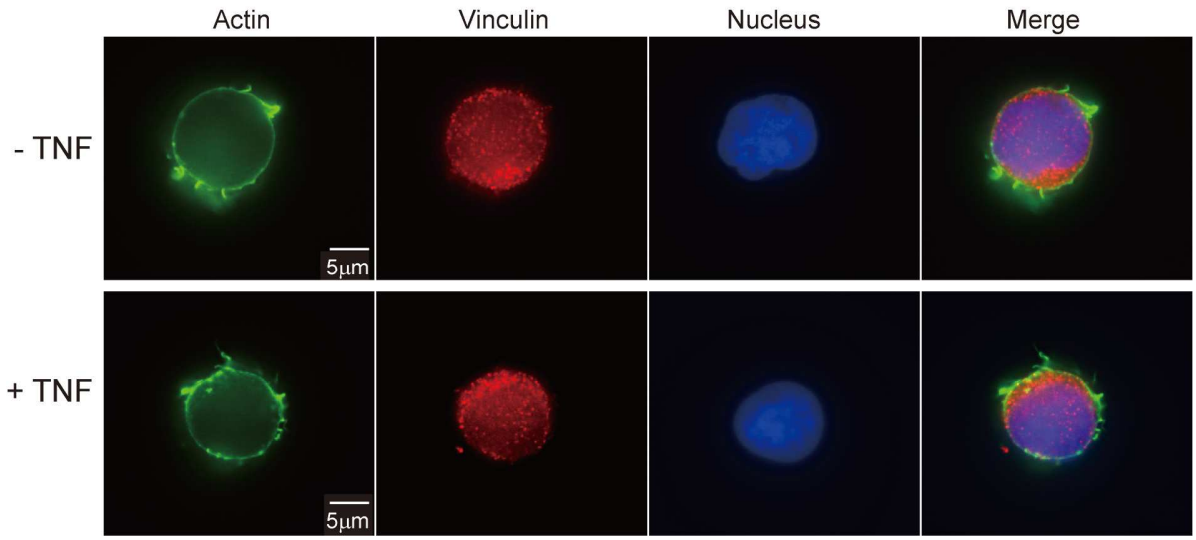

Fig. 64: Imaging of adhesion complex in TNF untreated cells (-TNF) and TNF treated cells (+TNF) on the surface of "control+cLDV" samples.

2.2.3 Discussion

With the peptide functionalized nanopatterned structures, it is convenient to manipulate and study cell adhesion and further migration dynamics with delicate designed distance of gold nanodots with the exact control of the involved binding partners. Furthermore, the nanopatterned functionalization is a great approach to understand the binding of integrins to the shortest functional peptides. In this study, a few cells adhered on cRGD functionalized nanostructures, which might be due to the extremely low expression level of α_5. However, on cLDV functionalized nanostructures, there was still a very small amount of cells. This could be due to two possibilities: (1) The PLL-g-PEG coating covers gold dots and the cells are not able to dig in the PLL-g-PEG and bind with the peptide; (2) The distance between the gold dots (50±5 nm) is still a bit large for the efficient integrin (expressed on Jurkat E6-1 cells) binding, as the distance reported for strong binding is 36±7 nm in hematopoietic stem cells (Muth et al., 2013), which might give a clue to the Jurkat E6-1 cell line. To solve the problem (1) salinization should be used to avoid the overcoating from PLL-PEG and to solve the problem (2) different block copolymer should be used for nanostructure preparation in order to shorten the distance of gold nanodots.

The high expression of actin and vinculin shows the adhesion complex at the cortex of the cell membrane. From the imaging of the proteins and their colocalization, it is hard to say whether TNF helps to recruit more actin or vinculin to the adhesion sites. Further approaches would include a quantification study of the expression of these proteins in response to TNF stimulation. Furthermore, by manipulating the distances of the gold dots, the dynamics of integrin binding density during cell adhesion would be revealed at nano-scales.

3. Summary

The goal of my thesis was to investigate the adhesion of T-lymphocytes as a function of TNF stimulation, which serves as a trigger in the integrin-mediated inside-out signaling pathway.

This work was carried out on a biomimetic fibronectin-coated surface that initiates cell adhesion and excludes the involvement of surface molecules on endothelial cells. Light microscopy imaging was used for measuring and comparing the number of adherent cells and cell size between cells not treated and those treated with TNF in phase contrast microscopy and PCS-based surface contrast microscopy. No difference due to TNF stimulation was detected, which was probably due to the restrictions of the technique in our study that the cell membrane might covers the real adhesion area under the whole cell body, and the long adhesion time. Therefore, an interference-based method, RICM, was used in the measurement. RICM is appropriate in detecting the close proximity of cells to the surface, i.e. precise cell adhesion area, protrusions emerging from cell membranes (e.g., microspikes) and noteworthy, all experiments were carried out with living cells. Although no difference on the cell adhesion area and length of microspikes could be detected in response to TNF stimulation, the dynamics of the protrusions to sense the environment was recorded and revealed that they were not in a balanced motion but elongation-retraction cycles were highly dynamic.

AFM-based single-cell force microscopy was used as the main strategy in my thesis to address the role of TNF in the cell adhesion to the surface, since it enables precise measurement of cell adhesion for shortest cell-surface contact time and also gives the information on single molecule ruptures. I found that cell adhesion strength increased with longer cell-surface contact time. Furthermore, the most important result was that within short contact time of no more than 10 sec, I detected striking differences in detachment force, detachment energy, number of ruptures until detachment in response to TNF stimulation. The greatest difference was found for the shortest contact time of only 0.2 sec. As well, for single-molecule ruptures forces, slight differences were found. In addition, TNF was assumed to modulate the viscosity of cells.

Microfluidics was used to study the rolling and adhesion of cells under defined shear stress. This

complementary technique realized the examination of the influence of TNF to the physical properties of cells in a more natural condition, i.e., simulating blood flow. I found that TNF stimulation slightly increased the percentage of adhering cells and decreased the speed of rolling cells at different shear stress and temperature.

The preliminary cell adhesion work with cRGD and cLDV functionalized nanostructures presented no difference on the adherent cell amount and cell morphology, however, the proteins in the adhesion structure were successfully visualized as well as their colocalization. It would be very interesting to study the dynamics of proteins in the adhesion structure in the living conditions.

Based on AFM and microfluidics results, it can be concluded that TNF stimulation accelerates the adhesion speed, enables more cells to adhere, and very strikingly, enhances cell adhesion strength in the very initial “probe” of cells to FN surface in a very short-term adhesion scale. Furthermore, these results indicate that the interplay of TNF is through the inside-out signaling pathway as all experiments were carried out in an endothelium-free environment. Meanwhile, the most probable effectors in the adhesion are assumed to be synergistic positive effects caused by the raised proportion of integrins binding with high affinity at the contact area and additional clustering.

In the future, further studies should decipher the cross talk of integrins, e.g., here α_4 and α_5 in response to TNF stimulation, genetic modifications can be applied. For instance, through upregulating and/or downregulating the expression of specific integrins, we can study if there is any compensation from other integrins, which is expected to reflect the change of cell adhesion strength. Undoubtedly, since the dynamics of integrin adhesion is very complex, there is no simple way to explicitly explain the way of their assembly and disassembly in the initial contact to the surface. Sophisticated experimental strategies with even minuscule resolutions, i.e., CLSM bounded AFM with microfluidics, are anticipated to shed light on the dynamics of single molecular binding. To a higher degree, improved understanding of the stimulation of cytokines on cell mechanics should provide new strategies for the diagnosis of the early pathological changes, i.e., changes of integrins, as well as for therapy strategies.

4. Materials

4.1 Cell Lines

Jurkat E6-1: ATCC
Ref 52 wt: Gift from the group of Prof. Joachim Spatz, MP1 for intelligent system, Stuttgart
Ref 52 YFP-Paxillin: Gift from the group of Prof. Joachim Spatz, MP1 for intelligent system, Stuttgart

4.2 Chemicals for cell culturing

Click's/ RPMI 1640: Applichem
DMEM: Biochrom
Ethanol: Walter CMP
FBS: Biochrom
HBSS: Biochrom
Penicillin/Streptomycin: Biochrom
PBS: Sigma-Aldrich
RPMI 1640 medium: Gibco
Trypsin-EDTA: Biochrom

4.3 Staining Chemicals

Alex Fluor® 488 Phalloidin: Life technologies
Alex Fluor® 555 Phalloidin: Life technologies
Calcein-AM: BD Biosciences
Hoechst: Life technology
Primary antibodies:
  Monoclonal anti-human CD49d: ImmunoTools
  Monoclonal anti-human CD49e: ImmunoTools
  Monoclonal vinculin antibody: Millipore
Prolong diamond antifade mountant with DAPI: life technologies
Secondary antibody:
  Goat anti-mouse IgG, (H+L) FITC conjugated: Millipore
  Goat anti-mouse IgG, Alex Fluor® 594: Life technologies
Vectashield: Vector laboratories

4.4 Other Chemicals

Biocompatible glue: JPK Instruments

Biotin-concanavalin A: Sigma-Aldrich
Biotin-BSA: Sigma-Aldrich
BSA: Sigma-Aldrich
cRGD: Panatecs
cLDV: Biosyntan
FN: Sigma-Aldrich
HEPES: Sigma-Aldrich
HBSS: Biochrom
P2VP: Polymer Source Inc.
PFA: Sigma-Aldrich
PLL-g-PEG: SurfaceSolutions
PS: Polymer Source Inc.
Streptavidin: Sigma-Aldrich
Tetrachlorogold (III) acid trihydrate (gold salt): Sigma-Aldrich
TNF: BASF Bioresearch
Toluene: Merck
Triton X-100: Sigma-Aldrich

4.5 Plastic ware

6-well plate: Sarstedt
Cantilevers (MLCT): Bruker
Flask: Sarstedt
μ-Slide $I^{0.4}$ flow chamber: Ibidi
Petri dish: TPP

4.6 Devices

Camera:
Imagingsource DFK31AF03, Olympus;
ProgRes MF cool, Jenoptik;
Hamamatsu digital camera C9300, Olympus.
Centrifuge: Biofuge primo, Heraeus
Chemical hood: Köttermann
CLSM: Zeiss
FACSCalibur flow cytometer: Becton Dickinson
Incubation: Binder
Laminar: Thermo Scientific
Microscopy:
CKX41, Olympus;
IX81, Olympus;
IX71, Olympus.
Surface Contrast Microscopy: installed by “Integrated Systems and Photonics” Lab in Faculty of Engineering, Kiel

Microfluidic pump: RS-485 system, PHD ULTRA ™ series, Harvard apparatus
AFM: Nanowizard III, CellHesion 200 and Petridishheater, Biocell, JPK;
Objectives:
Antiflex: Zeiss (only for RICM);
UPlanFLN 10×/0.3, UPlanFLN 20×/0.5, LUCPlanFLN40×/0.6, and UplanSApo 60×/1.35: Olympus
Oxygen plasma: Te-Pla, 100-E
Water bath: GFL

4.7 Software

BD CellQuest™ Pro software V.4.0.2: Becton Dickinson
Data processing software: JPK
Image J: Rasband WS. ImageJ. U.S. National Institutes of Health, Bethesda, MD. http://rsb.info.nih.gov/ij/ [Online]. 2005
Image J Plug-In Particle Tracker Classic

5. Methods

5.1 Cell culture

All Cell culture work was done in the laminar in sterile conditions.

For cell morphology observation and counting except those announced, the phase contrast microscope CKX41 was applied for all work with the camera Imagingsource DFK 31AF03. The objectives were 10×, 20× and 40×.

5.1.1 Ref52 wt

Ref52 wt cells were cultured in culture medium (DMEM supplemented with 10% FBS) at 37 ºC, with 5% CO_2 and 90% humidity in the incubator. Regular splitting was carried out as follows:

1. Discard the old medium from the culture flask (T-25);
2. Wash the cells once with 5 ml PBS;
3. Add 1 ml of trypsin/EDTA to the flask and shake it a bit to make sure that trypsin covers the bottom homogeneously, and place the flask back to the incubator at 37 °C for about 2 min;
4. Shake the flask and make sure most of the cells are detached from the bottom under the phase contrast microscopy;
5. Add 5ml of pre-warmed complete medium to the cells and pipette the bottom of the flask to make sure that all cells were detached;
6. Transfer the cell suspension to a 15 ml centrifugation tube and centrifuge at 800 g for 5 min;
7. Discard the supernatant, add another 5ml culture medium and pipette the cells to make sure they are dispersed homogeneously without cell clusters;
8. Take a desired amount of cells into a new flask with fresh medium and make sure the final volume is 5ml and shake the flask gently to distribute cells homogeneously. For example, if the splitting concentration at 1:50, then take 100µl cells and add 4.9ml fresh medium for the new passage. At this concentration, cells need 4 days to arrive 80-90% confluency again.

Ref 52 wt cells can be maintained before passage 50.

5.1.2 Ref52 YFP-Paxillin

The same culture process as Ref52 wt cells.

5.1.3 Jurkat E6-1

The culture medium for Jurkat E6-1 cells is Click's/ RPMI 1640 medium plus 10% fetal bovine serum, 10% L-glutamine and 100 μg/ml penicillin and streptomycin. They are cultured at 37˚C, 5% CO_2, and about 90% humidity. Cells were passaged twice a week and were maintained up to passage 10 by the following steps:

1. Cells are transferred to a 50 ml centrifuge tube, and centrifuged at 100 g for 8 min.
2. Cells were splitted at desirable concentration. For example, at 1:10, it needs about 3 days to arrive the same confluency as in the last passage. In a T75 flask, the total volume is 30 ml. The concentration of cells should not exceed 3×10^6 cells/ml.

Jurkart E6-1 cells were maintained up to passage 12.

5.2 Jurkat E6-1 cells stimulation with TNF

For stimulation with TNF, cells were incubated with TNF in culture medium at 37˚C for 25 min prior to an experiment. The working concentration of TNF is 100 ng/ml.

5.3 Fibronectin Functionalization

Human fibronectin was physisorbed on the substrate at 4 ˚C overnight at a concentration of 15 $\mu g/cm^2$ in a humid environment. To remove excess proteins, the FN surface was washed several times with PBS. The substrates used in this study were coverslips and PCS. The coverslip used for the AFM experiment was glued into a Petri dish with biocompatible glue before the FN coating.

5.4 Jurkat E6-1 cell counting on FN coated glass and size analysis on FN coated PCS

FN was coated on coverslips in a 12-well plate as described in 6.3. 4000 cells were seeded in a

well with 1ml medium volume of. 3 repeats were carried out for each experimental situation, i.e. with and without TNF-treatment of cells. Cells were incubated for 1h at 37˚C. Afterwards, cells were fixed with 4% PFA at room temperature for 25 min, after twice wash with PBS. Then, cells can be imaged directly in PBS. Cells in 20 ocular spectrums (avoid the border) were counted. This experiment was done once in triplicate.

For the cell size analysis, PCS substrates were coated with FN as described in 6.3. The samples were put into a 6-well plate, 5×10^5 cells were seeded per well. The incubation time and fixation procedure was the same as last paragraph. On a single sample, about 20-30 images were recorded with the surface contrast microscopy. Cell size was analyzed manually with Image J. This experiment was done twice in triplicate.

5.5 RICM

For RICM experiment, 3 different kinds of surfaces were used. One was the FN coated coverslip (diameter 24 mm), one was a normal glass coverslips (cleaned with soap) and the other one was PLL-g-PEG passivated glass. The passivation was achieved by first activating the glass with oxygen plasma (0.4 mbar O_2, 150 W, 10 min) followed by incubation in a PLL-g-PEG solution (0.1 mg/ml in HEPES) for 40 min. Prior to experiments, the samples were washed several times with PBS.

Before adding cells on samples, the substrate was mounted into the BioCell chamber at 37 °C. Cells (non-activated and activated with TNF) were allowed to attach to the surface for 20 minutes. The experiment was carried out four times in duplicate for both stimulated and unstimulated cells. The objective is Antiflex. Images were captured by the camera ProgRes MF cool. The adhesion area of 7-10 cells and 50 microspikes per image were analyzed. There were about 20 images included in the analysis. RICM data were manually analyzed with Image J.

5.6 Immunofluorescence check of integrin expression on Jurkat E6-1 cells

5.6.1 Coverslips Treatment

Coverslips were soaked in 33% HCl for 15 min, afterwards the acid was poured out and water was poured on the glass slides and wash 10 min twice. Then coverslips were soaked in 70% ethanol for 5min. Then they can be sterilized under 150 °C or dried overnight in a closed container.

5.6.2 Cell seeding and staining

Four coverslips (name them as S1, S2, S3, S4) were put in a 6-well plate, PLL (100μg/ml) was added to cover the coverslips as the adhesive surface and incubate at 37 °C for 30 min, afterwards, PLL was discarded and the coverslips were washed 3 times with PBS. 10^6 cells were seeded in each well, and incubate cells at 37 °C for 15min. Then, Cells were stained following the steps below:

1. Cells were fixed (same procedure as 6.4);
2. Add 2ml (same volume for the other solution if not specifically announced) of 1% Triton X-100, incubate at room temperature for 5min;
3. After once wash with PBS, add 1% BSA (dissolve in PBS) and incubate at room temperature for 1h with shaking.
4. After 3 times wash with PBS, add 1% BSA to S1 and S2 and add the primary antibodies monoclonal anti-human CD49d and monoclonal anti-human CD49d at the concentration of 10 μg/ml (antibodies were diluted in 1% BSA) to bind with integrin α_4 and α_5 respectively. Use aluminum paper to cover the samples and incubate at 4°C overnight.
5. After 3 times wash with PBS, add 1% BSA to S1, add secondary antibody goat anti-mouse IgG, (H+L) FITC conjugated to S2, S3 and S4. Samples were covered with aluminum paper and incubated at 37°C for 1h. Secondary antibody was also diluted in 1% BSA, the working concentration of it was 10μg/ml.
6. After extensive wash with PBS, samples were dip once in water; the excessive water was absorbed with a soft paper. A drop (12μl) of Prolong diamond antifade mountant with DAPI was added on the sample. Samples were put on slides and were ready for imaging overnight.

Samples were imaged with CLSM.

5.7 FACS for Jurkat E6-1 cells

1. Prepare 4 FACS tubes, in each tube add 2.5×10^5 cells in 1ml;
2. Centrifuge at 4°C, 300g, 5min;
3. Discard the supernatant rapidly, suck the excessive liquid at the mouth of the tube;
4. Wash the precipitant with 1% BSA, and add 250µl in each tube;
5. Repeat step 2-4 once;
6. Add 100 µl primary antibody (working concentration was 10µg/ml) to the tube and votex to resuspend cells for 3 seconds and incubate cells at 4°C for 1h;
7. Repeat step 2, 3 and 4;
8. Repeat step2;
9. Add 200µl secondary antibody (working concentration was 10µg/ml), repeat step 2;
10. Wash twice with 1% BSA;
11. Resuspend cells with 100µl 1% PFA, and vortex 3 seconds. Cells were kept at 4°C before FACS.

There are also 2 samples for negative control and positive control as 6.6.

Green fluorescence was measured on a FACSCalibur flow cytometer by the BD CellQuest^{TM} Pro software V.4.0.2

5.8 AFM

5.8.1 Cantilever Calibration

Cantilevers were first rinsed once with acetone for a couple of minutes. After clamping it to quartz block which fixes the cantilevers. The calibration was implemented in the Petri dish heater chamber filled with PBS and the cantilever was approached to the surface with the Nanowizard III motor. The laser spot was adjusted on the cantilever till the maximum sum signal was achieved, and both the lateral and vertical signal in photodiode was adjusted at 0V.

The automatic approach was applied to approach the cantilever to the surface within the valid range of piezo (15µm), where the position of the cantilever was stabilized in the middle of the piezo range (about 7.5 µm). The parameter for approaching was 1V, speed was 0.5 µm/s, and the pulling length was 1 µm. Afterwards, a single force-distance was run once to get the typical

curve for calibration. The sensitivity was obtained by fitting the linear part of the curve (can either be approach or retract curve), after accepting this value, the motor was lifted up by 500 µm and the spring constant was obtained, a correction factor (0.871) implemented in the AFM software was used to get the accurate spring constant. One cantilever was calibrated at least three times to get the average value of sensitivity and corrected spring constant. Calibration was carried out at room temperature.

5.8.2 Cantilever Functionalization

Calibrated cantilevers were incubated in biotin-BSA (0.5mg/ml in PBS) overnight at 37 ˚C in a Petri dish wrapped with parafilm. Afterwards, they were incubated with streptavidin (0.5 mg/ml PBS) for 10 minutes at room temperature, and then incubated 10 minutes in biotin-concanavalin A (0.2 mg/ml in PBS) at room temperature. Incubation was done in a humid environment. Between functionalization steps, cantilevers were rinsed extensively with PBS.

5.8.3 Single-cell Force Spectroscopy

Cell adhesion forces were measured using atomic force microscopy (AFM) installed on an inverted microscopy (IX71). In detail, a NanoWizard III head was used for sub-second cell-substrate contact time of 0 sec. The piezo range is up to 15 µm which is enough to completely detach the cell and a CellHesion 200 with 100 µm piezo travel length was used for longer cell-substrate contact times of 5sec and 10 sec.

For the adhesion force experiments, 2 ml RPMI 1640 medium supplemented with 100 µg/ml penicillin/streptomycin were added into the Petri dish containing a fibronectin-coated substrate (coverslip, diameter at 14mm). All experiments were carried out at approximately 36 °C in a heated fluid chamber. The functionalized cantilever was approached to the surface with the AFM and cantilever sensitivity was measured again because the position of the laser spot changed on the calibration day and the experiment day. Also if the cantilever was replaced or tilted during the experiment, the sensitivity should be measured once more, because sensitivity is necessary for the force calculation carried out after detecting cantilever bending with the photodiode.

Prior to the measurements, it is best to wait until the photodiode signal is equilibrated. This might take a while (about half an hour). A droplet of cell suspension (about 10^4 cells) was pipetted into the Petri dish far away from the FN-coated coverslip very gently to avoid bubbles. Then, the cantilever was pressed to a cell for several tens of seconds, a successful attachment can be reflected into an obvious change of the vertical deflection, where the photodiode signal increased till about 2 V over contact time. Afterwards, the cantilever can be lifted upwards by about 20 µm to check optically if the cell was attached at the right position, normally the whole cell body should be below the top of the cantilever. And also since the cantilever is translucent, abnormal cells are discarded although they might get attached. The image was taken with camera ProgRes MF cool, and the objective is 20×.

After successful cell attachment, the cell was allowed to relax at the cantilever for about 2 minutes, then the cantilever was lifted upwards for about 700 µm, this lifting should be very gentle to avoid shaking from the motor movement, e.g. step size 100 µm. Then the cantilever was moved on top of the FN-coated coverslip. The edge of the coverslip was considered not the good position due to the not perfect FN coating.

Before measuring a force-distance curve, the cell was approached to the surface again into the range of the piezo. The settings were: contact force was 500 pN, constant speed for both approaching and retraction was 3 µm/s for all curves, contact time was at 0 sec, 5 sec and 10 sec. Pulling length was varied from 15 µm to 80 µm, which depends on the contact time and whether cells were completely detached from the surface. Closed-loop and constant height mode were applied for all measurements. In the constant height mode, the cantilever position was kept at a constant height after the maximum contact force had been reached. Typically, the time difference between the first cell-surface contacts to reaching the maximum contact force is about 0.2 s. Only cells without change of their positions during the experiment were included for analysis. 11-15 cells in total 250 detachment curves were analyzed in each experimental situation.

5.8.4 Data analysis

Force-distance curves were analyzed with the commercial data processing software from JPK. The results were plotted with Origin 9.0 software (Originlab, USA).

5.9 Microfluidics

Jurkat E6-1 cells without or with TNF treatment were added in the syringe which is fixed with the pump and the control system.

Videos were obtained with IX81 phase contrast microscopy, the objective is 10×, the camera is Hamamastu C9300, and the software for recording is HCImage 2.1.1.0. Shear stress at 0.04 $\frac{dyn}{cm^2}$, 0.06 $\frac{dyn}{cm^2}$, 0.08 $\frac{dyn}{cm^2}$, were applied and resolution of images at 256×256 pixel with up to 151 frames per second only in the first experiment at approximately 22 °C were obtained. The other experiment situations and/or repeats were applied at the resolution of 640×480 pixel with up to 83 frames per second. For each experiment situation, videos of about 3 minutes were recorded and videos of about 2min were analyzed with Image J Plug-In Particle Tracker Classic.

5.10 Preparation of Nanostructures

Preparation of nanostructures was similar as the protocol in (Arnold et al., 2004). The micelle solution is prepared by dissolving PS (79000g/mol) and P2VP (36500g/mol) into toluene, the concentration of the micelle is 4mg/ml. Afterwards, gold salt is added into the micelle solution. Coverslips (24mm×24mm) were used as the substrate. The coverslips were cleaned with piranha solution (H_2O_2: H_2SO_4= 1:3) before dipping into the gold micelle solution. The micelle polymer shell is etched with a hydrogen plasma treatment at 0.4mbar, 150watt for 1h to exposure the elemental gold on the surface with defined distance. The nanostructures produced with dip coating method (the dipping speed is 10mm/min) were provided by Chengqi Xu and those with spin coating method (the spinning speed is 3000rpm) were provided by Laith Kadem.

5.11 Passivation and Functionalization of Nanostructures

The structures prepared from 6.10 were etched and activated with oxygen plasma for 10min at 0.4 mbar, afterwards the samples were incubated with PLL-g-PEG (0.1mg/ml in HEPES) for 40min, after extensive wash with water and dried. The samples were ready for functionalization. The procedure and concentration for peptides cRGD and cLDV were the same. Samples were incubated with 25μmol peptide (dissolved in water) for 4 hours, afterwards, samples were shaken for 24 hours to remove the excessive peptide. The samples can be used directly.

5.12 cLDV homogeneously coating on coverslips

Coverslips (diameter: 24mm) were incubated with 25μmol cLDV (dissolved in water) overnight at room temperature; afterwards, samples were washed several times with water.

5.13 Jurkat E6-1 cells seeding and staining

Four nanostrucured samples and four cLDV homogeneously coated coverslips were put into 6-well plates. About 7×10^5 cells (TNF untreated and TNF treated cells) were seeded in each well with 2 ml culture medium, for each experimental situation, two repeats of samples were used. After 1 h incubation at 37 ºC, cells were washed and fixed as described before (6.4). Cells were imaged with IX81 and Hamamastu camera, and cells in 10 pictures at 10× objective were counted. Since there were too less cells on the nanostructures, only cLDV homogeneously coated samples were stained. The staining procedure is as follows:

1. Add 2ml (same volume for the other solution if not specifically announced) of 1% Triton X-100, incubate at room temperature for 5min;
2. After one wash with PBS, add 1% BSA (dissolve in PBS) and incubate at room temperature for 1h with shaking.
3. After 3 times washing with PBS, add the primary antibody monoclonal anti vinculin at the concentration of 20 μg/ml (antibodies were diluted in 1% BSA). For each sample the volume was 250 μl, samples were incubated at 4 °C overnight in a humid environment.
4. After 3 times wash with PBS, dilute secondary antibody goat anti-mouse IgG, Alex Fluo® 594, Alex Fluo® 488 Phalloidin and Hoechst in 1% BSA, the working concentration of them were 1μg/ml, 5 units/ml and 10μg/ml respectively. The staining solution mixture was added to the samples, for each sample the volume was 250μl. Samples were covered with aluminium paper and incubated at room temperature for 1h in a humid environment.
5. After extensively washing with PBS, samples were dipped once into water; the excessive water drop on the edge of the sample was absorbed with a soft paper. A drop (8μl) of vectashield was added on the sample. Samples were put on slides and sealed with nail polish and they were imaged directly with IX81 microscopy and the camera was Hamamatsu, the objective was 60×.

6. Abbreviations

% (v/v)	Volume concentration (volume/volume)
% (w/v)	Mass concentration (weight/volume)
AFM	Atomic Force Microscopy
BSA	Bovine Serum Albumin
cLDV	cyclo (lysine-aspartic acid-valine)
CLSM	Confocal Laser Scanning Microscopy
cRGD	cyclo (arginine-glycine-aspatic acid)
°C	degree Celsius
cm	Centimeter
DAPI	4’, 6-diamidino-2-phenylindole
DMEM	Dulbecco’s Modified Eagle Medium
EDTA	Ethylenediaminetetraacetic acid
FACS	Fluorescence-activated cell sorting
FBS	Fetal Bovine Serum
FITC	Fluorescein isothiocyanate
FN	Fibronectin
HCl	Hydrochloric acid
HEPES	4-(2-hydroxyethyl)-1-piperazineethanesulfonic acid
IgG	Immunoglobulin
kD	kilo Dalton
µ	micro
µl	microliter
µm	micrometer
ml	milliliter
mm	millimeter
P2VP	poly-2-vinylpyridine
PBS	Phosphate buffered saline
PCS	Photonic Crystal Slabs
PFA	Paraformaldehyde
PLL-g-PEG	Poly-L-Lysine-graft-polyethylene glycol
PS	polystyrene
RICM	Reflection Interference Contrast Microscopy
RPMI	Roswell Park Memorial Institute
s, sec	second
SEM	Scanning Electronic Microscopy
TNF	Tumor Necrosis Factor
TNFR	Tumor Necrosis Factor Receptor
YFP	Yellow Fluorescence Protein
wt	Wilde type

7. List of Figures

8. Bibliography

Abram, C. L., & Lowell, C. A. (2009). The ins and outs of leukocyte integrin signaling. *Annual Review of Immunology*, *27*, 339–362.

Adams, E. L., & Czymmek, K. J. (2007). The combined application of AFM and LSCM: Changing the way we look at innate immunity. *Modern Research and Educational Topics in Microscopy*, 68–76.

Alberts, B., Johnson, A., Lewis, J., Raff, M., Roberts, K., & Walter, P. (2007). *Molecular Biology of the Cell* (Fifth Edit.). Garland Scicence, Taylor & Francis Group, LLC.

Alon, R., & Dustin, M. L. (2007). Force as a Facilitator of Integrin Conformational Changes during Leukocyte Arrest on Blood Vessels and Antigen-Presenting Cells. *Immunity*, *26*, 17–27.

Arnold, M., Cavalcanti-Adam, E. A., & Glass, R. et al. (2004). Activation of integrin function by nanopatterned adhesive interfaces. *Chemical Physics and Physical Chemistry*, *5*, 383–388.

Azari, H., Sharififar, S., Rahman, M., Ansari, S., & Reynolds, B. a. (2011). Establishing embryonic mouse neural stem cell culture using the neurosphere assay. *Journal of Visualized Experiments : JoVE*, (47), 1–4.

Bassous, E., Taub, H. H., & Kuhn, L. (1977). Ink jet printing nozzle arrays etched in silicon. *Applied Physics Letters*, *31*(2), 135.

Bearz, A., Tell, G., Formisano, S., Merluzzi, S., Colombatti, A., & Pucillo, C. (1999). Adhesion to fibronectin promotes the activation of the p125 FAK / Zap-70 complex in human T cells. *Immunology*, *98*, 564–568.

Beck, K., & Bereiter-Hahn, J. (1981). Evaluation of reflection interference contrast microscope images of living cells. *Microscopica Acta*, *84*(2), 153–178.

Bell, G. (1978). Models for the specific adhesion of cells to cells. *Science*, *200*, 618–627.

Benoit, M., Gabriel, D., Gerisch, G., & Gaub, H. E. (2000). Discrete interactions in cell adhesion measured by single-molecule force spectroscopy. *Nature Cell Biology*, *2*, 313–317.

Benoit, M., & Selhuber-unkel, C. (2011). Measuring cell adhesion forces: theory and principles. In P. C. Braga & D. Ricci (Eds.), *Atomic Force Microscopy in Biomedical Research* (Vol. 736, pp. 355–377). Totowa, NJ: Humana Press.

Billadeau, D. D., Nolz, J. C., & Gomez, T. S. (2007). Regulation of T-cell activation by the cytoskeleton. *Nature Reviews. Immunology*, *7*(2), 131–143.

Binnig, G., & Quate, C. F. (1986). Atomic force microscope. *Physical Review Letters*, *56*(9), 930–934.

Boecke, A., Sieger, D., Neacsu, C. D., Kashkar, H., & Krönke, M. (2012). Factor associated with neutral sphingomyelinase activity mediates navigational capacity of leukocytes responding to wounds and infection: live imaging studies in zebrafish larvae. *Journal of Immunology*, *189*(4), 1559–1566.

Boettiger, D. (2012). Mechanical control of integrin-mediated adhesion and signaling. *Current Opinion in Cell Biology*, *24*, 592–599.

Bouaouina, M., Blouin, E., Halbwachs-Mecarelli, L., Lesavre, P., & Rieu, P. (2004). TNF-induced beta2 integrin activation involves Src kinases and a redox-regulated activation of p38 MAPK. *Journal of Immunology*, *173*, 1313–1320.

Bradley, L. M. (2003). Migration and T-lymphocyte effector function. *Current Opinion in Immunology*, *15*, 343–348.

Brownlie, R. J., & Zamoyska, R. (2013). T cell receptor signalling networks: branched, diversified and bounded. *Nature Reviews. Immunology*, *13*, 257–269.

Butt, H.-J., Cappella, B., & Kappl, M. (2005). Force measurements with the atomic force microscope: Technique, interpretation and applications. *Surface Science Reports*, *59*, 1–152.

Cai, X., Xing, X., Cai, J., Chen, Q., Wu, S., & Huang, F. (2010). Connection between biomechanics and cytoskeleton structure of lymphocyte and Jurkat cells: An AFM study. *Micron*, *41*, 257–262.

Calderwood, D. a, Campbell, I. D., & Critchley, D. R. (2013). Talins and kindlins: partners in integrin-mediated adhesion. *Nature Reviews. Molecular Cell Biology*, *14*, 503–17.

Califano, J., & Reinhart-King, C. A. (2010). Substrate stiffness and cell area predict cellular traction stresses in single cells and cells in contact. *Cell and Molecular Bioengineering*, *3*(1), 68–75.

Cappella, B., & Dietler, G. (1999). Force-distance curves by atomic force microscopy. *Surface Science Reports*, *34*, 1–104.

Caputo, K. E., & Hammer, D. a. (2005). Effect of microvillus deformability on leukocyte adhesion explored using adhesive dynamics simulations. *Biophysical Journal*, *89*, 187–200.

Carlson, R. H., Gabel, C. V, Chan, S. S., Austin, R. H., & Brody, J. P. (1997). Self-Sorting of White Blood Cells in a Lattice. *Physical Review Letters*, *79*(11), 2149–2152.

Carrasco, Y. R., Fleire, S. J., Cameron, T., Dustin, M. L., Batista, F. D., & Fields, I. (2004). LFA-1 / ICAM-1 Interaction Lowers the Threshold of B Cell Activation by Facilitating B Cell Adhesion and Synapse Formation. *Immunity*, *20*, 589–599.

Chan, J. R., Hyduk, S. J., & Cybulsky, M. I. (2000). alpha4beta1 Integrin/VCAM-1 Interaction Activates alphaLbeta2 Integrin-Mediated Adhesion to ICAM-1 in Human T Cells. *The Journal of Immunology*, *164*, 746–753.

Chen, C. S., Alonso, J. L., Ostuni, E., Whitesides, G. M., & Ingber, D. E. (2003). Cell shape provides global control of focal adhesion assembly. *Biochemical and Biophysical Research Communications*, *307*, 355–361.

Chen, G., & Goeddel, D. V. (2002). TNF-R1 Signaling : A Beautiful Pathway The Fas Signaling Pathway : More Than a Paradigm. *Science*, *296*, 1634–1635.

Chu, J., Zhang, H., Huang, X., Lin, Y., Shen, T., Chen, B., … Li, J. (2013). Apelin ameliorates TNF-α-induced reduction of glycogen synthesis in the hepatocytes through G protein-coupled receptor APJ. *PloS One*, *8*(2), e57231.

Constantin, G., & Laudanna, C. (2012). Transmigration of effector T lymphocytes: changing the rules. *Nature Immunology*, *13*(1), 15–16.

Cox, D., Brennan, M., & Moran, N. (2010). Integrins as therapeutic targets: lessons and opportunities. *Nature Reviews. Drug Discovery*, *9*, 804–820.

Curtis, a S. G. (1964). A study by interference reflection microscopy. *Journal of Cell Biology*, *20*(1), 199–215.

Czeschik, J. C., Hagenacker, T., Schäfers, M., & Büsselberg, D. (2008). TNF-alpha differentially modulates ion channels of nociceptive neurons. *Neuroscience Letters*, *434*, 293–298.

De Fougerolles, A. R., Sprague, A. G., & Nickerson-nutter, C. L., et al. (2000). Regulation of inflammation by collagen-binding integrins α1β1 and α2β1 in models of hypersensitivity and arthritis. *The Journal of Clinical Investigation*, *105*(6), 721–729.

Delanoë-Ayari, H., Rieu, J. P., & Sano, M. (2010). 4D traction force microscopy reveals asymmetric cortical forces in migrating dictyostelium cells. *Physical Review Letters*, *105*, 248103–1–248103–4.

Dixit, N., Yamayoshi, I., & Nazarian, A., et al. (2011). Migrational guidance of neutrophils is mechanotransduced via high-affinity LFA-1 and calcium flux. *Journal of Immunology*, *187*, 472–481.

Engler, A. J., Griffin, M. A., & Sen, S., et al. (2004). Myotubes differentiate optimally on substrates with tissue-like stiffness: Pathological implications for soft or stiff microenvironments. *Journal of Cell Biology*, *166*(6), 877–887.

Erdmann, T., & Schwarz, U. S. (2004). Stability of Adhesion Clusters under Constant Force. *Physical Review Letters*, *92*(10), 108102–1–108102–4.

Erdmann, T., & Schwarz, U. S. (2006). Bistability of cell-matrix adhesions resulting from nonlinear receptor-ligand dynamics. *Biophysical Journal*, *91*(6), L60–L62.

Evans, E., & Ritchie, K. (1997). Dynamic strength of molecular adhesion bonds. *Biophysical Journal*, *72*(4), 1541–1555.

Faustman, D., & Davis, M. (2010). TNF receptor 2 pathway: drug target for autoimmune diseases. *Nature Reviews. Drug Discovery*, *9*(6), 482–93.

Fiedler, S., Shirley, S. G., & Schnelle, T. (1998). Dielectrophoretic sorting of particles and cells in a microsystem. *Anaytical Chemistry*, *70*, 1909–1915.

Fletcher, D. a, & Mullins, R. D. (2010). Cell mechanics and the cytoskeleton. *Nature*, *463*, 485–492.

Folch, A. (2000). Icroengineering of cellular interactions. *Annual Review of Biomedical Engineering*, *2*, 227–256.

Folger, R., Weiss, L., & Glaves, D., et al. (1978). Translational movements of macrophages through media of different viscosities. *Jounal of Cell Science*, *31*, 245–257.

Franz, C. M., Taubenberger, A., & Puech, Pi-H., et al. (2007). Studying integrin-mediated cell adhesion at the single-molecule level using AFM force spectroscopy. *Science's STKE*, *406*, pl5.

Galbraith, C. G., Yamada, K. M., & Galbraith, J. A. (2006). Polymerizing actin fibers position integrins primed to probe for adhesion sites. *Science*, *315*, 992–995.

Giagulli, C., Ottoboni, L., & Caveggion, E., et al. (2006). The Src family kinases Hck and Fgr are dispensable for inside-out, chemoattractant-induced signaling regulating beta 2 integrin affinity and valency in neutrophils,

but are required for beta 2 integrin-mediated outside-in signaling involved in sustained a. *Journal of Immunology*, *177*, 604–611.

Giblin, P. A., Hwang, S. T., & Katsumoto, T. R., et al. (1997). Ligation of L-selectin on T lymphocytes activates beta1 integrins and promotes adhesion to fibronectin. *Journal of Immunology*, *159*, 3498–3507.

Grabovsky, V., Feigelson, S., & Chen, Ch., et al. (2000). Subsecond Induction of alpha 4 Integrin Clustering by Immobilized Chemokines Stimulates Leukocyte Tethering and Rolling on Endothelial Vascular Cell Adhesion Molecule 1 under Flow Conditions. *The Journal of Experimental Medicine*, *192*(4), 495–505.

Gruys, E., Toussaint, M. J. M., & Niewold, T. A., et al. (2005). Acute phase reaction and acute phase proteins. *Journal of Zhejiang University.*, *6B*(11), 1045–1056.

Harris, A. K., Wild, P., & Stopak, D. (1980). Silicone Rubber Substrates: A New Wrinkle In The Study Of Cell Locomotion. *Science*, *208*(4440), 177–7–179.

Harrison, D. J., Manz, A., & Fan, Z.H., et al. (1992). capillary electrophoresis and sample injection systems integrated on a planar glass chip. *Analytical Chemistry*, *64*, 1926–1932.

Haubner, R., & Finsinger, D. (1997). AUFSATZE Stereoisomere Peptid-Bibliotheken und Peptidmimetika zum Design von selektiven Inhibitoren des a & -Integrins fur eine neuartige Krebstherapie. *Angewandte Chemie*, *109*, 1440–1456.

Head, B. P., Patel, H. H., & Insel, P. a. (2014). Interaction of membrane/lipid rafts with the cytoskeleton: impact on signaling and function membrane/lipid rafts, mediators of cytoskeletal arrangement and cell signaling. *Biochimica et Biophysica Acta*, *1838*(2), 532–545.

Helenius, J., Heisenberg, C.-P., & Gaub, H. E., et al. (2008). Single-cell force spectroscopy. *Journal of Cell Science*, *121*(Pt 11), 1785–1791.

Hersen, P., & Ladoux, B. (2011). Biophysics: Push it, pull it. *Nature*, *470*, 340–341.

Herter, J., & Zarbock, A. (2013). Integrin Regulation during Leukocyte Recruitment. *Journal of Immunology*, *190*, 4451–4457.

Hirschfeld-Warneken, V. C., Arnold, M., & Cavalcanti, A., et al. (2008). Cell adhesion and polarisation on molecularly defined spacing gradient surfaces of cyclic RGDfK peptide patches. *European Journal of Cell Biology*, *87*, 743–750.

Hoffmann, S., Hosseini, B. H., & Hecker, M., et al. (2011). Single cell force spectroscopy of T cells recognizing a myelin-derived peptide on antigen presenting cells. *Immunology Letters*, *136*, 13–20.

Hogg, N., Laschinger, M., & Giles, K., et al. (2003). T-cell integrins: more than just sticking points. *Journal of Cell Science*, *116*, 4695–4705.

Hogg, N., Patzak, I., & Willenbrock, F. (2011). The insider's guide to leukocyte integrin signalling and function. *Nature Reviews. Immunology*, *11*, 416–426.

Hosseini, B. H., Louban, I., & Djandji, D., et al. (2009). Immune synapse formation determines interaction forces between T cells and antigen-presenting cells measured by atomic force microsocopy. *Proceedings of the National Academy of Sciences*, *106*(42), 17852–17857.

Huang, H., Kamm, R. D., & Lee, R. T. (2004). Cell mechanics and mechanotransduction: pathways, probes, and physiology. *American Journal of Physiology. Cell Physiology*, *287*, C1–C11.

Hutter, J. L., & Bechhoefer, J. (1993). Calibration of atomic-force microscope tips. *Review of Scientific Instruments*, *64*(7), 1868–1873.

Hynes, R. O. (2002). Integrins : Bidirectional , Allosteric Signaling Machines. *Cell*, *110*, 673–687.

Ibelgaufts, H. (2013). Cytokines & cells online pathfinder encyclopedia.

Ingber, D. E. (2006). Cellular mechanotransduction: putting all the pieces together again. *The FASEB Journal*, *20*, 811–827.

Jacobson, S. C., & Ramsey, J. M. (1996). Integrated Microdevice for DNA Restriction Fragment Analysis. *Analytical Chemistry*, *68*, 720–723.

Jaczewska, J., Abdulreda, M. H., & Yau, Ch.Y., et al. (2014). TNF-α and IFN-γ promote lymphocyte adhesion to endothelial junctional regions facilitating transendothelial migration. *Journal of Leukocyte Biology*, *95*, 265–274.

Janmey, P. a, & McCulloch, C. a. (2007). Cell mechanics: integrating cell responses to mechanical stimuli. *Annual Review of Biomedical Engineering*, *9*, 1–34.

Kiersnowska-Rogowska, B., Lzycka, A., & Jabłońska, E. et al. (2006). Estimation of L-selectin expression on neutrophils and level of soluble L-selectin form in serum of patient with chronic myelogenic leukemia. *Przeql Lek*, *63*(9), 756–758.

Kinashi, T. (2005). Intracellular signalling controlling integrin activation in lymphocytes. *Nature Reviews. Immunology*, *5*, 546–559.

Koukouritaki, S. B., Vardaki, E. A., & Papakonstanti, E. A., et al. (1999). TNF-a Induces Actin Cytoskeleton Reorganization in Glomerular Epithelial Cells Involving Tyrosine Phosphorylation of Paxillin and Focal Adhesion Kinase. *Molecular Medicine*, *5*, 382–392.

Krauss, T. F., Richard, M., & Brand, S. (1996). Two-dimensional photonic-bandgap structures operating at near-infrared wavelengths. *Nature*, *383*, 699–702.

LaFleur-Brooks. M. (2008). *Exploring medical language: a student-directed approach* (7th ed., p. p398). St. Louis, Missouri, US: Mosby Elsevier.

Lampin, M., Legris, C., & Degrange, M. (1997). Correlation between substratum roughness and wettability, cell adhesion, and cell migration - Lampin - 1998 - Journal of Biomedical Materials Research.pdf. *Journal of Biomedical Materials Research.*, *36*, 99–108.

Lee, S., & Spencer, N. D. (2008). Adsorption Properties of Poly (L-lysine)-graft-poly (ethylene glycol) (PLL-g-PEG) at a Hydrophobic Interface : Influence of Tribological Stress , pH , Salt Concentration , and Polymer Molecular Weight. *Langmuir*, *24*, 9479–9488.

Lee, S.-Y., Zaske, A.-M., & Novellino, T. et al. (2011). Probing the mechanical properties of TNF-α stimulated endothelial cell with atomic force microscopy. *International Journal of Nanomedicine*, *6*, 179–195.

Legate,L.R., Wickström, S. A., & Fässler, R. (2009). Genetic and cell biological analysis of integrin outside-in signaling. *Genes & Development*, *23*, 397–418.

Leick, A. (1904). *Annalen Der Physik*, *14*, 139.

Leitinger, B., & Hogg, N. (2002). The involvement of lipid rafts in the regulation of integrin function. *Jounal of Cell Science*, *115*(5), 963–972.

Ley, K., Laudanna, C., Cybulsky, M. I., & Nourshargh, S. (2007). Getting to the site of inflammation: the leukocyte adhesion cascade updated. *Nature Reviews. Immunology*, *7*, 678–689.

Li, P. C. H., & Harrison, D. J. (1997). Transport , Manipulation , and Reaction of Biological Cells On-Chip Using Electrokinetic Effects. *Analytical Chemistry*, *69*, 1564–1568.

Liliental, J., & Chang, D. D. (1998). Rack1, a receptor for activated protein kinase C, interacts with integrin beta subunit. *The Journal of Biological Chemistry*, *273*(4), 2379–2383.

Limozin, L., & Sengupta, K. (2009). Quantitative reflection interference contrast microscopy (RICM) in soft matter and cell adhesion. *Chemical Physics and Physical Chemistry*, *10*, 2752–2768.

Lokuta, M. A., & Huttenlocher, A. (2005). TNF- alpha promotes a stop signal that inhibits neutrophil polarization and migration via a p38 MAPK pathway. *Journal of Leukocyte Biology*, *78*, 210–219.

Luo, B., Carman, C. V, & Springer, T. A. (2007). Structural basis of integrin regulation and signaling. *Annual Review of Immunol*, *25*, 619–647.

Luo, J. X., Li, C. F., & Xu, T. Sh., et al. (2014). PI3K is involved in β1 integrin clustering by PSGL-1 and promotes β1 integrin-mediated Jurkat cell adhesion to fibronectin. *Molecular and Cellular Biochemistry*, *385*, 287–295.

Maciaszek, J. L., Partola, K., & Zhang, Ji., et al. (2014). Single-cell force spectroscopy as a technique to quantify human red blood cell adhesion to subendothelial laminin. *Journal of Biomechanics*, *47*, 3855–3861.

Majstoravich, S., Zhang, J. Y., & Nicholson-Dykstra, S., et al. (2004). Lymphocyte microvilli are dynamic, actin-dependent structures that do not require Wiskott-Aldrich syndrome protein (WASp) for their morphology. *Blood*, *104*, 1396–1403.

Mao, Y., & Schwarzbauer, J. E. (2005). Fibronectin fibrillogenesis, a cell-mediated matrix assembly process. *Matrix Biology*, *24*, 389–399.

Marshall, B. T., Long, M., & Piper, J.W., et al. (2003). Direct observation of catch bonds involving cell-adhesion molecules. *Nature*, *423*, 190–193.

Maton, D., Hopkins, J., & McLaughlin, C. W. et al. (2008). *Human biology and health*. Englewood Cliffs, New Jersey, USA: Prentice Hall.

Mattila, P. K., & Lappalainen, P. (2008). Filopodia: molecular architecture and cellular functions. *Nature Reviews. Molecular Cell Biology*, *9*, 446–454.

Millard, T. H., & Martin, P. (2008). Dynamic analysis of filopodial interactions during the zippering phase of Drosophila dorsal closure. *Development*, *135*, 621–626.

Muth, C. A., Steinl, C., & Klein, G., et al. (2013). Regulation of hematopoietic stem cell behavior by the nanostructured presentation of extracellular matrix components. *PloS One*, *8*(2), e54778.

Müller, D. J., & Engel, A. (2007). Atomic force microscopy and spectroscopy of native membrane proteins. *Nature Protocols*, *2*(9), 2191–2197.

Nazirizadeh, Y., Becker, T., & Reverey, J., et al. (2012). Photonic crystal slabs for surface contrast enhancement in microscopy of transparent objects. *Optics Express*, *20*(13), 14451–14459.

Nazirizadeh, Y., Müller, J. G., & Geyer, U., et al. (2008). Direct Observation of Photonic Modes in Photonic Crystal Slabs. *IEEE*, 72–75.

Nazirizadeh, Y., Reverey, J., & Geyer, U., et al. (2013). Material-based three-dimensional imaging with nanostructured surfaces. *Applied Physics Letters*, *102*, 011116.

Nourshargh, S., & Alon, R. (2014). Leukocyte Migration into Inflamed Tissues. *Immunity*, *41*, 694–707.

Ornatsky, O., Bandura, D., & Baranov, V., et al. (2010). Highly multiparametric analysis by mass cytometry. *Journal of Immunological Methods*, *361*, 1–20.

Osborn, L., Hession, C., & Tizard, R., et al. (1989). Direct Expression Cloning of Vascular Cell Adhesion Molecule 1, a Cytokine-Induced Endothelial Protein That Binds to Lymphocytes. *Cell*, *59*, 1203–1211.

Paguirigan, A. L., & Beebe, D. J. (2008). Microfluidics meet cell biology: Bridging the gap by validation and application of microscale techniques for cell biological assays. *BioEssays*, *30*, 811–821.

Pankov, R., & Yamada, K. M. (2002). Fibronectin at a glance. *Journal of Cell Science*, *115*(20), 3861–3863.

Park, S., Koch, D., & Cardenas, R., et al. (2005). Cell motility and local viscoelasticity of fibroblasts. *Biophysical Journal*, *89*, 4330–4342.

Partridge, M. A., & Marcantonio, E. E. (2006). Initiation of Attachment and Generation of Mature Focal Adhesions by Integrin-containing Filopodia in Cell Spreading. *Molecular Biology of the Cell*, *17*, 4237–4248.

Pasche, S., Textor, M., & Meagher, L. et al. (2005). Relationship between Interfacial Forces Measured by Colloid-Probe Atomic Force Microscopy and Protein Resistance of Poly (ethylene glycol) -Grafted Poly (L-lysine) Adlayers on Niobia Surfaces. *Langmuir*, *21*, 6508–6520.

Paszek, M. J., Boettiger, D., & Weaver, V. M., et al. (2009). Integrin clustering is driven by mechanical resistance from the glycocalyx and the substrate. *PLoS Computational Biology*, *5*(12), e1000604.

Patterson, K. C., Yang, R., & Zeng, B.X., et al. (2013). Measurement of cationic and intracellular modulation of integrin binding affinity by AFM-based nanorobot. *Biophysical Journal*, *105*, 40–47.

Pawley, J. B. (2006). *handbook of biological confocal microscopy* (3rd ed.). Berlin: Springer.

Peters, J. . H., Sporn, L. . A., & Ginsberg, M. H., et al. (1990). Human endothelial cells synthesize, process, and secrete fibronectin molecules bearing an alternatively spliced type III homology (ED1). *Blood*, *75*(9), 1801–1808.

Petersen, K. E. (1979). Fabrication of an interated, planar silicon ink-jet structure. *IEEE Transactions on Electron Devices*, *ED-26*(12), 1918–1920.

Philipp, S., Puchert, M., & Adam-Klages, S., et al. (2010). The Polycomb group protein EED couples TNF receptor 1 to neutral sphingomyelinase. *Proceedings of the National Academy of Sciences of the United States of America*, *107*(3), 1112–1117.

Pober, J. S., & Sessa, W. C. (2007). Evolving functions of endothelial cells in inflammation. *Nature Reviews. Immunology*, *7*, 803–815.

Provenzano, P. P., & Keely, P. J. (2011). Mechanical signaling through the cytoskeleton regulates cell proliferation by coordinated focal adhesion and Rho GTPase signaling. *Journal of Cell Science*, *124*, 1195–1205.

Puls, A., Eliopoulos, A. G., Nobes, C. D., Bridges, T., & Young, L. S. (1999). Activation of the small GTPase Cdc42 by the inflammatory cytokines TNF α and IL-1 , and by the Epstein-Barr virus transforming protein LMP1. *Journal of Cell Science*, *112*, 2983–2992.

Ramsden, J. J., & Horvath, R. (2009). Optical biosensors for cell adhesion. *Journal of Receptor and Signal Transduction Research*, *29*(3-4), 211–223.

Rape, A.D., Guo, W.H., & Wang, Y. L. (2011). *Responses of cells to adhesion-mediated signals: a universal mechanism*. (A. W. Johnson & B. A. Harley, Eds.) (pp. pp1–10). Springer US.

Rico, F., Chu, C., & Abdulreda, M.H., et al. (2010). Temperature modulation of integrin-mediated cell adhesion. *Biophysical Journal*, *99*, 1387–1396.

Rietzler, M., Bittner, M., & Kolanus, W., et al. (1998). The human WD repeat protein WAIT-1 specifically interacts with the cytoplasmic tails of β7-integrins. *Journal of Biological Chemistry*, *273*(42), 27459–27466.

Rinker, K. D., Prabhakar, V., & Truskey, G. A. (2001). Effect of Contact Time and Force on Monocyte Adhesion to Vascular Endothelium. *Biophysical Journal*, *80*, 1722–1732.

Roduit, C., van der Goot, F. G., & De Los Rios, Paolo, et al. (2008). Elastic membrane heterogeneity of living cells revealed by stiff nanoscale membrane domains. *Biophysical Journal*, *94*(4), 1521–1532.

Ruoslahti, E., & Pierschbacher, M. D. (1987). New Perspectives in Cell Adhesion : RGD and Integrins. *Science*, *238*, 491–497.

San Lek, H., Morrison, V. L., & Conneely, M., et al. (2013). The spontaneously adhesive leukocyte function-associated antigen-1 (LFA-1) integrin in effector T cells mediates rapid actin- and calmodulin-dependent adhesion strengthening to ligand under shear flow. *Journal of Biological Chemistry*, *288*, 14698–14708.

Sariisik, E., Docheva, D., & Padula, D., et al. (2013). Probing the interaction forces of prostate cancer cells with collagen I and bone marrow derived stem cells on the single cell level. *PloS One*, *8*(3), e57706.

Schmitz, J., Manevich, E., & Tschöpe, M., et al. (2009). Linking single integrin–ligand bond properties to cell adhesiveness under external forces exemplified by the VLA-4–VCAM-1 bond. *Soft Matter*, *5*, 4141–4151.

Schneider, U., Schwenk, H.-U., & Bornkamm, G. (1977). characterization of EBV-genome negative “null” and “T” cell lines derived from children with acute lymphoblastic leukemia and leukemic transformed non-hodgkin lymphoma. *International Journal of Cancer*, *19*, 621–626.

Selhuber-Unkel, C. (2006). Biological adhesion on nanopatterned substrates studied with force spectroscopy and microinterferometry. *phD Dissertation*.

Selhuber-Unkel, C., López-García, M., Kessler, H., & Spatz, J. P. (2008). Cooperativity in adhesion cluster formation during initial cell adhesion. *Biophysical Journal*, *95*, 5424–31.

Seminario, M., Sterbinsky, S. A., & Bochner, B. S. (1998). beta 1 Integrin-dependent binding of Jurkat cells to fibronectin is regulated by a serine-threonine phosphatase. *Journal of Leukocyte Biology*, *64*, 753–758.

Shimaoka, M., Xiao, T., & Liu, J. H., et al. (2003). Structures of the αL I domain and its complex with ICAM-1 reveal a shape-shifting pathway for integrin regulation. *Cell*, *112*, 99–111.

Shimizu, Y. J., Van Seventer, G. J. A., & Horgan, K.J., et al. (1990). Costimulation of proliferative responses of resting CD4+ T cells by the interaction of VLA-1 and VLA-5 with fibronectin or VLA-6 with laminin. *The Journal of Immunology*, *145*, 59–67.

Song, K. H., Kwon, K. W., Choi, J.-C., Jung, J., Park, Y., Suh, K.-Y., & Doh, J. (2014). T cells sense biophysical cues using lamellipodia and filopodia to optimize intraluminal path finding. *Integrative Biology*, *6*, 450–459.

Springer, T. a., & Dustin, M. L. (2012). Integrin inside-out signaling and the immunological synapse. *Current Opinion in Cell Biology*, *24*, 107–115.

Stadtmann, A., Germena, G., & Block, H., et al. (2013). The PSGL-1-L-selectin signaling complex regulates neutrophil adhesion under flow. *The Journal of Experimental Medicine*, *210*(11), 2171–2180.

Svitkina, T. M., Bulanova, E. A., & Chaga, O.Y., et al. (2003). Mechanism of filopodia initiation by reorganization of a dendritic network. *Journal of Cell Biology*, *160*, 409–421.

Tamkun, J. W., Desimone, D. W., Fonda, D., Patel, R. S., Buck, C., Horwitz, A. F., & Hynes, R. (1986). Structure of Integrin , a G lycoprotein Involved in the Transmembrane Linkage between Fibronectin and Actin. *Cell*, *46*, 271–282.

Taubenberger, A. V. (2009). Quantifying adhesive interactions between cells and extracellular matrix by single-cell force spectroscopy. *phD Dissertation*.

Taylor, T. B., Winn-deen, E. S., & Picozza, E., et al. (1997). Optimization of the performance of the polymerase chain reaction in silicon-based microstructures. *Nucleic Acids Research*, *25*(15), 3164–3168.

To, W. S., & Midwood, K. S. (2011). Plasma and cellular fibronectin: distinct and independent functions during tissue repair. *Fibrogenesis & Tissue Repair*, *4*, 21.

Tulla, M., Helenius, J., & Jokinen, J., et al. (2008). TPA primes alpha2beta1 integrins for cell adhesion. *FEBS Letters*, *582*, 3520–3524.

Vaday, G. G., Hershkoviz, R., Rahat, M. A., Lahat, N., & Cahalon, L. (2000). Fibronectin-bound TNF- alpha stimulates monocyte matrix metalloproteinase-9 expression and regulates chemotaxis, *68*, 737–747.

Vanderslice, P., Ren, K., & Revelle, J. K., et al. (1997). A cyclic hexapeptide is a potent antagonist of alpha 4 integrins. *Journal of Immunology*, *158*(4), 1710–1718.

Wang, N., Tytell, J. D., & Ingber, D. E. (2009). Mechanotransduction at a distance: mechanically coupling the extracellular matrix with the nucleus. *Nature Reviews. Molecular Cell Biology*, *10*, 75–82.

Wang, Y. X., Botvinick, E. L., & Zhao, Y. H., et al. (2005). visualizing the mechanical activation of Src. *Nature*, *434*, 1040–1045.

Whitesides, G. M. (2006). The origins and the future of microfluidics. *Nature*, *442*, 368–373.

Wilson, S. M., & Bacic, A. (2012). Preparation of plant cells for transmission electron microscopy to optimize immunogold labeling of carbohydrate and protein epitopes. *Nature Protocols*, *7*, 1716–1727.

Witte, V., Laffert, B., & Rosorius, O., et al. (2004). HIV-1 Nef Mimics an Integrin Receptor Signal that Recruits the Polycomb Group Protein Eed to the Plasma Membrane. *Molecular Cell*, *13*, 179–190.

Woolf, E., Grigorova, I., & Sagiv, A., e al. (2007). Lymph node chemokines promote sustained T lymphocyte motility without triggering stable integrin adhesiveness in the absence of shear forces. *Nature Immunology*, *8*(10), 1076–1085.

Yamada, K. M., & Kennedy, D. W. (1979). Fibroblast cellular and plasma fibronectins are similar but not identical. *The Journal of Cell Biology*, *80*(25), 492–498.

Yeung, T., Georges, P. C., & Flanagan, L. A., et al. (2005). Effects of substrate stiffness on cell morphology, cytoskeletal structure, and adhesion. *Cell Motility and the Cytoskeleton*, *60*, 24–34.

Zaidel-Bar, R., Cohen, M., & Addadi, L., et al. (2004). Hierarchical assembly of cell-matrix adhesion complexes. *Biochemical Society Transactions*, *32*, 416–420.

Zamir, E., & Geiger, B. (2001). Molecular complexity and dynamics of cell-matrix adhesions. *Journal of Cell Science*, *114*(20), 3583–3590.

Zhang, K., & Chen, J. F. (2012). The regulation of integrin function by divalent cations. *Cell Adhesion & Migration*, *6*(1), 20–29.

Zhang, X. H., Wojcikiewicz, E. P., & Moy, V. T. (2006). Dynamic adhesion of T lymphocytes to endothelial cells revealed by atomic force microscopy. *Experimental Biology and Medicine*, *231*, 1306–1312.

Zhu, D. M., Dustin, M. L., & Cairo, C. W., et al. (2007). Analysis of two-dimensional dissociation constant of laterally mobile cell adhesion molecules. *Biophysical Journal*, *92*, 1022–1034.

Zilker, A., Engelhardt, H., & Sackmann, E. (1987). Dynamic reflection interference contrast (RIC-) microscopy : a new method to study surface excitations of cells and to measure membrane bending elastic moduli. *Journal de Physique*, *48*, 2139–2151.

9. Acknowledgements

Some years ago, I thought that I would not choose biophysics for the further research field until now I studied biomechanics and measured the tiny force of single molecules. Without the kindest help from many people, I am not able to accomplish my PhD research.

First of all, I would like to sincerely thank my supervisor, Prof. Christine Selhuber-Unkel to allow me to work in the interesting project and the very patient guidance in the physical field as well as for the financial support during the whole research period. I want to also thank Prof. Dieter Adam for his nice guidance in immunology. Specially, I benefited a lot from the efforts of the above two professors and learned a lot in the interdisciplinary field. I am very grateful to Prof. Thomas Bosch for inviting me to realize my research abroad and for his agreement of my official supervisor, without his facilitation, today's work is just a dream. Additionally, I would like to thank the encouraging from Dr. Konstantin Khalturin and his guidance in improving my presentation.

Secondly, I am very appreciating the warmest help from my colleagues. The early guidance from Dr. Saskia Viebig in the biomaterials study and her support in my work gave me a lot of confidence. Dr. Constanze Lamprecht introduced to me how to use the AFM, which made my measurements very effective and efficient. As well, Sören Gutekunst helped me very patiently on the fluorescence microscopies and also I thank his time for making my life abroad easy. Benjamin Spetzler helped me for installing the RICM and the following imaging was very smooth and also his bachelor thesis and Hiwi work made my project more integrated. Equally, I thank Manuela Lieb for her many help in the technician help in the lab and Ellen Riemer for her general help in office. Meanwhile, I thank my HiWi students Katharina Siemsen, Anneke Möhring and my master student Chengqi Xu for the nice work time together. Indispensable, I thank Hendrikje Neumann, Mohammadreza Taale, Dr. Tobias Tellkamp, Dr. Julia Reverey, Michael Timmermann, Katharina Göpfert, Laith Kadem for their harmonious and encouraging work environment.

Thirdly, I would like to thank the help from the people within collaborations. Justyna Sosna

helped me every time I asked for the CLSM imaging and was accompanied during the immunofluorescence and FACS experiment. I also benefited a lot from the discussion with her. Sabine Mathieu prepared the culture medium and TNF many times. I also want to thank Yousef Nazirizadeh for the providing PCS and the imaging help with surface contrast microscopy and the people prepared the biocompatible samples: Michelle Holz, Grace Suana, Ahmed Zayed, Klaas Loger, Kristina Schlüter, Melike Baytekin-Gerngroß. Furthermore, I would like to thank the entire Bosch group, where I spent the first two months very happily.

Particularly and importantly, I would like to thank my parents for their support all the time in my education.

Last but not least, I thank Wei for his forever belief in my academic ability whenever I felt frustrated as well as the best accompany and care in my daily life.

10. Appendix

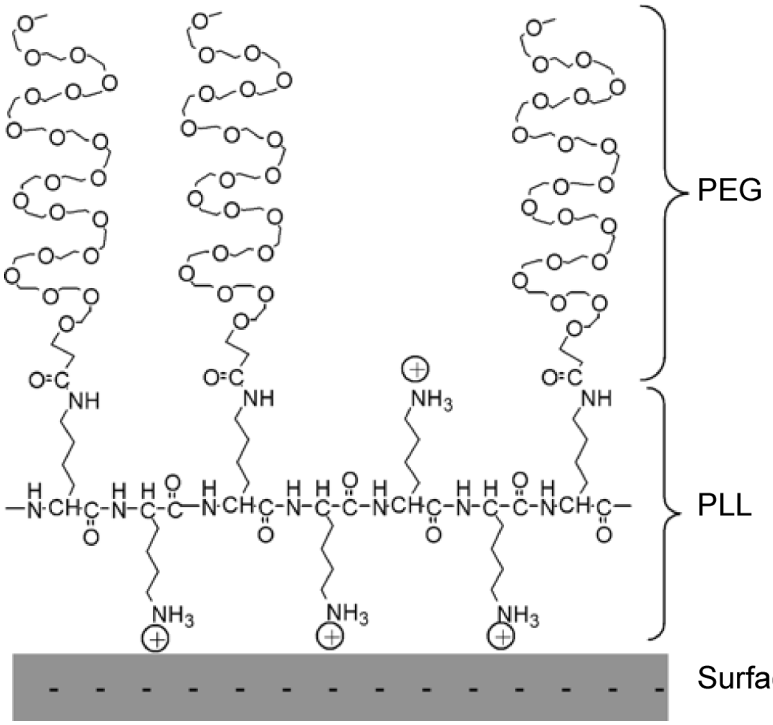

Fig. 65: Interfacial structure of adsorption of PLL-g-PEG on the surface. The surface is negatively charged and PLL has positive charge (modified from Pasche et al., 2005).

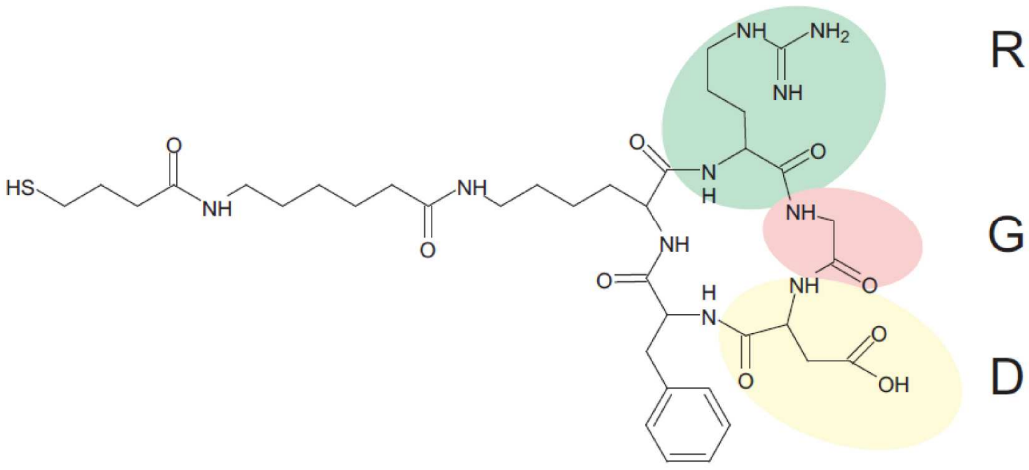

Fig. 66: Chemical structure of cRGD. (Selhuber-Unkel, 2006)

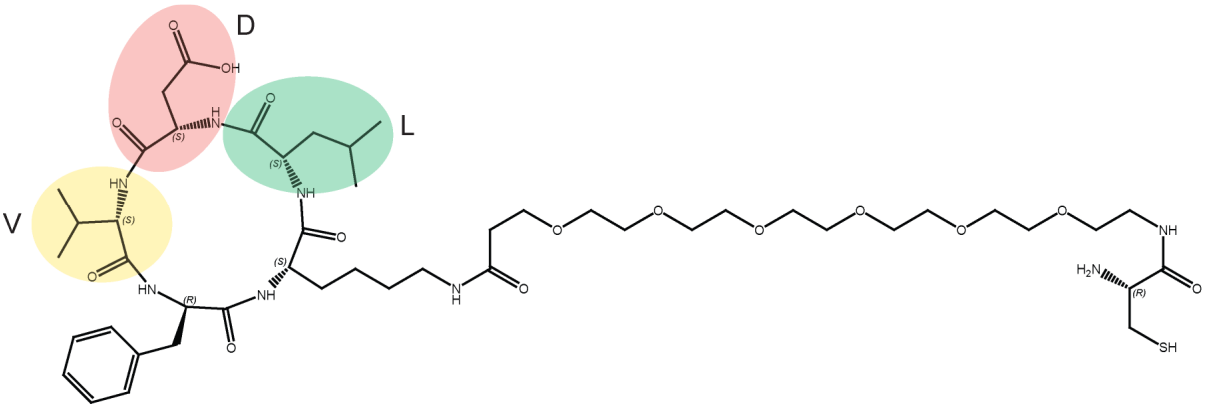

Fig. 67: Chemical structure of cLDV.

11. Erklärung

Hiermit erkläre ich, dass ich die vorliegende Dissertation nach den Regeln guter wissenschaftlicher Praxis selbst verfasst habe. Dabei habe ich keine Hilfe, außer der wissenschaftlichen Beratung durch meinen Doktorvater Prof. Dr. Thomas C. G. Bosch in Anspruch genommen. Des Weiteren erkläre ich, dass ich noch keinen Promotionsversuch unternommen habe.

Kiel, den 28. April 2015

_____

Qian Li